CR-180868

NASA

National Aeronautics and
Space Administration

FULL SCALE TECHNOLOGY DEMONSTRATION OF A MODERN COUNTERROTATING UNDUCTED FAN ENGINE CONCEPT

COMPONENT TEST

December 1987

by
GE Aircraft Engines
GE36 Project Department
Cincinnati, Ohio 45215

Prepared for

National Aeronautics and Space Administration

(NASA-CR-180868) FULL SCALE TECHNOLOGY DEMONSTRATION OF A MODERN COUNTERROTATING UNDUCTED FAN ENGINE CONCEPT: COMPONENT TEST (GE) 109 p CSCL 21E

N90-10047
Unclas
G3/07 0237151

These limitations shall be considered void after two (2) years after date of such data.
This legend shall be marked on any reproduction of these data in whole or in part.

NASA-Lewis Research Center
Contract NAS3-24210

CR-180868

National Aeronautics and
Space Administration

FULL SCALE TECHNOLOGY DEMONSTRATION OF A MODERN COUNTERROTATING UNDUCTED FAN ENGINE CONCEPT

COMPONENT TEST

FOREWORD

The testing described in this report was conducted by GE Aircraft Engines in Cincinnati, Ohio for the NASA Lewis Research Center in Cleveland, Ohio under Contract NAS3-24210. The program was carried out under the technical cognizance of Mr. R.D. Hager of the Advanced Turboprop Project Office. The contract effort was conducted at the GE Evendale Plant by the GE36 Project Department.

TABLE OF CONTENTS

Section		Page
1.0	SUMMARY	1
2.0	INTRODUCTION	2
3.0	COMPONENT BENCH TESTING - FAN BLADES	5
	3.1 Fan Blade Bench Testing - Results and Conclusions	5
4.0	COMPONENT VERIFICATION TESTING	19
	4.1 Turbine Blade Dynamic Analysis Correlation Testing	19
	4.2 Turbine Blade Frequency and Strain Distribution Testing	20
	4.3 Turbine Spool Frequency Test	34
	4.4 Seal Material Rub Test	39
	4.5 Mixer Frame Test	42
5.0	CONTROL SYSTEM DEVELOPMENT TESTING AND EVALUATION	50
	5.1 Fan Pitch Actuation Results	52
	5.2 Fuel System Test Results	59
	5.3 Control Computer Test Results	63
	5.4 Transient Response Evaluation	64
	5.5 Functional Test of Electronic Control Unit	65
	5.6 Functional Test of the EIU	68
	5.7 Conclusions	70
	5.8 Recommendations	71
6.0	ADDITIONAL COMPONENT TESTING	72
	6.1 Carbon Seal Component Testing	72
	6.2 IGV/OGV Frequency Test	79
	6.3 Turbine Blade Damper Development and Verification Test	81
7.0	SYMBOLS/ABREVIATIONS	91
8.0	REFERENCES	93

LIST OF ILLUSTRATIONS

Figure		Page
1.	Cross Section of Unducted Fan Engine.	3
2.	Cross Section of UDF™ Engine (Enlarged View).	4
3.	Strain Survey Gage Distribution.	6
4.	Engine Strain Gage Locations.	7
5.	F7 Mode Shape Comparison.	9
6.	Fan Blade Static Pull Test.	12
7.	Schematic of Ballistic Impact Testing Facility.	14
8.	Projectile Direction.	14
9.	Impact Energy at Takeoff Versus Percent Span.	15
10.	Damage Assessment for Shot No. 5.	17
11.	Damage Assessment for Shot No. 6.	17
12.	Damage Assessment for Shot No. 7.	18
13.	Blade Dynamic Analysis Correlation Test, Base Effect on Fundamental Modes.	21
14.	Blade Dynamic Analysis Correlation Test, Stiffener Effect on Panel Modes.	22
15.	Turbine Blade Dynamic Analysis, Modeling Improvements.	23
16.	Turbine Blade Dynamic Analysis, Model Assessment.	24
17.	Turbine Blade Frequency Test, Status.	26
18.	Turbine Blade Frequency Results Summary.	27
19.	Turbine Blade Frequency Results, Stages 3, 4, 6, and 7.	28
20.	Turbine Blade Frequency Results, Stages 8 through 10.	29
21.	Stage 8 Design Modification.	30
22.	Stage 8 Blade Test Results, Analysis Versus Test.	31
23.	Final Stage 8 Blade Design.	32
24.	Turbine Blade, Frequency Results.	33
25.	Stage 9 Blade Instrumented Frequency Test.	35
26.	Stage 9 Blade Instrumented Frequency Test Results.	36
27.	Forward Outer Spool Frequency Test Results, Tested with Fixture.	37
28.	Forward Outer Spool Frequency Test Results, Tested Unrestrained.	38
29.	Forward Seal Rub Material Test.	41

PAGE iv INTENTIONALLY BLANK

PRECEDING PAGE BLANK NOT FILMED

LIST OF ILLUSTRATIONS (Concluded)

Figure		Page
30.	Internal Flow Test.	44
31.	Internal Flow Test, Test Hole Pattern Adjusted for Simulation of Internal Flow/Mach Number.	45
32.	Flow Test Results, No Service Tube Blockage.	47
33.	Flow Tests Results with Service Tube Blockage.	48
34.	External Flow Test, Instrumentation.	49
35.	System Test Setup.	51
36	Fan Pitch Actuation System.	54
37.	Fan Pitch Actuation System.	55
38.	Schematic-Fan Pitch Actuation System - Before System Bench Test.	56
39.	Schematic-Fan Pitch Actuation System - Engine Ground Test Configuration.	57
40.	HP Rotor Speed Governing Schedule.	60
41.	Duct Bleed LVDT Characteristics.	62
42.	Forward and Aft Intershaft Carbon Seal.	73
43	Forward Intershaft Seal Flow Test Results.	75
44.	Test Setup for Assembly Test No. 1.	76
45.	Engine -001 Sump Leakage, Tests 2 and 3 Results.	78
46.	Engine -001 Sump Seal Leakage, Assembly Tests.	80
47.	IGV Frequency Test Results.	82
48.	OGV Frequency Test Results.	83
49.	Whirligig Damper Test.	85
50.	Whirligig Test Results Summary.	86
51.	Whirligig Damper Test Results.	87
52.	Turbine Blade Fix.	89

LIST OF TABLES

Table		Page
1.	Frequency Comparison Analysis Versus Bench Test.	8
2.	UDF™ Blade Impact Test Results.	13
3.	Spool Frequency Test Results.	39
4.	Forward Flowpath Seal - Resonant Interaction Margin.	42
5.	HP Shaft Speed Scaling.	65
6.	IP Shaft Speed Calibration.	66
7.	Interturbine Temperature Scaling.	66
8.	Inlet Temperature Scaling.	67
9.	Fuel Valve Calibration.	67
10.	IP Compressor Stator Actuator LVDT.	68
11.	Inlet Total Pressure.	69
12.	Duct Total Pressure.	69
13.	Interturbine Pressure.	70
14.	Turbine Blade Damper Development.	88

1.0 SUMMARY

A number of tests were performed on UDF™ engine components to verify component function or integrity. This report covers the UDF™ component tests as specified by NASA Contract NAS3-24210 in Exhibit A - Statement of Work. The topics covered by this statement of work are as follows:

Task No.	Description
2.1.6	Component Bench Testing
	• Fan Blades
2.2.3	Component Verification Testing
	• Rotor Turbine Blades
	• Rotor Turbine Spools
	• Mixer Frame
	• Seal Material
2.3.3	Control Test and Evaluation

Additional component test topics not specified in the contract are also included as a matter of interest. These topics are as follows:

- Carbon Seal
- Inlet Guide Vanes
- Outlet Guide Vanes
- Turbine Blade Dampers

2.0 INTRODUCTION

The UDF™ engine is a new aircraft engine concept that is based on an ungeared, counterrotating, unducted, ultra-high-bypass turbofan configuration. This engine is being developed by GE to provide a high thrust-to-weight ratio power plant with exceptional fuel efficiency for subsonic aircraft application.

The engine encompasses the operational flexibility and fuel efficiency of a two-spool core gas generator with the propulsive efficiency of a propeller (moderate diameter and tip speed). The engine is based on an aft-mounted, counterrotating power turbine that aerodynamically couples with a basic gas generator engine and provides for direct conversion of the gas generator engine power into propulsive thrust without requiring a gearbox or additional shafting. The concept of counterrotating fan blades is being used to capitalize on the full propulsive efficiency of this configuration; that is, the exit swirl from the first blade row is recovered by the second row and converted into propulsive thrust. The turbine transmits its power through two counterrotating power turbine frames, upon which polygonal support rings are mounted to carry the unducted fan blades. In this configuration, the turbine frames transmit power to the fan blades through the polygonal support rings which act as the primary-load carrying support structure for the fan blades. This isolates the turbine flowpath from out-of-round distortions from the fan blade loads.

The counterrotating turbine rotors, power turbine frames, fan blades, and static structures are components which comprise the "propulsor" for the UDF™ engine. Mounted in front of the propulsor is a gas generator engine which provides the required gas horsepower. The gas generator is a modified production F404 turbofan engine. A cross-sectional view of the UDF™ engine is shown in Figure 1. An enlarged cross section of the propulsor is shown in Figure 2.

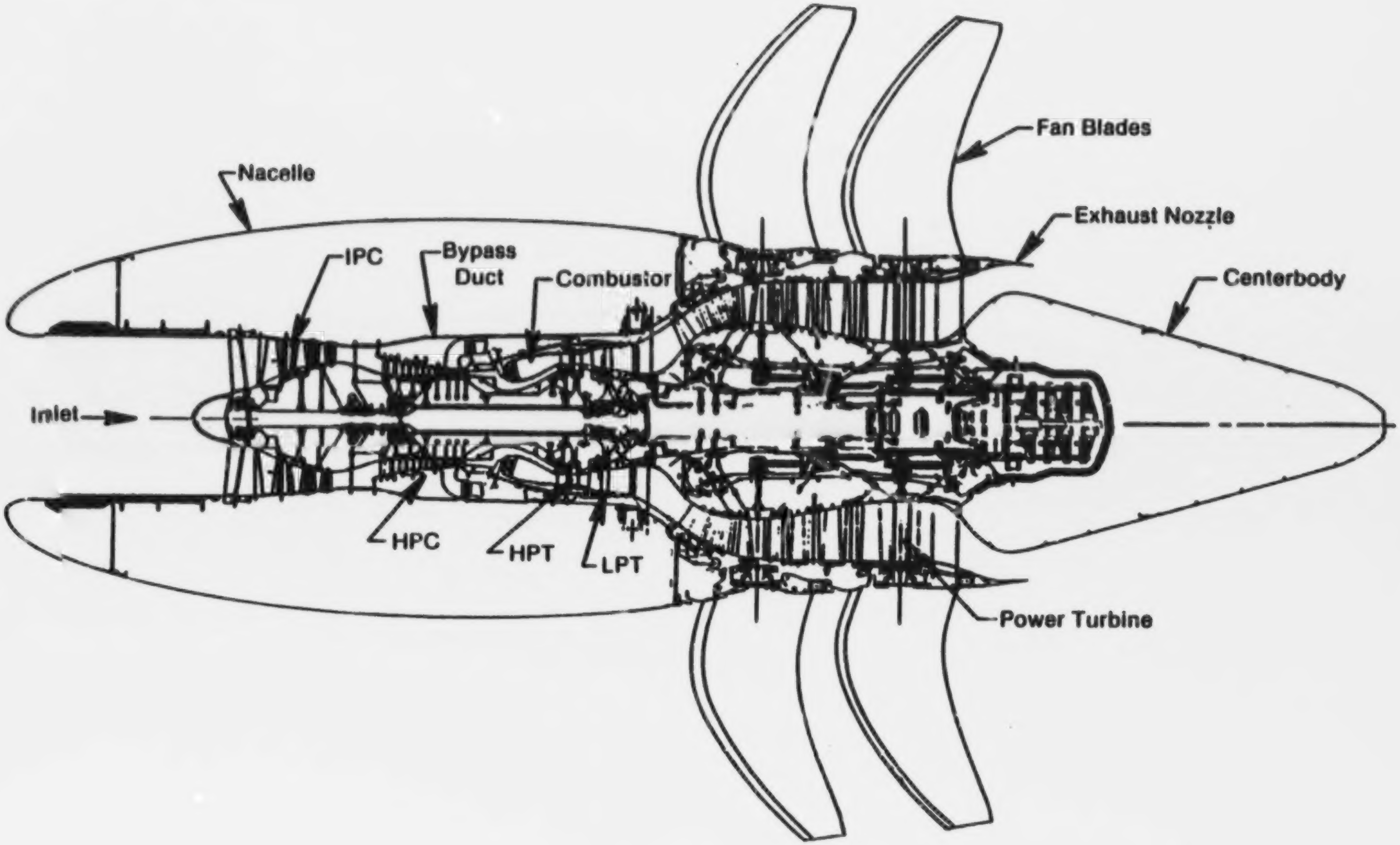
Fan Blades
Nacelle
Exhaust Nozzle
IPC
Bypass Duct
Combustor
Centerbody
Inlet
HPC
HPT
LPT
Power Turbine

Figure 1. Cross Section of Unducted Fan Engine.

ORIGINAL PAGE IS
OF POOR QUALITY

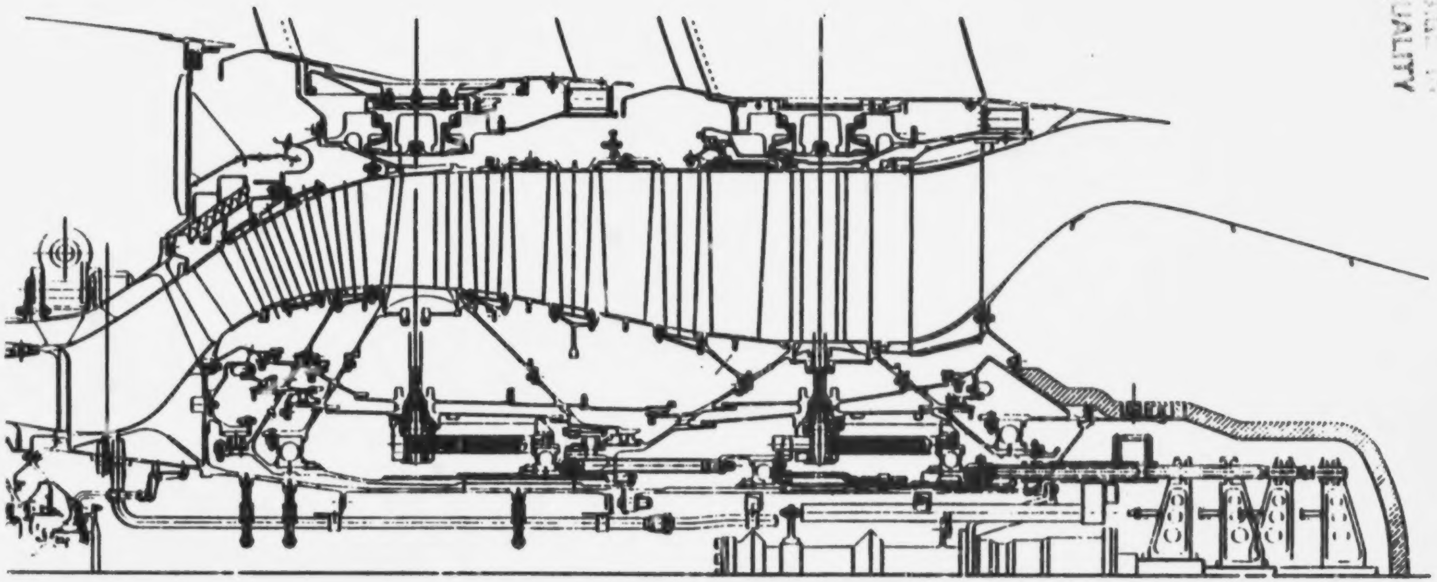

Figure 2. Cross Section of UDF™ Engine (Enlarged View).

3.0 COMPONENT BENCH TESTING - FAN BLADES

Introduction

The UDF™ fan blades are advanced designs aerodynamically and mechanically. They consist of a composite shell or airfoil on a titanium core or spar. The bottom of the spar forms a dovetail which enables the blade to be held by the blade retention hardware. These new fan blades make this type of engine conceivable and the success of the UDF™ hinges upon them. This makes the component testing of these blades extremely important.

Overview

Nondestructive and destructive mechanical tests of the UDF™ fan blades were conducted to determine vibration response, life, and strength of the blades. A strain survey was conducted to determine the blade vibrational response and mode shape. Data from this testing were also used to select strain gage locations for the fan blade static HCF and engine tests. A high cycle fatigue test was performed to establish the cyclic life of the blades. A static pull test was conducted to verify the mechanical integrity of the blade and primary retention mechanism. The impact resistance capability was investigated by static impact testing conducted to simulate aircraft velocities and bird sizes used in impact tests of GE's CFM56-3 engine (which is the same thrust class as the UDF™) and to simulate impact conditions corresponding to large bird ingestion at aircraft rotational velocity.

3.1 FAN BLADE BENCH TESTING - RESULTS AND CONCLUSIONS

Strain Survey

Utilizing special blade fixtures, vibratory strain surveys were conducted on one blade per stage. The blades were excited by siren. Unidirectional strain gages (147) were mounted on each blade along the leading and trailing edges, tip chord, and maximum thickness locations (Figure 3) to obtain the strain distribution of each vibrational mode.

Based on the strain survey test and analytical results, four strain gage locations (Figure 4) were selected for the fan blade static HCF and engine

ORIGINAL PAGE IS
OF POOR QUALITY

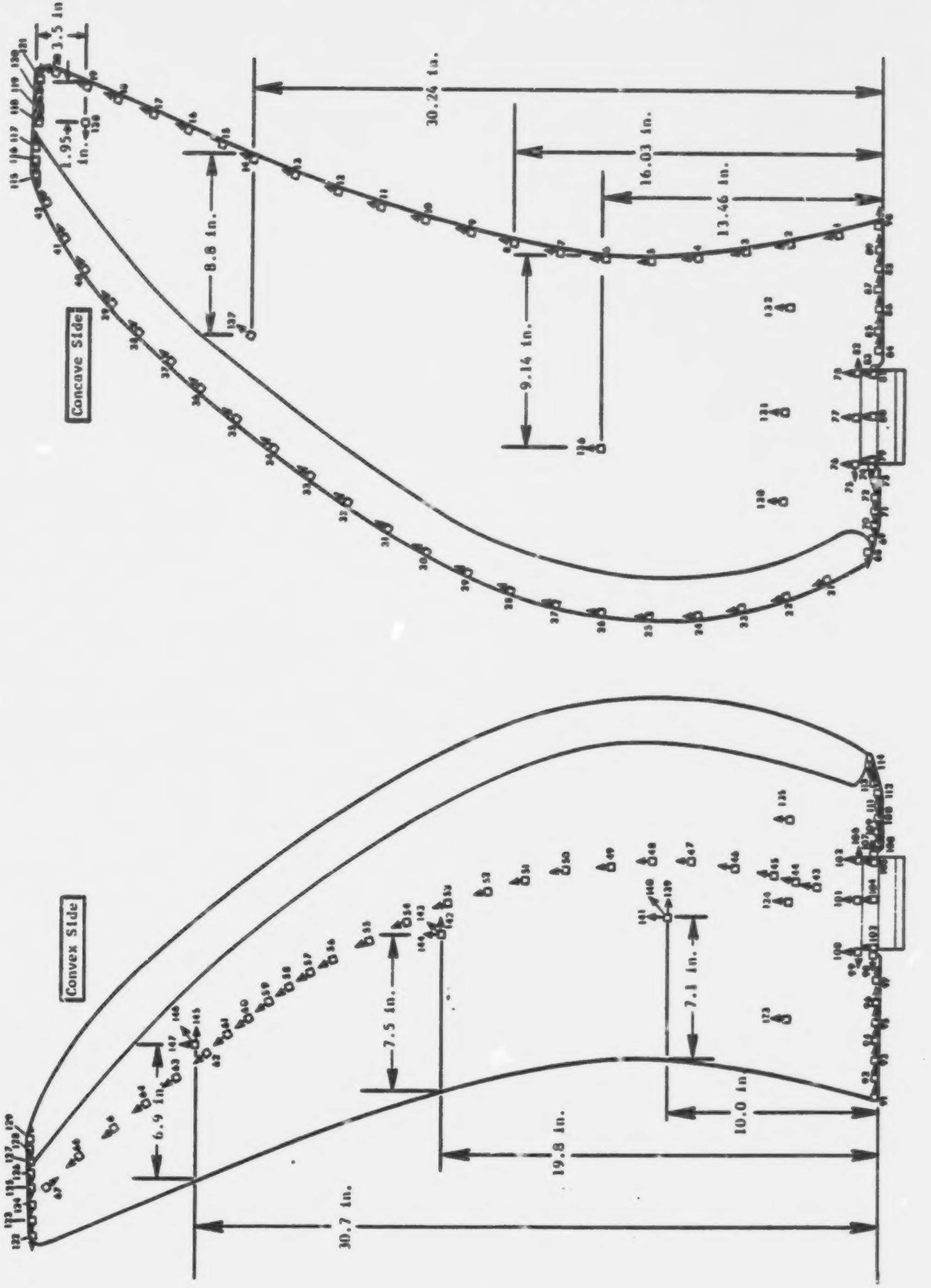
Concave Side
3.5 in.
30.24 in.
16.03 in.
13.46 in.
1.95 in.
8.8 in.
9.14 in.
Convex Side
6.9 in.
7.5 in.
7.1 in.
10.0 in.
19.8 in.
30.7 in.

Figure 3. Strain Survey Gage Distribution.

ORIGINAL PAGE IS
OF POOR QUALITY

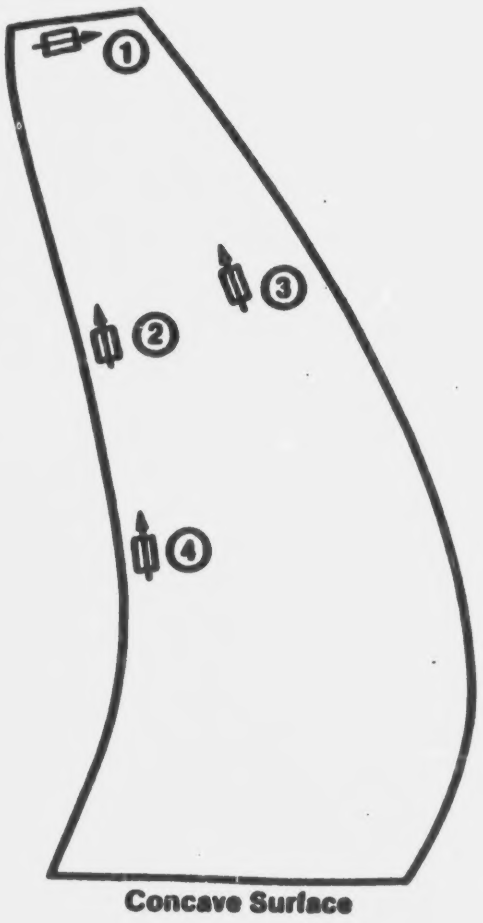

- Total Of 16 Gages Per Stage
  4 Gages/Blade And 4 Blades/Stage

① - Gage - Sensitive To 1 Torsion And High Order Modes

② - Gage - Sensitive To 2 Flex And I/P Forced Response

③ - Gage - Sensitive To Axial Mode And High Order Flex Modes

④ - Gage - Location of Highest SS Stress And 1 Flex Vibratory Stress

Figure 4. Engine Strain Gage Locations.

tests. Of all the gages, No. 4 (located at the highest steady-state stress point) is the most important for the engine test. This gage is very sensitive to the first flex mode, which was the most responsive mode during the engine test. Hence, the No. 4 gage was often named as the reference gage, or simply as the airfoil gage in the component or engine tests.

The data obtained during this testing was used for comparison to a frequency/mode shape analysis. Because the accuracy of the fan blade stability prediction is highly dependent on the accuracy of the frequency/mode shape calculation, it is imperative to validate the calcualtion. The frequency/mode shape comparisons are presented in Table 1 and Figure 5, and show excellent agreement for the first five modes; however, the mode shape agreement for the higher modes is less desirable, although the agreement in frequencies is good. Aeromechanically and aeroelastically, these higher modes are not as important as the lower modes, particularly the first three modes.

Table 1. Frequency Comparison Analysis Versus Bench Test.

Mode	Analytic	Bench Test
1st Flex (1F)	23.5	24
2nd Flex (2F)	73.6	73
1st Torsion (1T)	108.6	106
3rd Flex (3F)	154.0	148
2nd Torsion (2T)	176.0	175
3rd Torsion (3T)	291.0	251
4th Flex (4F)	263.0	261
4th Torsion (4T)	384.0	339
5th Flex (5F)	395.0	363
Two Stripe (2S)	408.0	415

Static HCF Tests

A stair-step HCF test was performed on two Stage 2 fan blades which were excited at the first flex resonance frequency on a shaker table. The reference gage was mounted on each blade for setting the stress level at each test step. Run-out at each step was one million cycles.

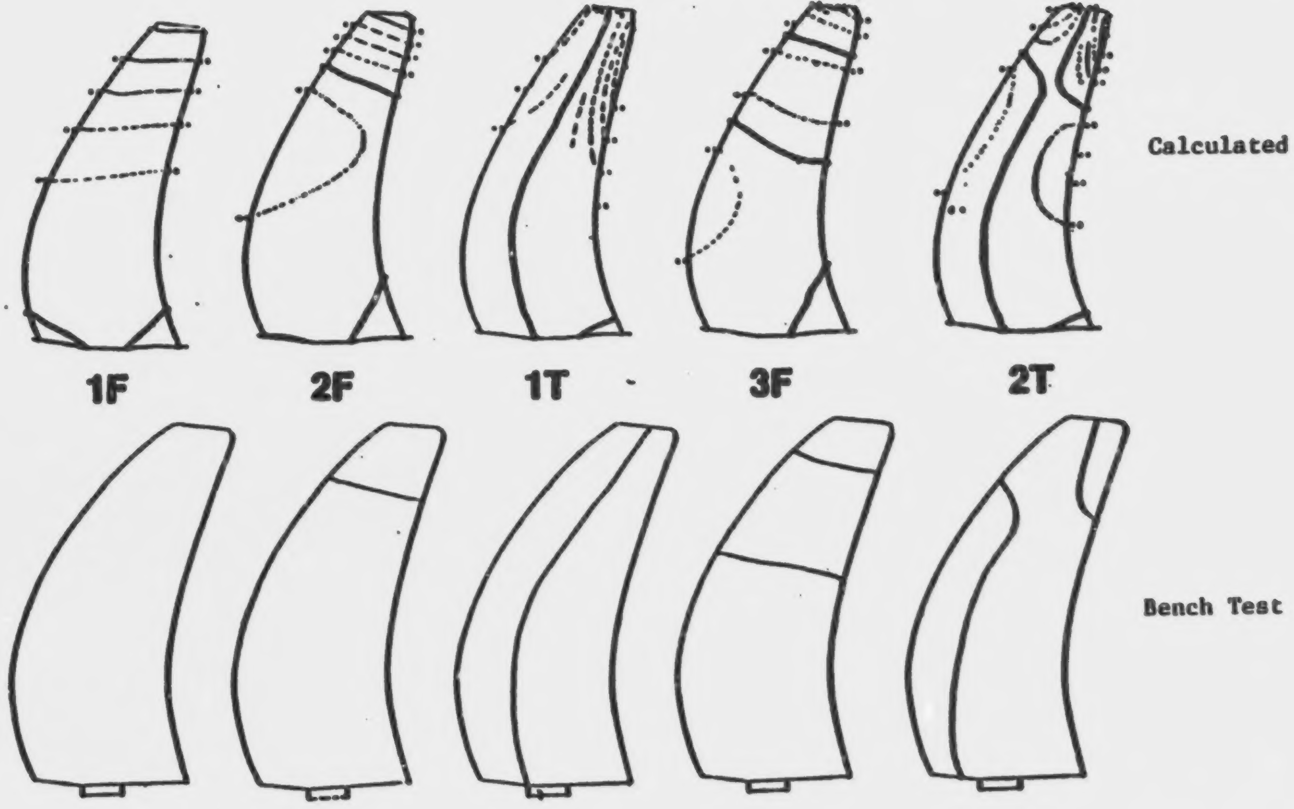
Calculated
1F
2F
1T
3F
2T
Bench Test

Figure 5. F7 Mode Shape Comparison.

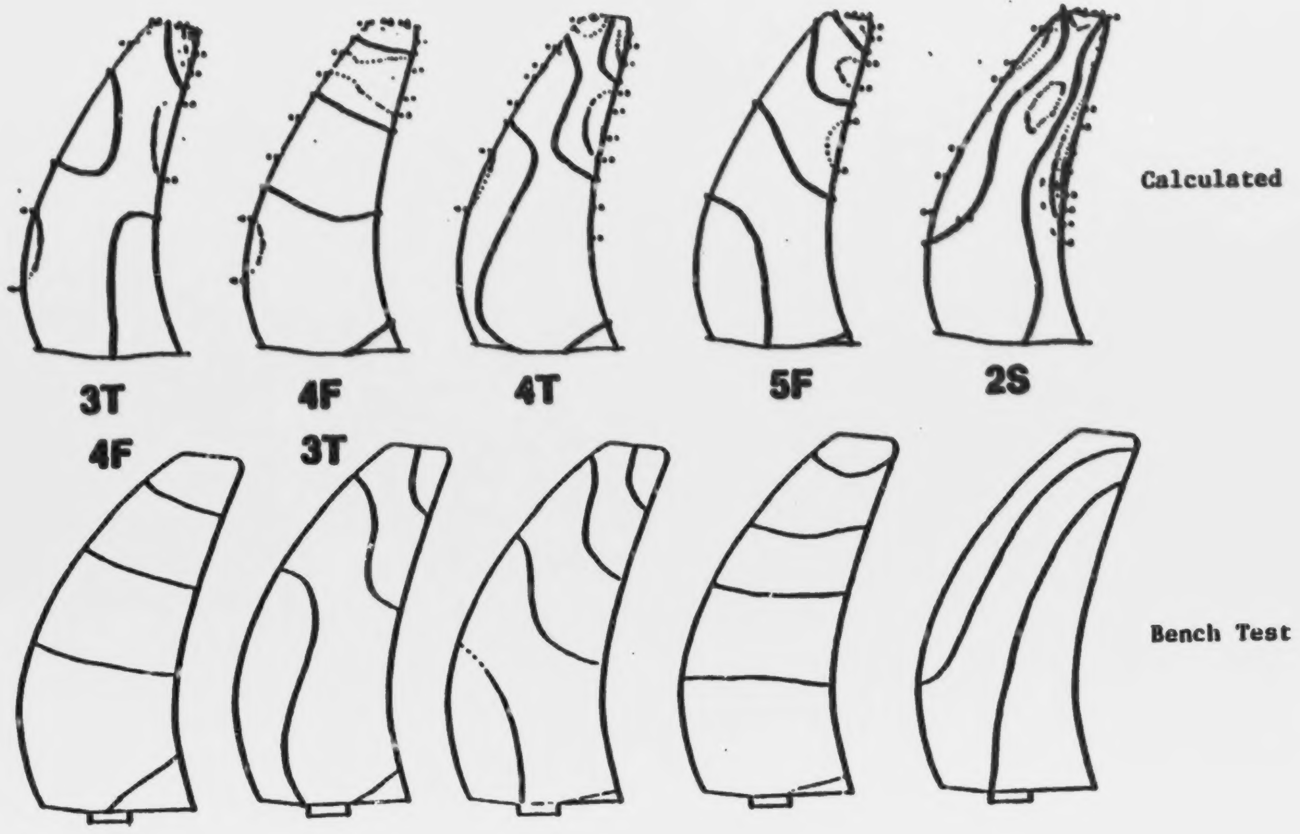
Calculated
3T
4F
4T
5F
2S
4F
3T
Bench Test

Figure 5. F7 Mode Shape Comparison (Continued).

On the first blade, the first set of cycles was run at 17.7 ksi; the next step was to 29.5 ksi (at which the blade failed). A smaller stress increment of about 2.2 ksi was set to test the second blade. This blade was tested from 12 ksi to failure at 25.2 ksi, accumulating a total of 6.3 million cycles.

Both blades failed in the titanium spar along the EB weld bottom line. These failures resulted from shell debonding which initiated at the base of the spar and progressed upward. The shell debonding reached the weld line and beyond, increasing the stress in the EB weld, and resulted in a weld fatigue failure.

It is apparent that stress levels which initiate shell debonding should be considered in defining the fan blade safe operating limits for the engine test.

Static Pull Test

A static pull test was conducted to verify the mechanical integrity of the fan blade and the primary retention mechanism. The test setup is depicted in Figure 6. A maximum pull load of 110,635 pounds was applied. The load pulled was more than 2X the desired capability of the blade and trunnion; however, due to a facility limitation, only about 1.7X the desired capacity was demonstrated on the thrust race and threads.

The strain readings behaved lineraly for the entire pull test; posttest evaluation revealed no distortion or damage.

Static Impact Test

The impact resistance capability of the UDF™ blades was investigated by static impact testing, conducted at the University of Dayton. The testing was performed to simulate aircraft velocities and bird sizes used in impact tests for the recently certified CFM56-3 engine and to simulate impact conditions corresponding to large-bird ingestion at rotation velocity for the UDF™ concept. Table 2 details the impact conditions used in the test program for simulation of bird ingestion. For the bird impacts, cylindrical (L/D = 2.0) simulated birds composed of a gelatin/microballoon mixture were used. A hard body impact test was also performed to simulate ingestion of a section of tire tread. It is noted that only one Stage 1 blade was used for all seven impact tests.

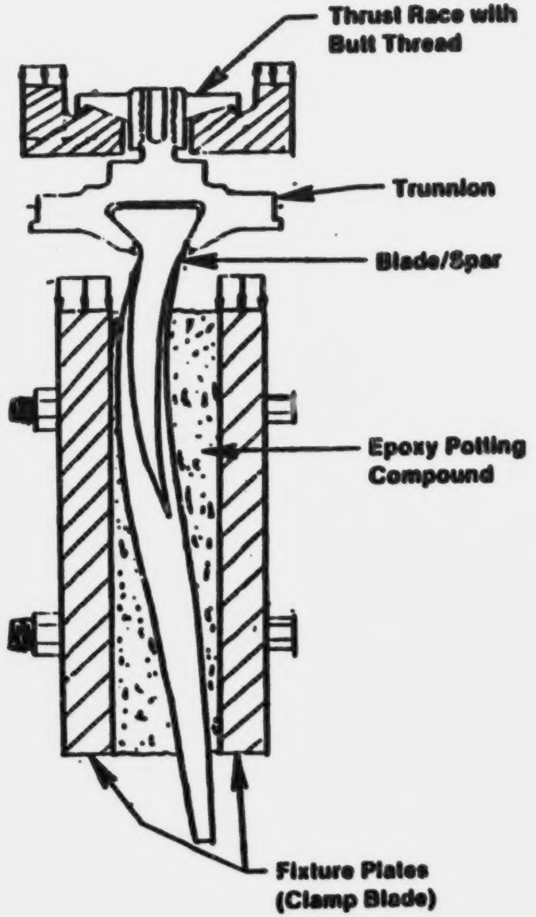
Thrust Race with
Butt Thread
Trunnion
Blade/Spar
Epoxy Potting
Compound
Fixture Plates
(Clamp Blade)

- Static Pull Test To Verify Mechanical Integrity Of Blade And Primary Retention Components
- Maximum Applied Load 110,635 Pounds

- Blade/Spar	2.46 x Takeoff
- Trunnion	2.35 x Takeoff
- Butt Thread	1.78 x Takeoff
- Thrust Race	1.68 x Takeoff

- Post Test Evaluation
  - No Distortion Or Visible Sign Of Damage
  - Strain Rate Linear

Figure 6. Fan Blade Static Pull Test.

Table 2. UDF™ Blade Impact Test Results.

- Stage 1 Blade Tested
- Static Conditions - Blade Fixed
- Rigid Foundation
- Blades Damaged but Capable of Maintaining Power

Shot	% Span	Bird Weight	Effective Weight	Aircraft Velocity	Relative Velocity	Incidence Angle	Normal KE	Test Date
1	60	1.5	1.2	366	756	9.4	396	10/31/85
2	30	1.5	1.5	366	634	10.8	326	11/06/85
3	90	1.5	0.64	366	885	6.8	109	11/08/85
4	60	4.0	1.8	428	788	7.3	287	11/12/85
5	60	1.5	1.5	250	708	14.6	743	11/14/85
6	60	4.0	3.7	250	708	14.6	1813	11/19/85
7	60	---	1.5 (Tire Tread)	250	708	14.6	---	11/21/85

The ballistic impact testing facility is depicted schematically in Figure 7. The blade was set up horizontally on a stand, in the cantilevered mode and positioned to achieve impact at the desired incidence angle to the path of the incoming simulated bird.

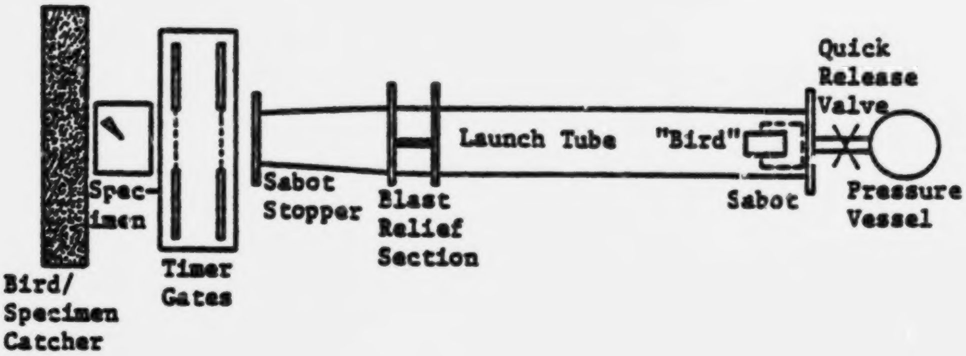
Quick Release Valve
Launch Tube
"Bird"
Spec-imen
Sabot Stopper
Blast Relief Section
Sabot
Pressure Vessel
Bird/ Specimen Catcher
Timer Gates

Figure 7. Schematic of Ballistic Impact Testing Facility.

The aiming point was set at the desired span location so that the edge of the projectile extends slightly beyond the leading edge in the chord direction, as illustrated in Figure 8.

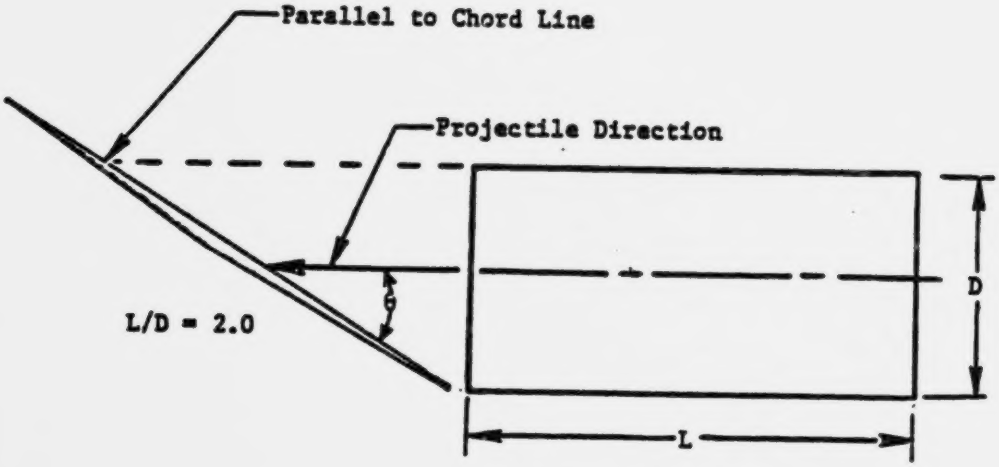
Parallel to Chord Line
Projectile Direction
θ
L/D = 2.0
D
L

Figure 8. Projectile Direction.

These impact tests were designed to simulate a leading edge impact. Bird impact energy on a blade depends on the bird size, incidence angle, and relative velocity to the blade. Figure 9 demonstrates the impact energy spanwise distributions for the Stage 1 blade corresponding to the aircraft velocity during rotation for the GE36 engine. For the 4-pound bird impact, the impact energy peaks at 45% span, although there is not a great deal of difference in the energy levels for span positions less than or equal to 60%. The 60% span location was selected as the impact location, in addition to the 90% location.

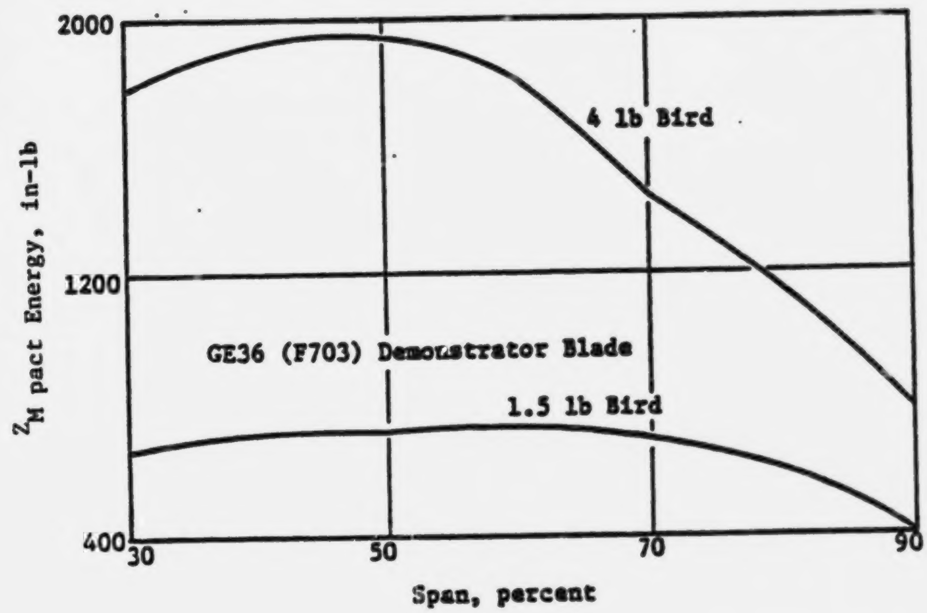

Figure 9. Impact Energy at Takeoff Versus Percent Span.

Impact Damage

As revealed by the high speed movies, the desired impact conditions were basically achieved for all shots, except for Shot 4. In this case, the bird missed the leading edge and initiated contact with the blade at the last 25% of the chord. This was essentially a trailing edge impact.

- Shot 1 - Minor local debonding of leading edge protection at the tip of the blade; the blade was repaired.
- Shot 2 - No damage.

- Shot 3 - Local delamination (splitting) at the blade tip, about 1 inch forward of the trailing edge; blade repair was achieved by re-epoxying the delaminated area.

- Shot 4 - Local polyurethane protection layer separation from the composite near the trailing edge at 70% span.

- Shot 5 - Delamination at the tip trailing edge about 2 inches in and 2 inches down along the trailing edge (Figure 10); repair was made in the delaminated areas.

- Shot 6 - Delamination occurred across the blade tip and down the trailing edge approximately 12 inches from the tip; a small area of the tip trailing edge and the tip leading edge protection was missing. Total mass loss less the one ounce (Figure 11); the blade was repaired.

- Shot 7 - No blade damage was sustained at the impact location; however, the blade tip trailing edge had several large cracks through the thickness. No pieces were completely severed, but the internal delamination appears to have propagated beyond the previously damaged area. The leading edge strip also debonded approximately 6 inches down from the tip (Figure 12).

Less damage may have been sustained in Shot 6 if the test had been conducted on a new blade. Delamination had already initiated in the tip-trailing area from Shots 3 and 5, which propagated during Shot 6.

Impact testing was concluded with Shot 7. For this shot, a hard-bodied impactor, consisting of a section of tire tread 5-inches wide by 12-inches long by 3/4-inch thick and weighing approximately 1.5 pounds, was used with impact conditions of a 14.6° incidence angle and a relative velocity of 708 feet per second. Upon impact, the tread was sliced its entire length.

In its final condition, the blade retention capability remained intact, and it is assumed that the engine would still be able to produce at least 90% of its original thrust.

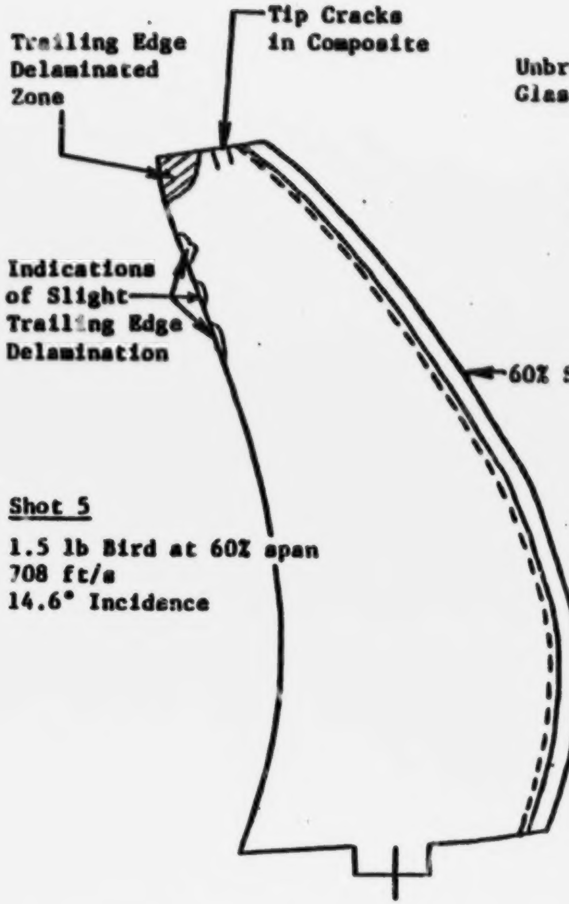
Trailing Edge Delaminated Zone
Tip Cracks in Composite
Indications of Slight Trailing Edge Delamination
60% Span
Shot 5
1.5 lb Bird at 60% span
708 ft/s
14.6° Incidence

Figure 10. Damage Assessment for Shot No. 5.

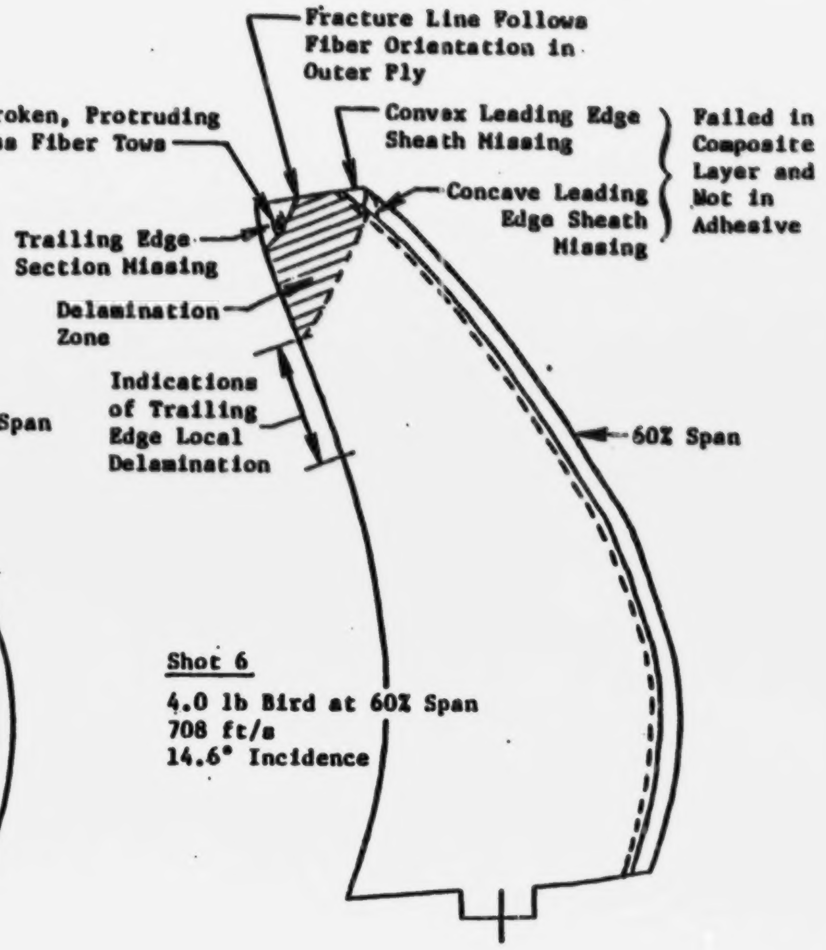
Fracture Line Follows Fiber Orientation in Outer Ply
Unbroken, Protruding Glass Fiber Tows
Convex Leading Edge Sheath Missing
Concave Leading Edge Sheath Missing
Failed in Composite Layer and Not in Adhesive
Trailing Edge Section Missing
Delamination Zone
Indications of Trailing Edge Local Delamination
60% Span
Shot 6
4.0 lb Bird at 60% Span
708 ft/s
14.6° Incidence

Figure 11. Damage Assessment for Shot No. 6.

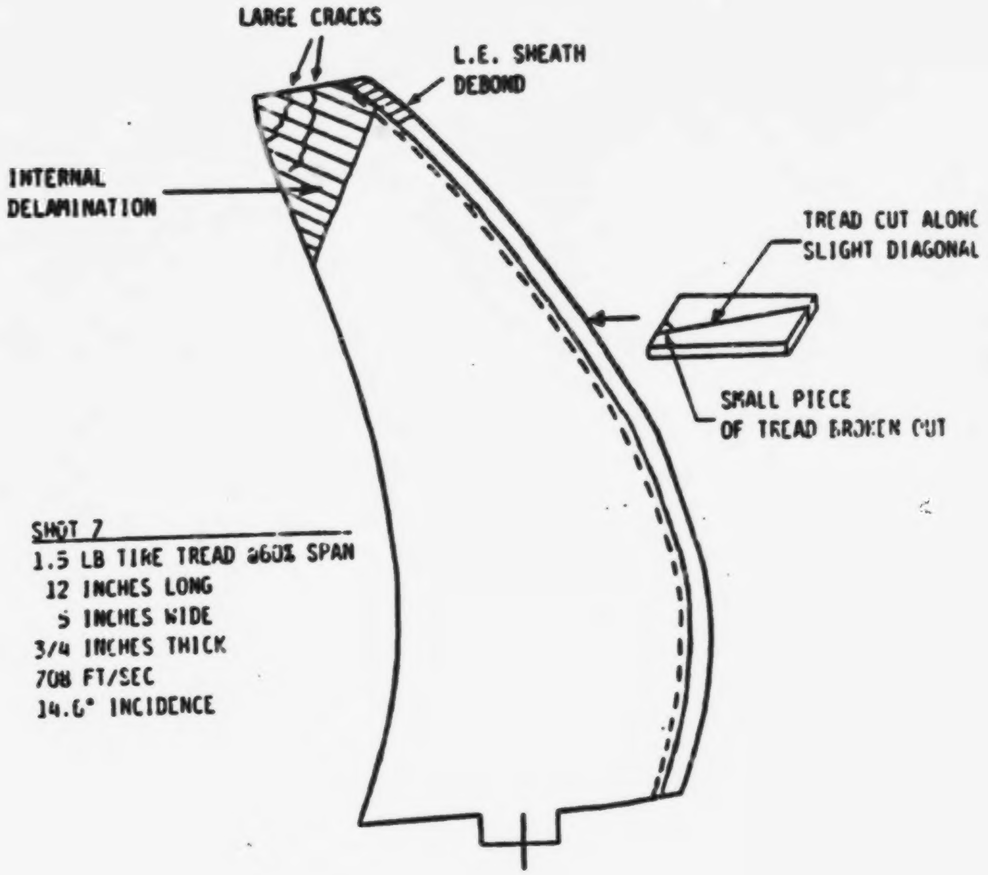
LARGE CRACKS
L.E. SHEATH DEBOND
INTERNAL DELAMINATION
TREAD CUT ALONG SLIGHT DIAGONAL
SMALL PIECE OF TREAD BROKEN OUT
SHOT 7
1.5 LB TIRE TREAD @60% SPAN
12 INCHES LONG
5 INCHES WIDE
3/4 INCHES THICK
708 FT/SEC
14.0° INCIDENCE

Figure 12. Damage Assessment for Shot 7.

4.0 COMPONENT VERIFICATION TESTING

4.1 TURBINE BLADE DYNAMIC ANALYSIS CORRELATION TEST

Introduction

Dynamic analysis and frequency tuning of the turbine blades was recognized early as a major detail design effort. Selection of a nonconventional method of manufacture (sheet metal fabrication) created some uncertainty about the ability of conventional dynamic analysis techniques applied to this job. Up front correlation between analysis and component test was utilized to verify the accuracy of the analytic techniques used for detail design of the blades.

Overview

Two concerns existed relative to using 3D finite element dynamic analysis with eight-noded brick elements for the detail design of the turbine blading. Conventional blade designs generally have platforms that produce stiffnesses significantly greater than that of the airfoil alone, while the UDF™ blading utilizes sheet metal fabricated platforms whose stiffness plays a major role in resonant frequency and mode shape. Additionally, the UDF™ utilizes corrugated sheet metal inserts brazed inside the hollow airfoils to control panel modes. Two tests were conducted to evaluate the capability of the analytical techniques to simulate the sheet metal platform and internal stiffness effects on frequency and mode shape:

1. Existing J79 Stage 7 compressor vanes utilize a solid airfoil brazed and welded to a sheet metal fabricated platform similar to the UDF™ turbine blade design. These were bench frequency checked as an airfoil alone (bronzed in a block) and as an assembly (clamped at the dovetail rails). Results were compared to analytical predictions using analysis and modeling techniques planned for the UDF™ blading.

2. Hollow sheet metal airfoil specimens of the UDF™ Stage 8 blade, both with and without an internal stiffener, were bench frequency checked (airfoil alone brazed in a block). Results were compared to analytical predictions using analysis and modeling techniques planned for the UDF™ blading.

Test Results and Conclusions

The J79 compressor vane test results correlated within 8% or less of analysis for the first four nodes in both the airfoil alone and vane assembly configurations. This is within the analytical correlation error for conventional designs and is considered substantiation for the UDF™ modeling and analysis techniques used to simulate the fabricated platforms. Additionally, the vane assembly frequency was divided by the airfoil-alone frequency to obtain a base effect ratio for both test and analysis results. The analysis ratio agreed within 15% of the test ratio. This result provides adequate substantiation for using simplified airfoil-alone models during the preliminary design and frequency tuning phase of development as seen in Figure 13.

Stage 8 airfoil specimen test results showed good correlation with analysis (less than 10% error) for all modes except first flex (1F) and two stripe (2S) (error was less than 14% for these modes), as seen in Figure 14. Better definition of material modulus of elasticity and modeling refinements in the leading and trailing edge and stiffness regions improved the 1F correlation to less than 2% but did not help 2S, as seen in Figure 15. Because the original analysis showed much better 2S correlation without the internal stiffer than with (Figure 13), it was concluded that the modeling technique resulted in too high stiffness for the 2S mode, and a correlation factor based on the test results should be applied to all 2S predictions, as seen in Figure 16.

4.2 TURBINE BLADE FREQUENCY AND STRAIN DISTRIBUTION TEST

Introduction

Frequency bench testing of representative samples from all 10 stages of turbine blading was conducted prior to engine assembly to confirm analytical predictions and to identify potential resonant modes that would be excited in the operating range of the engine. Strain distributions were determined for each stage to establish scope limits for the modes of interest.

Overview

Modes were identified by "ping" testing one blade from each stage using Hewlett-Packard Spectral Analysis equipment which allowed animated

- Correlate Base Effect on Fundamental Modes
- Test J79 Stage 7 Compressor Vane
  - Airfoil Brazed in Block
  - Vane Assembly Fixed at D/T Rails
  - Model/Analyze Like Power Turbine Blades

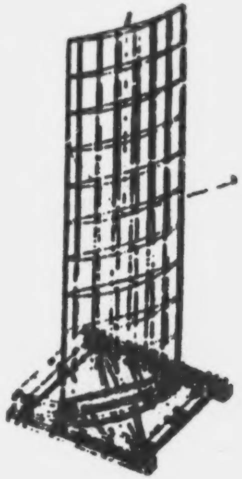

	Airfoil	Assembly	Base Effect
Test Results (Average of 5)	431	395	.916
	1959	1696	.866
	2167	1813	.837
	2712	2226	.836
Analytical Prediction	426	399	.937
	1970	1820	.924
	1995	1919	.962
	2871	2204	.768
Percent Error	-1.2	+1.0	+2.2
	+0.6	+7.3	+6.7
	-7.9	+5.8	+14.9
	+5.9	-2.7	-8.1

Figure 13. Blade Dynamic Analysis Correlation Test, Base Effect on Fundamental Modes.

- Correlate Stiffener Effect on Panel Modes
- Test Actual Stage 8 Airfoil Specimens
  - With and Without Stiffener
  - Brazed in Block

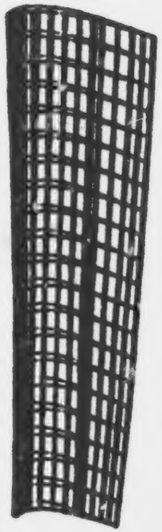

		Airfoil Only		Airfoil With Stiffener		
Mode	Test	Prediction	% Error	Test	Prediction	% Error
1 - 1F	234	258	+10.3	232	263	+13.4
2 - 1AX	584	558	- 4.5	624	640	+ 2.6
3 - 1T	830	871	+ 4.9	904	957	+ 5.9
4 - 2F	1082	1055	- 2.5	1330	1446	+ 8.7
5 - 2T	1330	1334	+ .3	2252	2312	+ 2.7
6	1592	1736	+ 9.0	2688	2746	+ 2.2
7 - 2S	1860	1808	- 2.8	2722	3157	+13.9
8	1980	2042	+ 3.1	3234	3466	+ 7.2
9 - 2AX	2632	2595	- 1.4	3710	3796	+ 2.3
10	2968	2677	- 9.8	4150	4392	+ 5.8

Figure 14. Blade Dynamic Analysis Correlation Test, Stiffener Effect on Panel Modes.

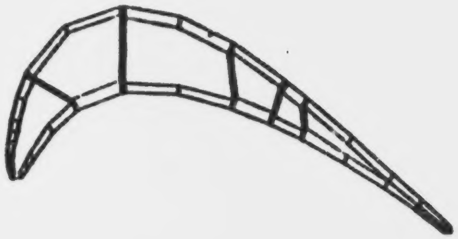

- Changes Based on Analysis Correlation Test
  - Refined Leading Edge Geometry
  - 4 Element Stiffener Ribs
  - Increased Wall Thickness at Rib Attachment
  - Corrected Elastic Modulus

		Initial Correlation		Final Correlation	
Mode	Test Results	Analytical Results	% Δ Rel to Test	Analytical Results	% Δ Rel To Test
(1) 1 FLX	232	263	+13.4	243	+ 4.7
(2) 1 AX	624	640	+ 2.6	618	- 1.0
(3) 1 TOR	904	957	+ 5.9	902	- .2
(4) 2 FLX	1330	1446	+ 8.7	1380	+ 3.8
(5) 2 TOR	2252	2312	+ 2.7	2230	- 1.0
(6)	2688	2746	+ 2.2	2668	- .7
(7) 2-STR	2772	3157	+13.9	3140	+13.3
(8)	3234	3466	+ 7.2	3390	+ 4.8
(9) 2 AX	3710	3796	+ 2.3	3695	- .4
(10)	4150	4392	+ 5.8	4284	+ 3.2

Figure 15. Turbine Blade Dynamic Analysis, Modeling Improvements.

- **Results of Test Correlation**
  - Base Effects Accurately Predicted
  - Airfoil Modes Accurately Predicted Except 2S
  - 2S Mode Predicts High Because of Bend Radius

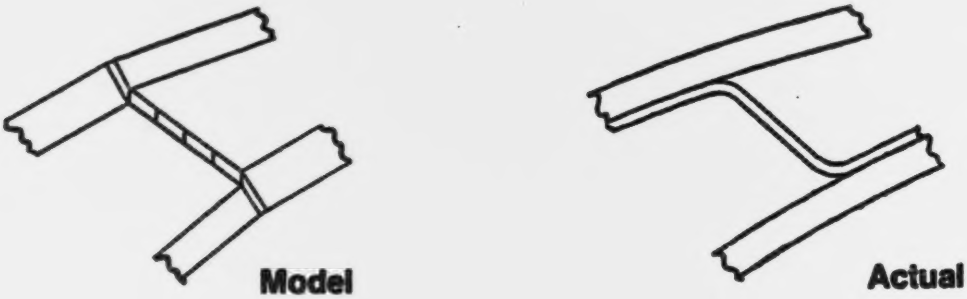
Model

Actual

- **Conclusions**
  - Apply .883 Factor to Predicted 2S Frequency
  - Use Other Frequencies as Calculated
  - ±15% Margin to Significant Excitations

Figure 16. Turbine Blade Dynamic Analysis, Model Assessment.

visualization of the modes. Samples of each stage ranging from 12 to 53 were then tested using electromagnetic excitation to establish frequency scatter for the individual modes. Frequency results for each stage were corrected for speed and temperature effects and potential engine resonances were identified. One blade from each stage was instrumented, including the engine gage location, to determine response of the engine gage as a percent of the maximum vibratory stress location for each mode so that allowable engine gage response could be determined.

Test Results and Conclusions

Typical "ping" test spectral analysis frequency results (Stage 9 blades) are summarized and compared to analytical predictions in Figure 17. Modes were identified from these data by animated graphic playback of each of the resonant frequency seals.

Electromagnetic excitation of representative samples of all stages yielded an assessment of scatter. The data were reduced as ±3 standard deviation limits and compared to analytical predictions. Results are summarized in Figures 18 through 20. In general, average test results correlated well with predictions except for the 2S mode, where frequencies were higher than expected. Scatter was within the ±15% design margin.

Results for Stage 8 (Figure 20) reflect the final design after incorporation of a design modification to address the 2S mode correlation. Preliminary test results from other stages indicated Stage 8 would have an unacceptable 2S resonance with the upstream Stage 7 blade passing frequency. Three specimens were obtained for test to assess capability to modify the design to move the frequency lower and avoid resonance. A design modification based on bench test results was incorporated in the engine hardware, as seen in Figures 21 through 23.

Test results for the six modes of interest were corrected to engine conditions to determine potential resonances. Five potential resonances were identified in the operating range affecting Stages 1, 2, 3, and 10. These modes were believed to have either relatively weak excitations or high damping but were identified as the primary responses to monitor during engine test, as seen in Figure 24.

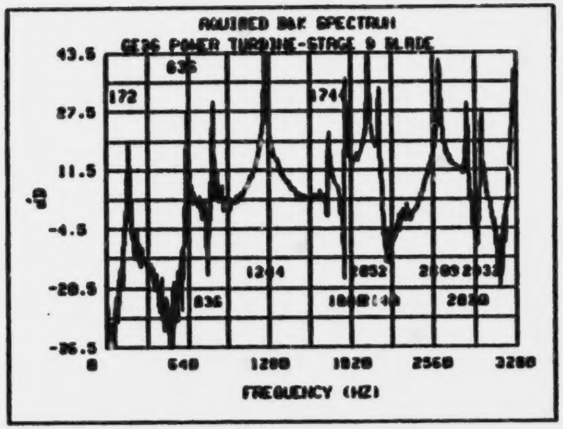

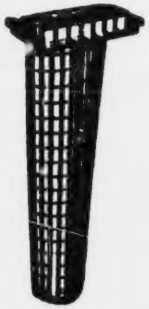

- System Checked Out — Stages 9 and 11 Pilot Parts
- Correlation Obtained for Stage 9

Test	Analysis	% Error
172	187	+8.7
636	651	+2.4
836	889	+6.3
1244	1280	+2.9
1744	1907	+9.3
1880	1917	+2.0
2052	2122	+3.4
2140	2279	+6.5
2608	2714	+4.1
2820	2968	+5.2

Figure 17. Turbine Blade Frequency Test, Status.

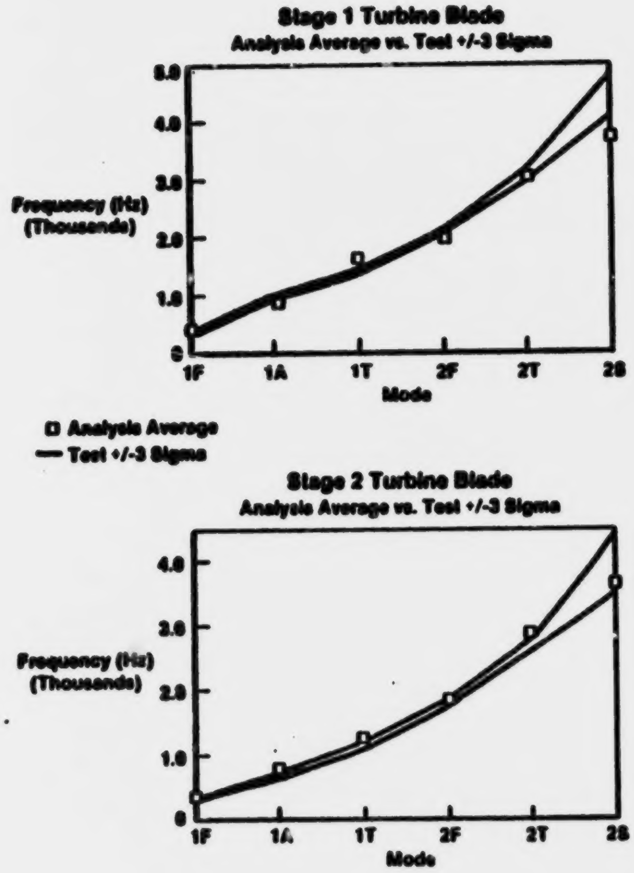

- **Results Shown at Take-Off Speed and Temperature**
- **Excellent Correlation Except 2S Mode**
  - **Test Higher Than Analysis**
  - **Stages 1 and 3 Resonant with Downstream Excitation**
  - **CF6 LPT and Booster Data Indicates Low Response Amplitude**
- **All Stages Instrumented**

Figure 18. Turbine Blade Frequency Results Summary.

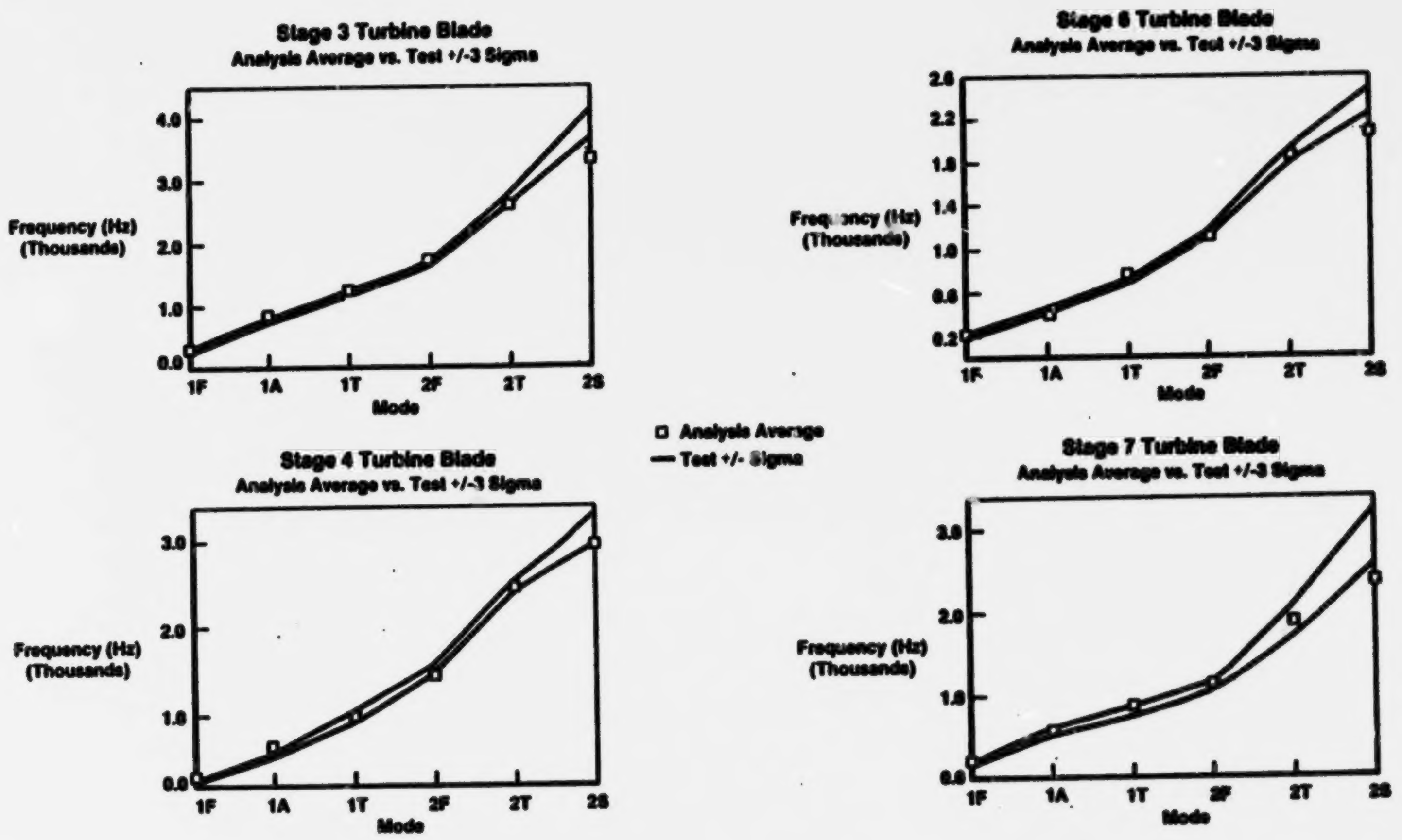

Figure 19. Turbine Blade Frequency Results, Stages 3, 4, 6, and 7.

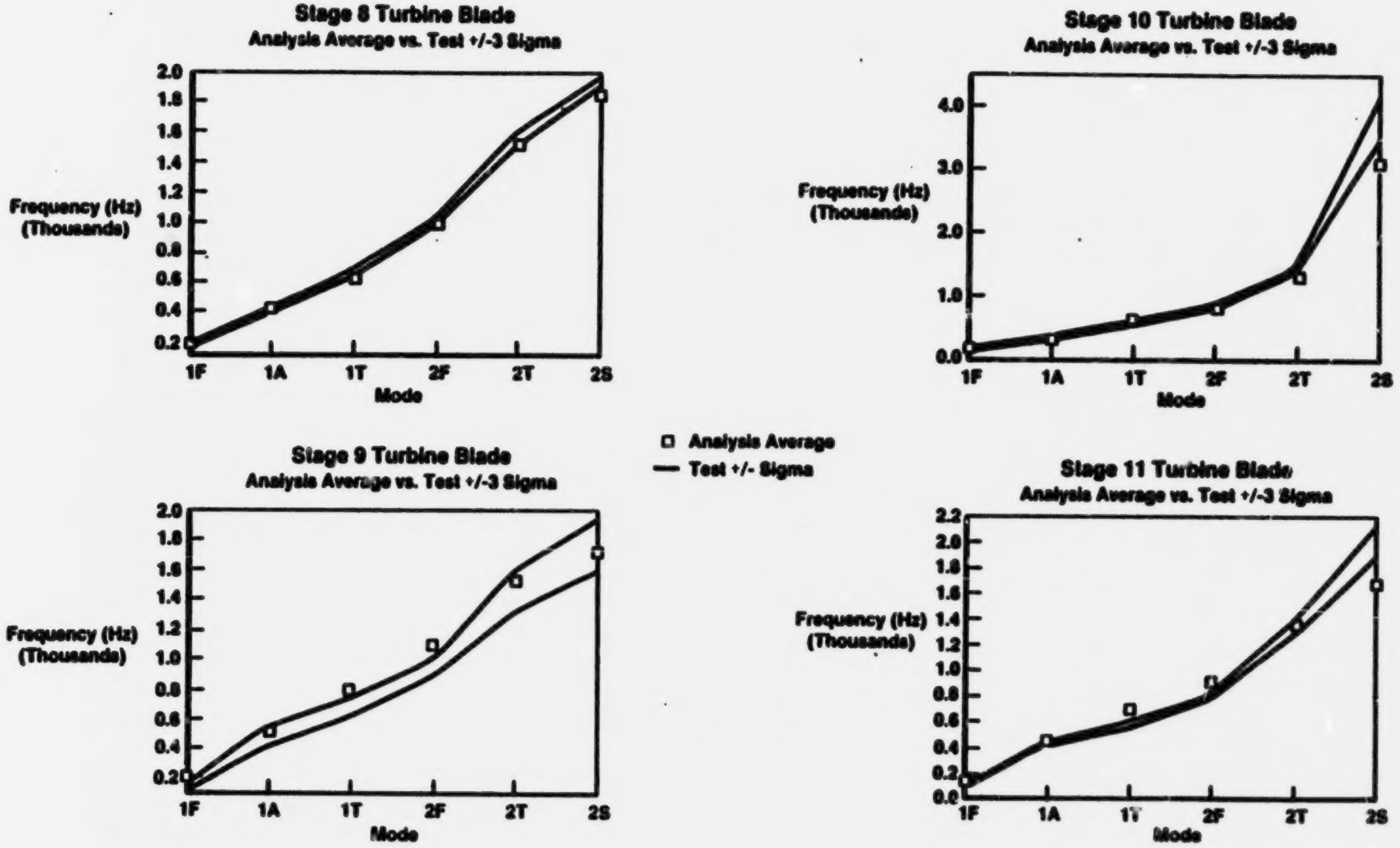
Stage 8 Turbine Blade
Analysis Average vs. Test +/-3 Sigma

Stage 10 Turbine Blade
Analysis Average vs. Test +/-3 Sigma

Stage 9 Turbine Blade
Analysis Average vs. Test +/-3 Sigma

Stage 11 Turbine Blade
Analysis Average vs. Test +/-3 Sigma

Figure 20. Turbine Blade Frequency Results, Stages 8 through 10.

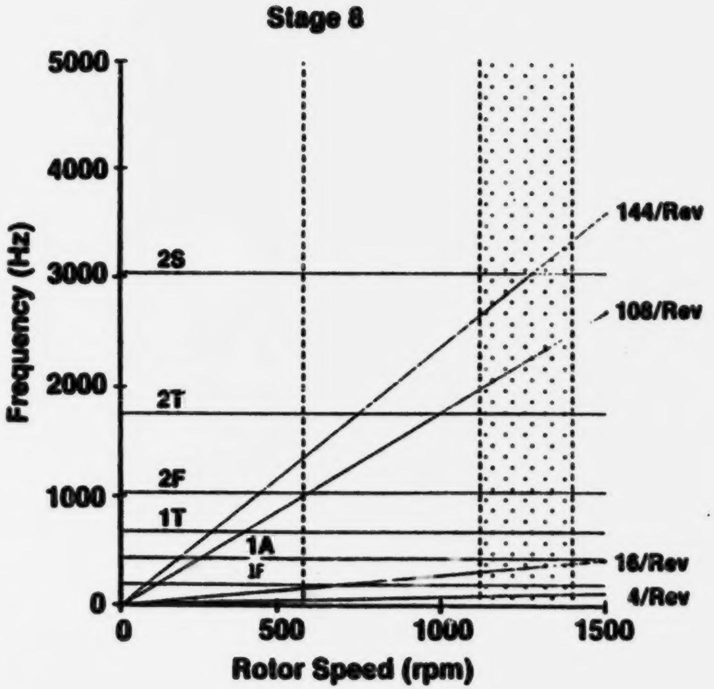

- **Problem**
  - 2-Stripe Resonance in Operating Band
  - Unable to Increase Frequency to Avoid
  - Hardware Ready to Manufacture

- **Approach**
  - Bench Test 3 Specimens
    - Original Design
    - Delete Transverse Ribs
    - Delete Transverse Ribs and Stiffener (Hollow)
  - Correlate Analysis
  - Revise Design and Confirm by Test

Figure 21. Stage 8 Design Modification.

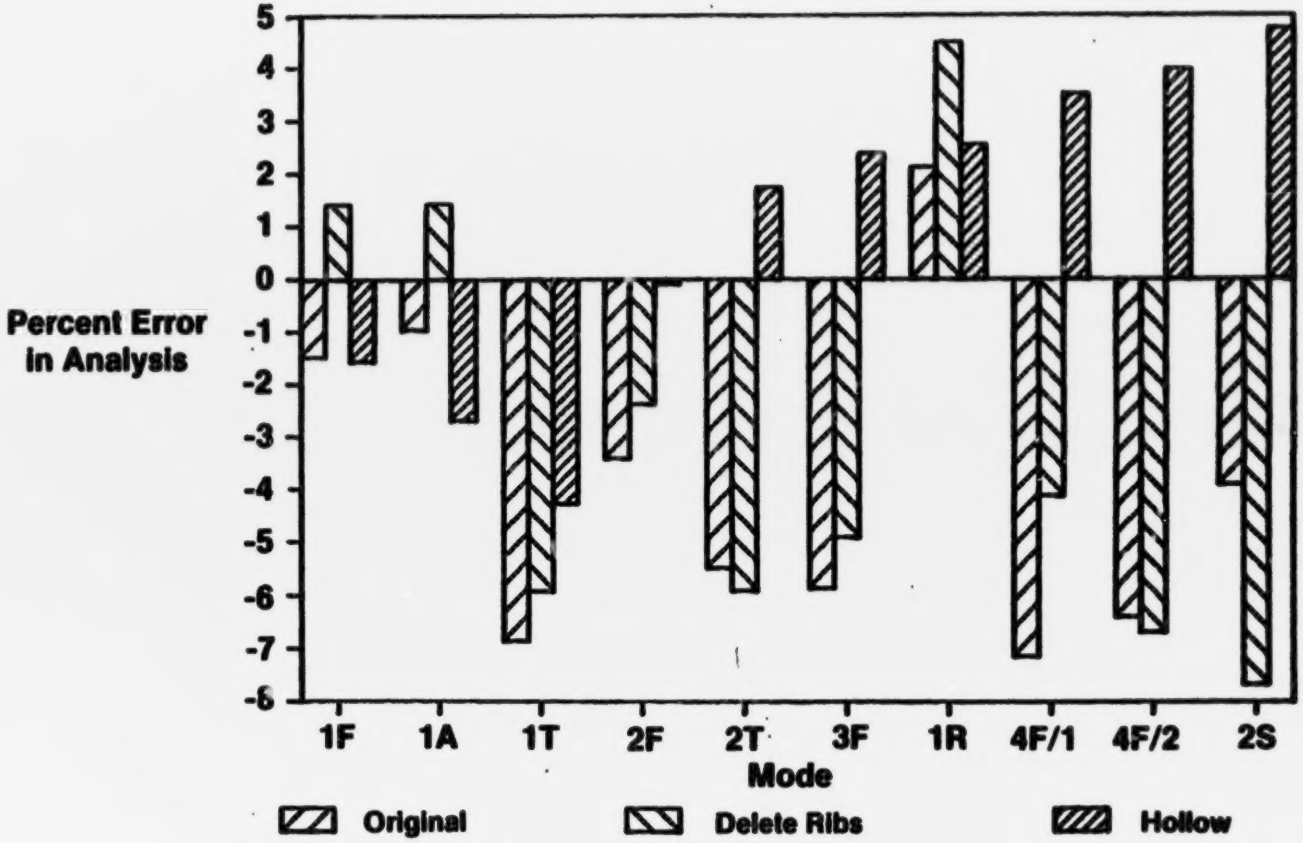

Figure 22. Stage 8 Blade Test Results, Analysis Versus Test.

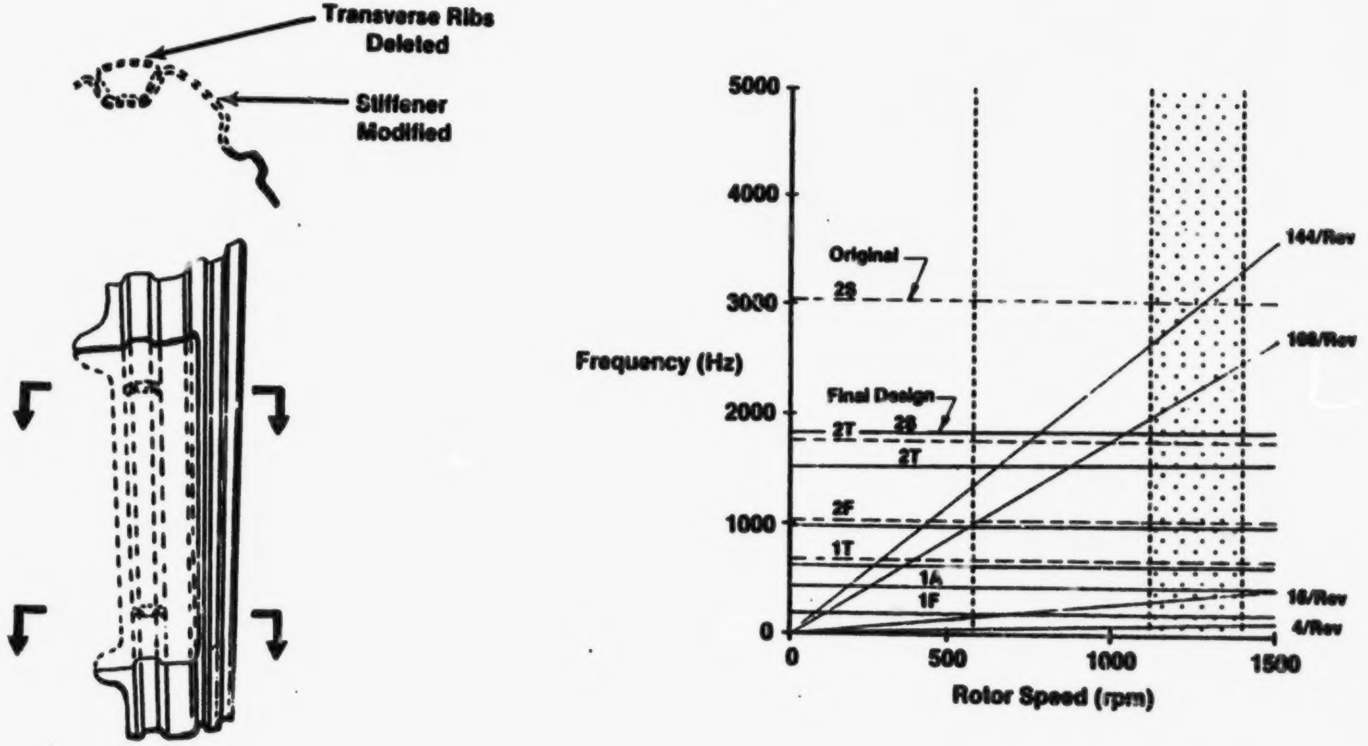

Figure 23. Final Stage 8 Blade Design.

- All 10 Stages Shown
- Average Bench Test Corrected for Speed and Temperature
- 4/Rev, 16/Rev, 60/Rev, Upstream and Downstream Crossing

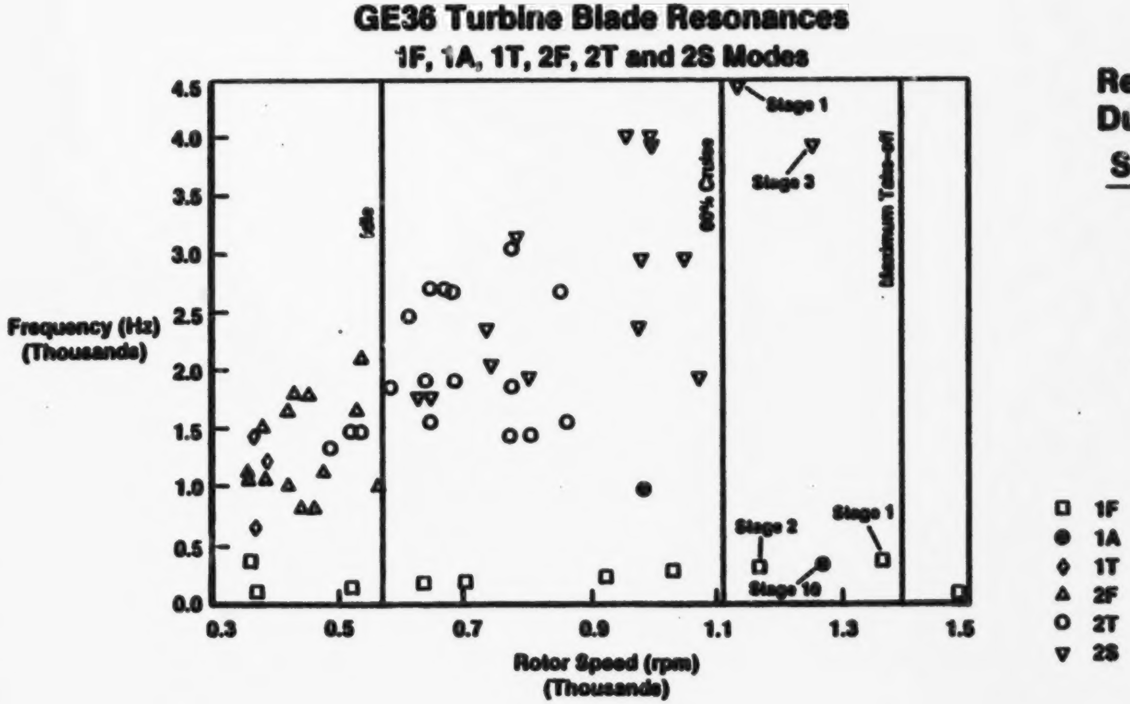

Responses to Watch During Test:

Stage	Mode
1	1F, 2S
2	1F
3	2S
10	1A

Figure 24. Turbine Blade, Frequency Results.

Strain distribution testing was conducted to help locate the position of the strain gage that will be used during engine test and experimentally determine response factors for the six modes of interest; Figures 25 and 26 show typical results (Stage 9). These data were used to establish scope limits for engine test monitoring.

4.3 TURBINE SPOOL FREQUENCY TEST

Introduction

Component frequency "ping" tests were conducted to correlate analytical predictions of turbine rotor spool modal diameter frequencies.

Overview

Testing was initially conducted by bolting spools or spool assemblies to steel fixtures which simulated the power frame attachment point. Testing was conducted using Hewlett-Packard Spectral Analysis equipment which allowed animated visualization of the modes. Testing showed poor correlation for low order modes because of the significant participation of the fixtures. Good correlation was obtained for all modes without the fixtures (free-free), but the frequencies were unrepresentative of the engine frequencies without the stiffness provided by the foundation of the power frame fixtures.

Testing was repeated on the actual rotor assemblies during rotor stack prior to final buildup. Correlation could be achieved by proper selection of boundary conditions.

Test Results and Conclusions

Typical test results with and without the steel fixture are shown in Figures 27 and 28 for the forward outer spool assembly. Note the improved correlation without the fixture and significant shift in frequencies.

The testing was repeated during rotor assembly (unbladed spools). Poor initial correlation was obtained for all modes. Correlation could be obtained by modeling the rabbeted flange joints as soft springs. This was attributed to the relatively light loading of the rabbets under static room temperature conditions.

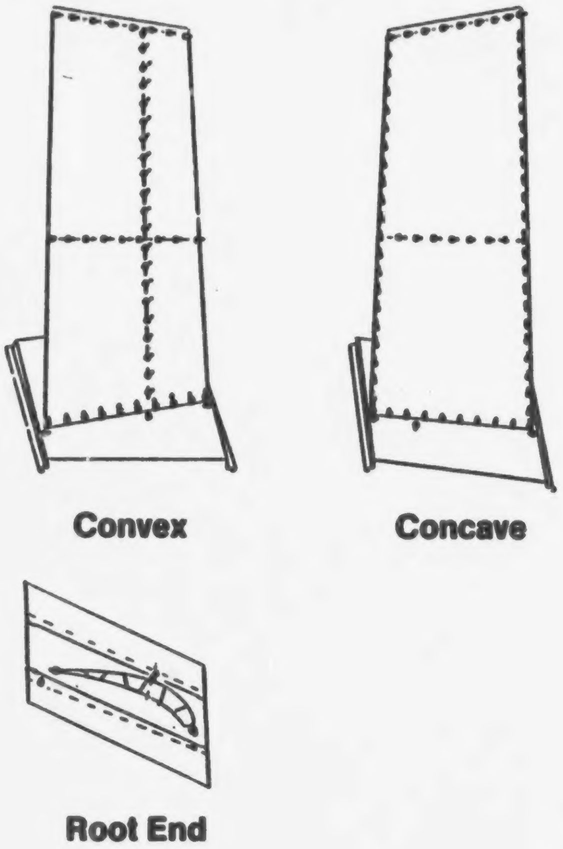
Convex
Concave
Root End

- Determine Peak Response Location vs. Mode
- Select Location for Engine Gages
- Determine % Response at Engine Gage vs. Mode

Figure 25. Stage 9 Blade Instrumented Frequency Test.

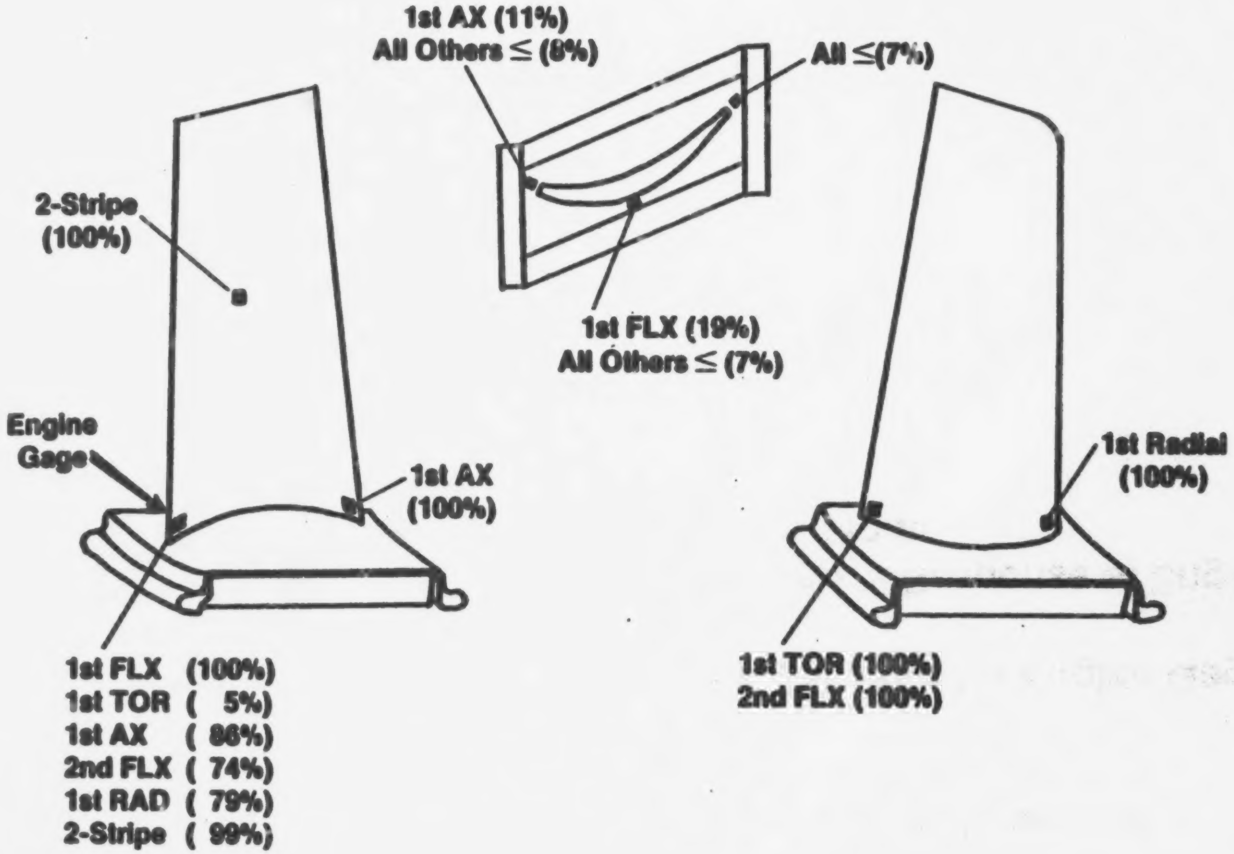
1st AX (11%)
All Others ≤ (8%)
All ≤(7%)
2-Stripe
(100%)
1st FLX (19%)
All Others ≤ (7%)
Engine
Gage
1st AX
(100%)
1st Radial
(100%)
1st FLX (100%)
1st TOR (5%)
1st AX (86%)
2nd FLX (74%)
1st RAD (79%)
2-Stripe (99%)
1st TOR (100%)
2nd FLX (100%)

Figure 26. Stage 9 Blade Instrumented Frequency Test Results.

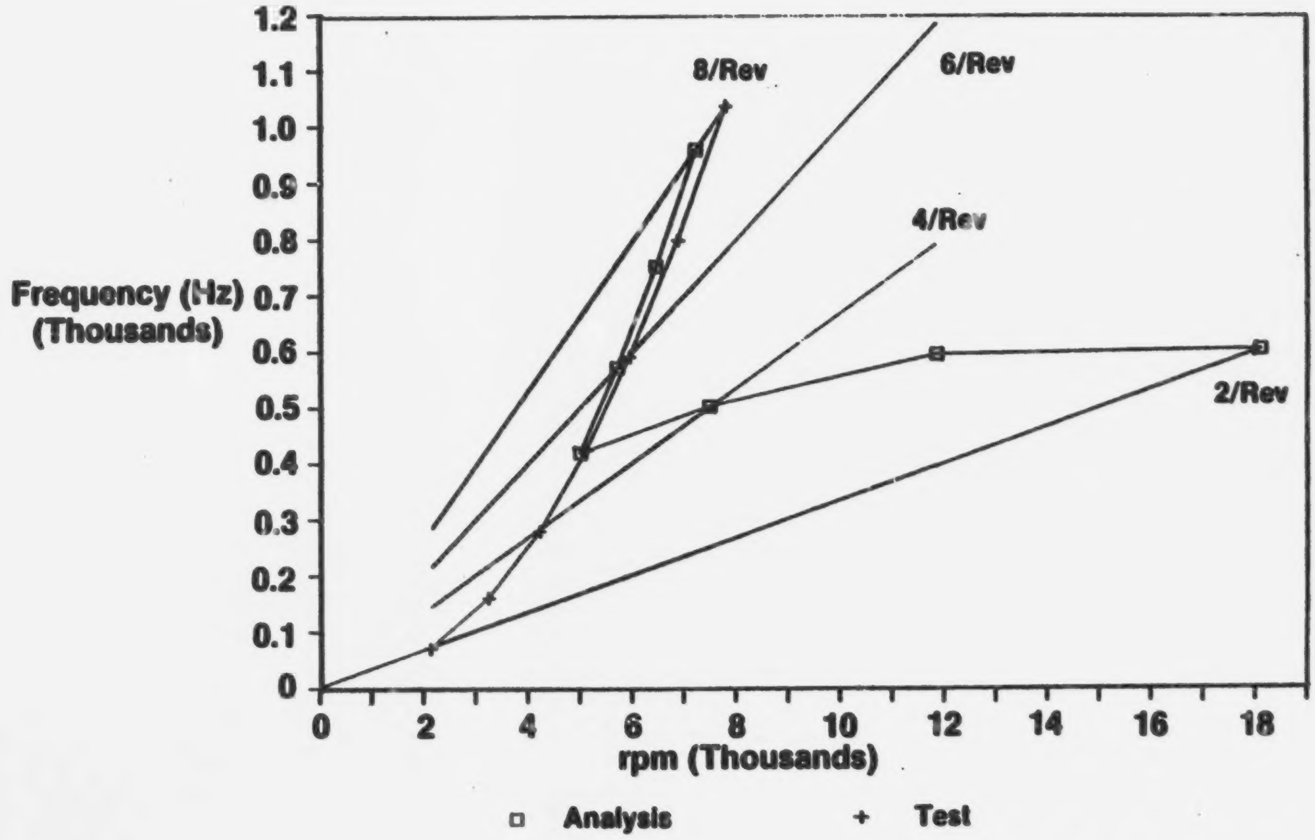

Figure 27. Forward Outer Spool Frequency Test Results, Tested with Fixture.

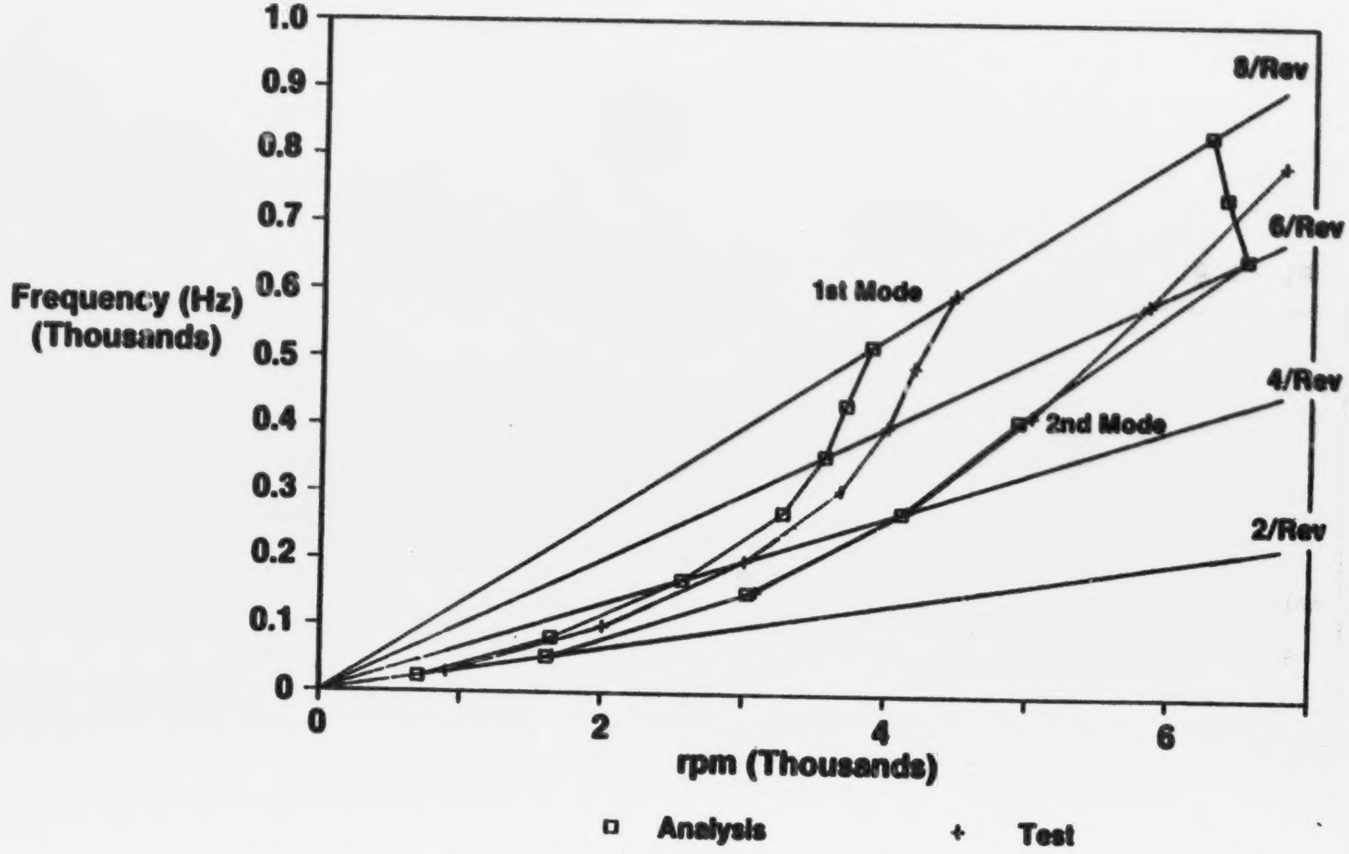

Figure 28. Forward Outer Spool Frequency Test Results, Tested Unrestrained.

A different analytical solution technique, subspace iteration, was applied and correlation was achieved with the original test results. Analytical predictions for engine operation with this technique were insignificantly affected. The final conclusion was that the analytical technique accurately predicted shell frequencies given proper boundary conditions and that predicted frequencies at engine operating conditions were accurate, as seen in Table 3.

Table 3. Spool Frequency Test Results.

Individual Spools on Fixtures

Good Correlation N = 4 and up

Analysis Boundary Condition Sensitive N = 2 and 3

Rotor System Test

Poor Initial Correlation

Insensitive to Power Frame Spring Constants

Correlated Frequency but not Mode Shape by Modeling Flanges with Springs

Reanalyzed Individual Spools on Fixtures

Subspace Iteration/No Boundary Conditions

Correlated all Modes

Conclusions

Rotor Dynamic Analysis Sensitive to Modeling

Original Analyses Representative

4.4 SEAL MATERIAL RUB TEST

Introduction

Initial design trade studies indicated a performance advantage for the use of a solid seal rub material instead of conventional open cell honeycomb in the static forward flowpath seal. Solid rubber was selected, but no information was available to validate its performance when fuel soaked or at the low rub speeds of its intended use. Component tests were conducted to validate these characteristics. Rubber proved to be unsuitable. Teflon was validated as an acceptable solid material but conventional honeycomb was ultimately selected.

Overview

Samples of the selected rubber were soaked in fuel and found to experience unacceptable volumetric swelling which could result in a severe rub. Planned low speed rub testing was discontinued and the test program was restructured around validating the bond strength of solid Teflon. While Teflon was found suitable for use in this seal, conventional open cell honeycomb was ultimately selected for other mechanical design related reasons.

Test Results and Conclusions

The degree of swelling of the rubber material during fuel soak made it totally unacceptable for this application since fuel exposure was possible. As a result, planned low speed rub testing was cancelled. A literature and experience search of other possible solid rub materials indicated Teflon was suitable, but the bond strength of Teflon to the A286 stainless steel seal was unknown.

Testing was restructured around evaluation of the Teflon bond strength. Specimen tensile and shear tests were conducted and properties validated as adequate for this application. However, the size of the seal and steep cone angle at the bond joint would require some process development to incorporate Teflon into the design.

Detail design development continued with the intention of utilizing Teflon, as seen in Figure 29. A dynamics evaluation of the rotating and stationary seal members revealed an unacceptable resonant interaction margin for the three-nodal diameter mode. Studies indicated little help for changing the rotating seal frequency, because there were already two distinct modes: seal only and seal-spool combined modes. Lowering the static seal frequency moved the three-nodal diameter interaction outside the operating range but caused other nodal diameter interactions. Because of the seal configuration, adding stiffness was not practical. However, Teflon material weight was 9 pounds

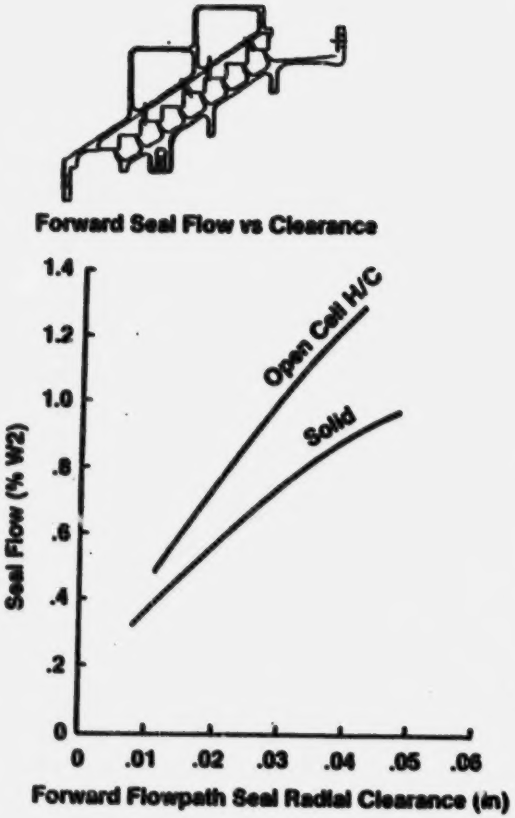

- **Background**
  - Solid Seal Provides Performance Advantage
    - Less Leakage Than Open Cell Honeycomb
    - Performance Derivative (1% W2 = 0.5% SFC)
  - Solid Rubber Selected
    - Within Experience Except Fuel Soak, Low Rub Speed
    - Less Heat Input During Rub
- **Test Results**
  - Unacceptable Swelling of Rubber During Fuel Soak
  - Test Restructured Around Teflon
  - Teflon Bond Strength at Temperature Validated
- **Conclusions**
  - Rubber Unacceptable
  - Teflon Technically Acceptable, Requires Manufacturing Process Development
  - Pursue Teflon, Keep Honeycomb Back-up

Figure 29. Forward Seal Rub Material Test.

greater than conventional open-cell honeycomb, and the substitution of honeycomb material significantly improved the dynamic margin of the seal, as seen in Table 4. Honeycomb rub material was selected for the final design because it offered the best compromise between dynamics, weight, and leakage. An additional penalty of +0.13 lb/sec leakage flow at takeoff (+0.65% sfc) was the predicted result relative to the use of a solid rub material.

Table 4. Forward Flowpath Seal - Resonant Interaction Margin.

Nodal Diameter	Teflon Static Seal		Honeycomb Static Seal	
	Fwd Wave, %	Bwd Wave, %	Fwd Wave, %	Bwd Wave, %
2	18	11	18	11
3	2	28	11	38
4	13	72	29	94
5	21	115	33	130
6	19	118	26	117
8	5	77	10	72
16	30	Interaction	31	6
ΔWeight	+9 lb		-9 lb	
ΔLeakage (@ T/O)	0		+ 0.13 lb/sec	

4.5 MIXER FRAME FLOW TESTS

Introduction

A major concern of the UDF™ engine, in terms of both cooling and aerodynamic design, was the mixer frame performance. As the fan bypass air exits the duct diffuser, it must turn 90° downward to enter the mixer frame struts. If the flow separates off the leading edge (LE), locally low film hole and impingement hole supply pressures could significantly lower cooling effectiveness and possibly result in hot gas inflow. Similarly, the sudden bend in the mixer frame flowpath could cause the core flow to separate off the frame outer band, resulting in a loss of engine performance.

Overview

In order to study mixer frame flow behavior, flow tests were performed, using full-scale plastic models. Pressure measurements were taken and visual studies were performed by placing tufts in the regions of concern. Overall, there was good agreement between test results and analysis. Problem areas were pinpointed and the design was modified accordingly.

Mixer Frame Internal Flow Test Results and Conclusions

This test was performed to study the possibility of flow separation within the mixer frame strut. The major concern was that fan bypass flow might separate off the strut LE, resulting in locally low static pressures and possibly hot gas inflow. A plastic model was constructed of 54° segments of the mixer frame consisting of three struts and the bypass duct diffuser. The model is shown in Figure 30.

Since all strut measurements were taken from the center strut, only that strut contained film holes. A comparison between the test strut and real strut is shown in Figure 31. The real strut hole pattern is duplicated in the LE region since flow separation is most likely to occur there. Because flowpath pressure distribution that will exist in the engine could not be duplicated in the flow test, much of the model film hole pattern was altered to simulate a pressure distribution.

In addition to the strut film holes, other exit holes were drilled in the plastic frame to attain the same flow split as in the real frame. Each hole was calibrated individually to determine flow rates as a function of pressure ratio.

Engine conditions were simulated in the flow test by matching flow functions. Since film hole exit pressure is ambient, the supply pressure in the bypass duct is established by matching the frame pressure ratio. If the bypass duct flow function is matched to engine conditions, the total flow rate is established.

To simulate the effect of service tube blockage, an oval pipe, duplicating the tube shape, was inserted in the strut during portions of the test. Pressure measurements were taken along the diffuser and at all film holes. A

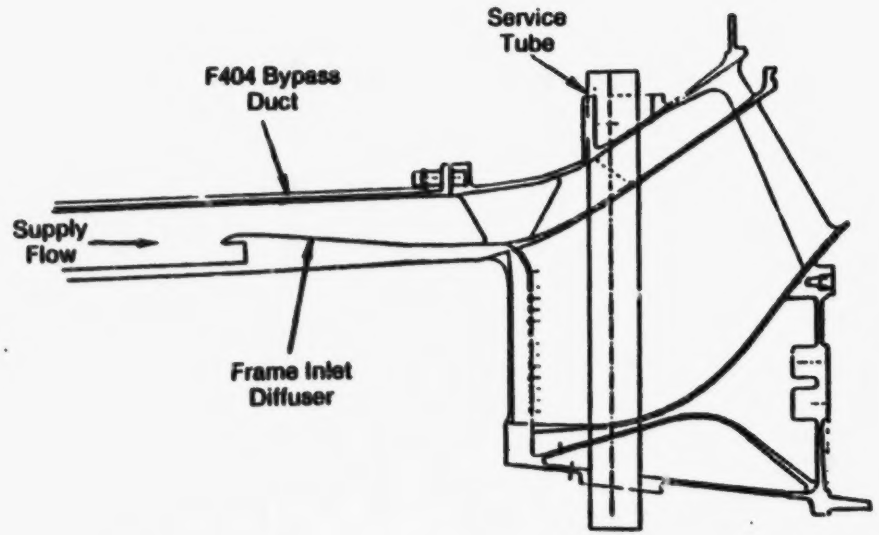
Service
Tube
F404 Bypass
Duct
Supply
Flow
Frame Inlet
Diffuser

- 3 Strut Frame Model
  - Center Strut Has Adjusted Hole Pattern
- Bypass Duct and Diffuser Model of Internal Passages
- Service Tube Blockage
- Engine Conditions Simulated by Matching Flow Functions
- Full Range of Flow Conditions Tested

Figure 30. Internal Flow Test.

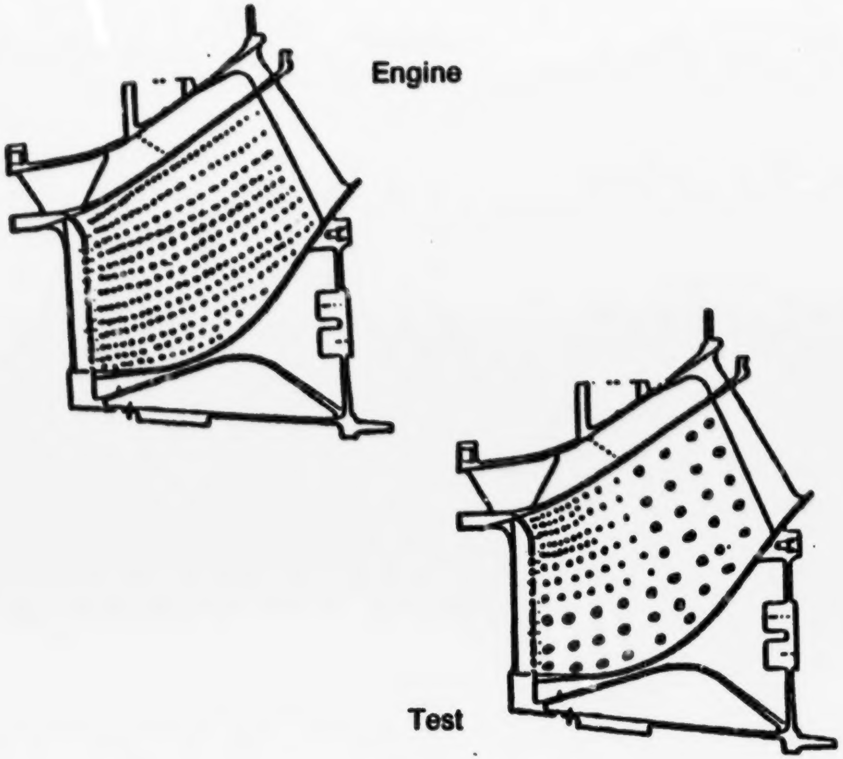

- Engine
  - Gas Side Pressure Level and Distribution
  - Heat Flux
- Test
  - Uniform (Ambient) Gas Side Pressure
  - No Heat Flux
  - Revised Hole Pattern

Figure 31. Internal Flow Test, Test Hole Pattern Adjusted for Simulation of Internal Flow/Mach Number.

visual flow study was conducted using a wand with tufts. By placing the wand inside the strut the flow pattern could be studied.

When testing without the service tube blockage, recirculation occurred within the strut. The total film hole flow and the internal pressure distribution was near predicted. However, in several holes which were near the center of the recirculation zone the pressure readings indicated zero flow. A comparison of predicted and measured pressures is shown in Figure 32.

When testing with the service tube blockage, no recirculation occurred. Again the flow and pressure distribution were near predicted. The service tube blockage did result in a higher velocity around the LE turn and low static pressures in that region. However, there were no indications of zero flow. A comparison of predicted and measured pressures is shown in Figure 33.

As a result of the flow test, service tubes will be placed in all 20 struts to prevent recirculation and possible gas ingestion. In addition, the outer leading edge impingement hole was moved inward and away from the region of low static pressure.

Mixer Frame Flowpath Flow Test Results and Conclusions

This flow test was performed to determine if flow separation will occur along with mixer frame outer flowpath. The test setup is shown in Figure 34. The model consists of two struts, a segment of the bypass duct, and a segment of the gas flowpath annulus. There are two separate supply flows to simulate both the fan bypass flow and the core flow. Turning vanes upstream of the frame simulate F404 exit swirl. The frame flow exits to ambient pressure. The bypass and core supply pressures are varied to cover the full range of flow conditions.

Wall static pressure measurements were taken along the bypass duct and the frame outer wall. A rake at the frame exit measures total pressure and can be rotated circumferentially. A wedge probe is used to measure swirl angle. A tuft is placed in the flowpath to visually study the flow pattern.

There was no evidence of flow separation within the entire range of flow conditions tested. The outer flowpath static pressures were near predicted.

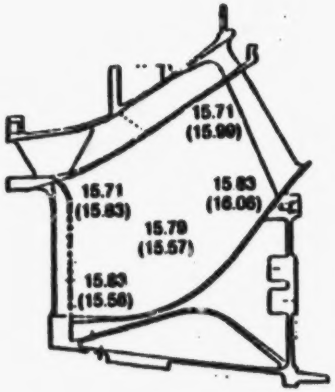
15.71
(15.99)
15.71
(15.83)
15.83
(16.06)
15.79
(15.57)
15.83
(15.58)

Test
- Predicted
- (Measured)

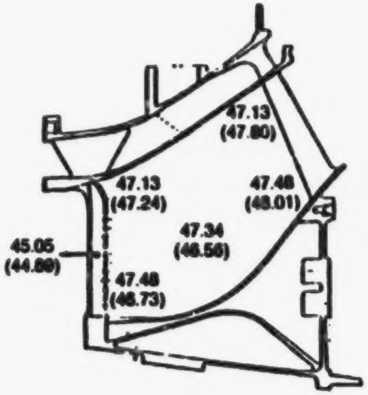
47.13
(47.80)
47.13
(47.24)
47.48
(48.01)
47.34
(46.56)
45.06
(44.89)
47.48
(46.73)

Engine
- Predicted
- (Measured)

- Measured Test Pressures Converted to Engine Operating Conditions
- Low Pressures Measured at Center of Recirculation

Figure 32. Flow Test Results, No Service Tube Blockage.

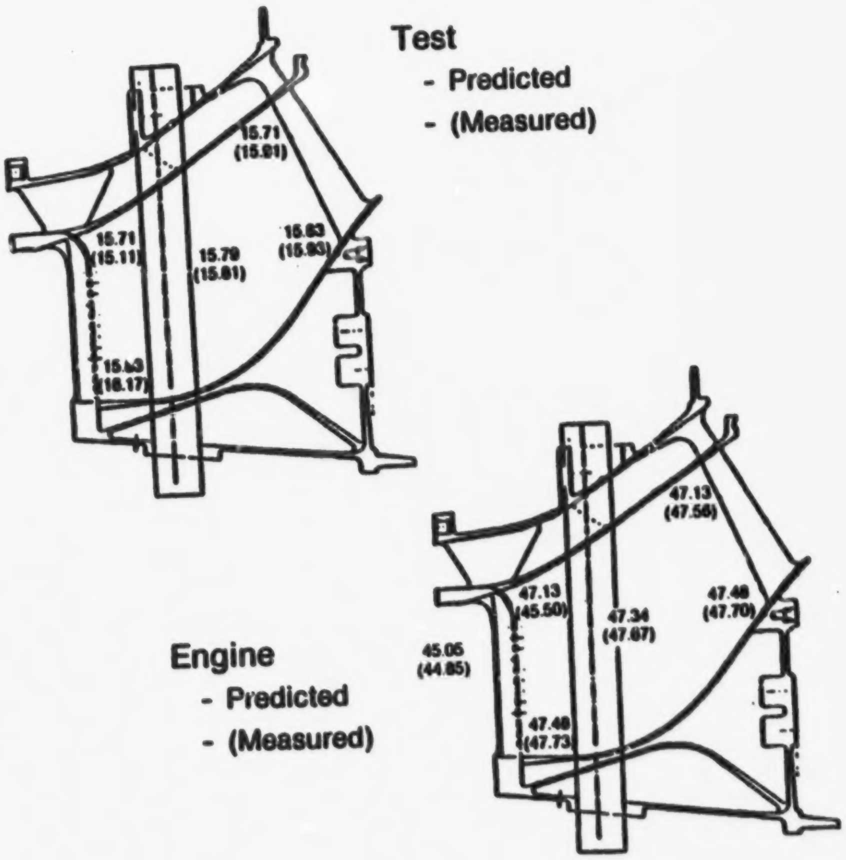

Test
- Predicted
- (Measured)
15.71
(15.91)
15.71
(15.11)
15.79
(15.81)
15.83
(15.93)
15.83
(16.17)
Engine
- Predicted
- (Measured)
47.13
(47.56)
47.13
(45.50)
47.34
(47.67)
47.48
(47.70)
45.06
(44.85)
47.48
(47.73)

- Measured Test Pressures Converted to Engine Operating Conditions
- High Mach Number Turn Causes Lower Than Predicted Pressure at Leading Edge Tip
- Move Outer Leading Edge Impingement Hole

Figure 33. Flow Test Results with Service Tube Blockage.

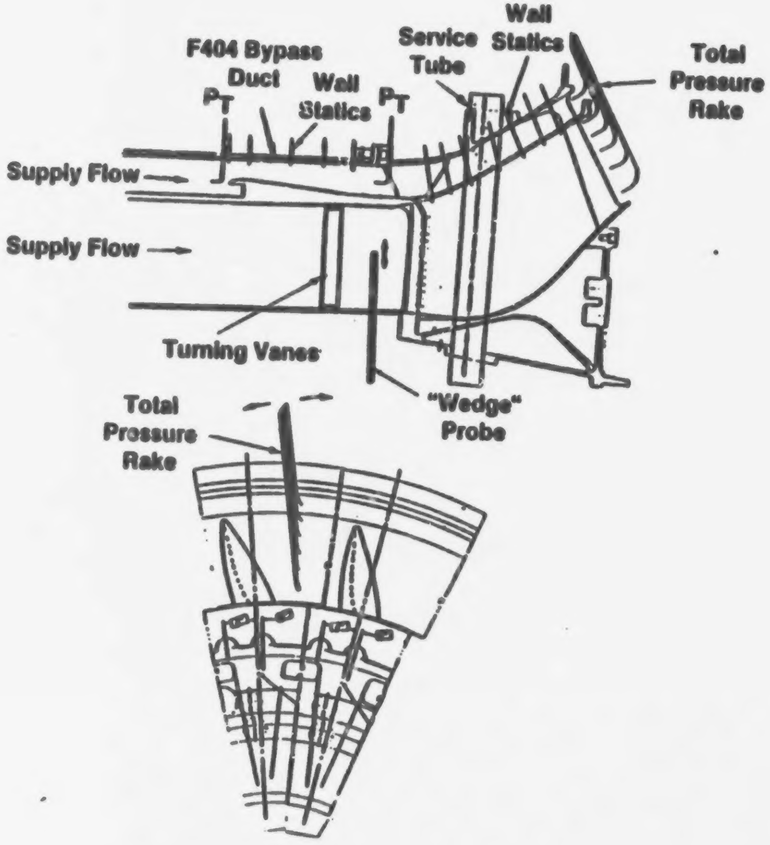
F404 Bypass Duct
P_T
Wall Statics
P_T
Service Tube
Wall Statics
Total Pressure Rake
Supply Flow
Supply Flow
Turning Vanes
"Wedge" Probe
Total Pressure Rake

- **Bypass Duct**
  - Total Pressure
  - Wall Statics
- **Frame**
  - Strut Cooling Air Total Pressure
  - Outer Flowpath Wall Statics
  - Exit Total Pressure Rake
    - 6 Elements
    - Can Be Rotated Circumferentially
  - "Wedge" Probe
    - To Measure Swirl
  - Tuft

Figure 34. External Flow Test, Instrumentation.

5.0 CONTROL SYSTEM DEVELOPMENT TESTING AND EVALUATION

Introduction

This program was conducted in order to demonstrate the functional characteristics of the GE36 demonstrator engine control system prior to its use on an engine.

Overview

A component test of the GE36 fan pitch actuation system, duct bleed system, fuel system, LPVG actuation and electronic control were conducted prior to engine installation and ground testing.

The test parts were set up in Cell 13, Building 500 at the Evendale, Ohio plant. The various test parts were set up as shown in Figure 35 and were used to check out the following:

- Functional test of the fan pitch actuation system
- Functional test of the fuel system
- Functional test of the control computer in wet bench environment
    - Pitch position control
    - Fuel flow override
    - Fuel powered duct bleed, IP compressor stator controls
- Transient response evaluation (Step changes into position loops)
- Functional test of Electronic Control Unit (ECU)
- Functional test of Electrical Interface Unit (EIU).

Power to the control computer, overspeed unit, and peripheral computer, is 120vac, 60 Hz, and was supplied from the test cell. Prior to power-up a continuity test was conducted on all electrical circuity. All system fault warnings were checked by forcing sensor values out of the acceptable tolerance range. These warnings are visible on the PCS' (Peripheral Computer Systems) CRT screen which was located in the control room.

ORIGINAL PAGE IS
OF POOR QUALITY

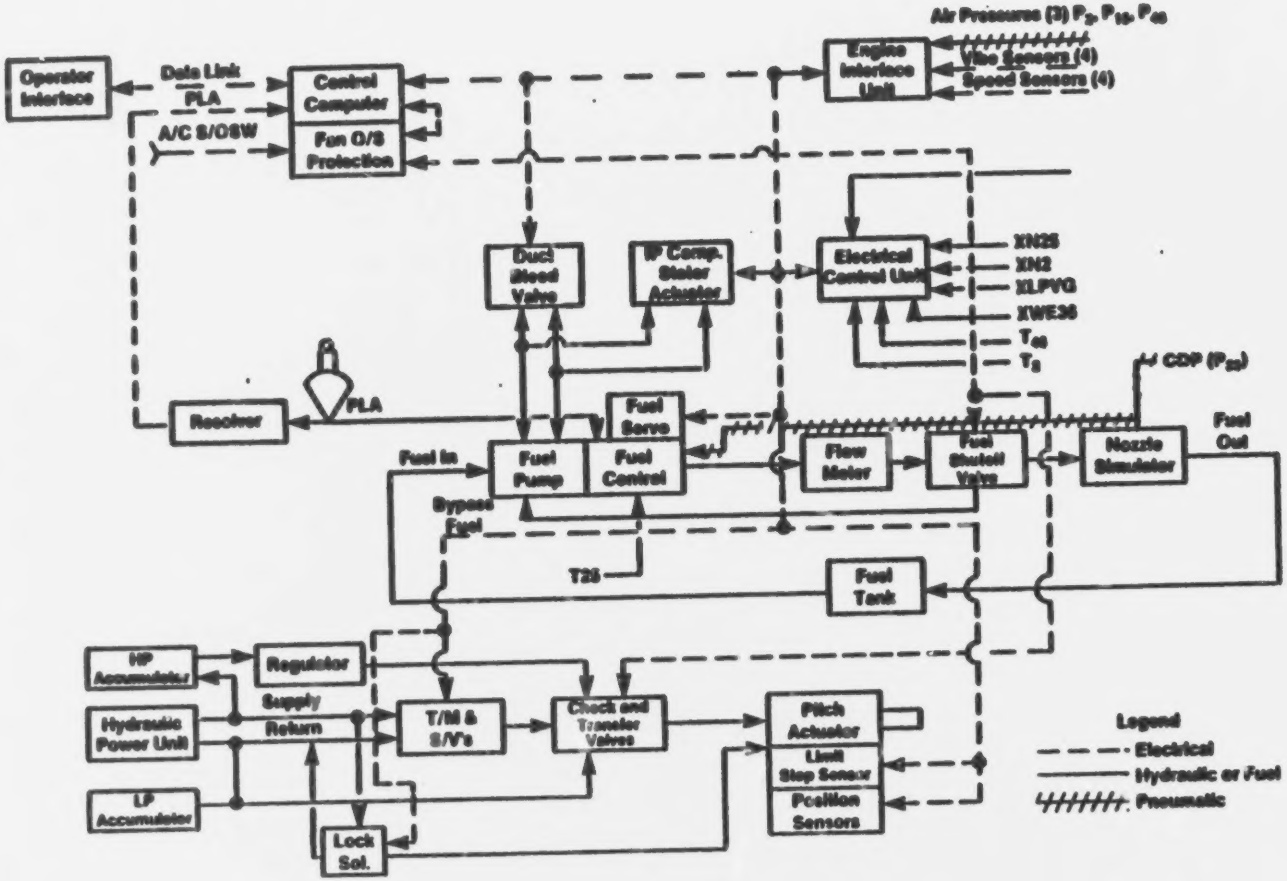
Operator Interface
Data Link
PLA
A/C S/OSW
Control Computer
Fan O/S Protection
Engine Interface Unit
Air Pressures (3) P2, P13, P48
Vibe Sensors (4)
Speed Sensors (4)
Duct Bleed Valve
IP Comp. Stator Actuator
Electrical Control Unit
XN25
XN2
XLPVG
XWE36
T48
T2
CDP (PS3)
Receiver
PLA
Fuel Servo
Fuel In
Fuel Pump
Fuel Control
Flow Meter
Fuel Shutoff Valve
Nozzle Simulator
Fuel Out
Bypass Fuel
T25
Fuel Tank
HP Accumulator
Regulator
Supply
Return
Hydraulic Power Unit
T/M & S/V's
Check and Transfer Valves
Pitch Actuator
Limit Stop Sensor
Position Sensors
LP Accumulator
Lock Sol.
Legend
Electrical
Hydraulic or Fuel
Pneumatic

Figure 35. System Test Setup.

Test Parts

Engine Hardware

Nomenclature

Actuator
Actuator LVDTs
Hydraulic Pump
Servo Assembly (2)
Transfer Valve (2)
3-Way Valve (pitch lock solenoid)
Accumulator Assembly (2)
P2/T2 Sensor
Quick Disconnects (2)
Filter Assembly (2)
Check Valve (2)
Relief/Check Valve (4)
Oil Cooler Assembly
Orifice for HP Accumulated Charging
Orifice for Blade Feathering Rate
Orifice to Dampen Lock Stroke Rate
Main Fuel Pump
Hydromechanical Fuel Control
Fuel Shutoff Valve
Duct Bleed Actuator
IP IGV Actuator
Nozzle Simulator
Engine Interface Unit (EIU)
Electrical Control Unit (ECU)
PLA Resolver Assembly
Cables

Control Room Equipment

Control Computer System (CCS)
Overspeed Unit (OSU)
Peripheral Computer System (PCS)
Vibration Amplifier
1 SPDT Switch for Air/Gnd ind
1 DPDT Switch for Stopcock ind

5.1 FAN PITCH ACTUATION TEST RESULTS

General

The fan pitch hydraulic system provides two independently controlled hydraulically actuated rod outputs operating in response to signals provided from the control computer. In addition, the system must have the capability to drive both pistons from full-extend (full reverse) to full-retract (feather) and to engage pitch locks to hold the pistons in the full retract position. The system test was conducted to validate these features and to identify necessary modifications as required for satisfactory operation. Prior to powering-up the system, a continuity check of all electrical circuits was conducted to validate correct electrical inter-connections.

Results

During initial start-up testing the HP Accumulator charge rate was greater than the hydraulic pump boost stage capacity causing piston pump inlet cavitation (Figure 36). The system was modified by adding a charge rate control (R_1), charging pump return from the LP Accumulator, and increasing Nitrogen precharge of the LP Accumulator from 25 to 40 psig. Figure 37 shows results for a Nitrogen precharge of 25 and 40 psig. Note that the 40 psig precharge always stays above the vendors recommended minimum return pressure.

The control system was designed to shut off fuel flow and drive the fan pitch to feather upon receipt of a shutdown signal. During initial testing, the drive to feather was uncontrolled causing high pump return and pump housing pressure. A flow feather rate control (R_2) was added (Figure 38). Final R_2 sizing was determined during engine test (200 Lohm - 0.061 in diameter).

During vendor component DAT (Design Assurance Testing) on the fan pitch actuator, it was determined that an uncontrolled pitch lock signal rate caused high impact loads on the pitch lock piston pin. A flow rate control (R_3) was added in the pitch lock signal line and the lock piston pin diameter was increased. The pitch lock piston was then tested to 10,000 cycles by the vendor with an uncontrolled flow rate (that is, worst case).

The hydraulic pump is a modified Variable Exhaust Nozzle (VEN) power unit and is a pressure compensated variable displacement pump. Inspection after a 50 hour endurance test at 2800/3000 psig discharge, with a 1 gpm flow rate, revealed no pump deterioration.

The fan pitch actuation system schematic is shown before and after system bench test (Figure 39) with the modifications described above incorporated.

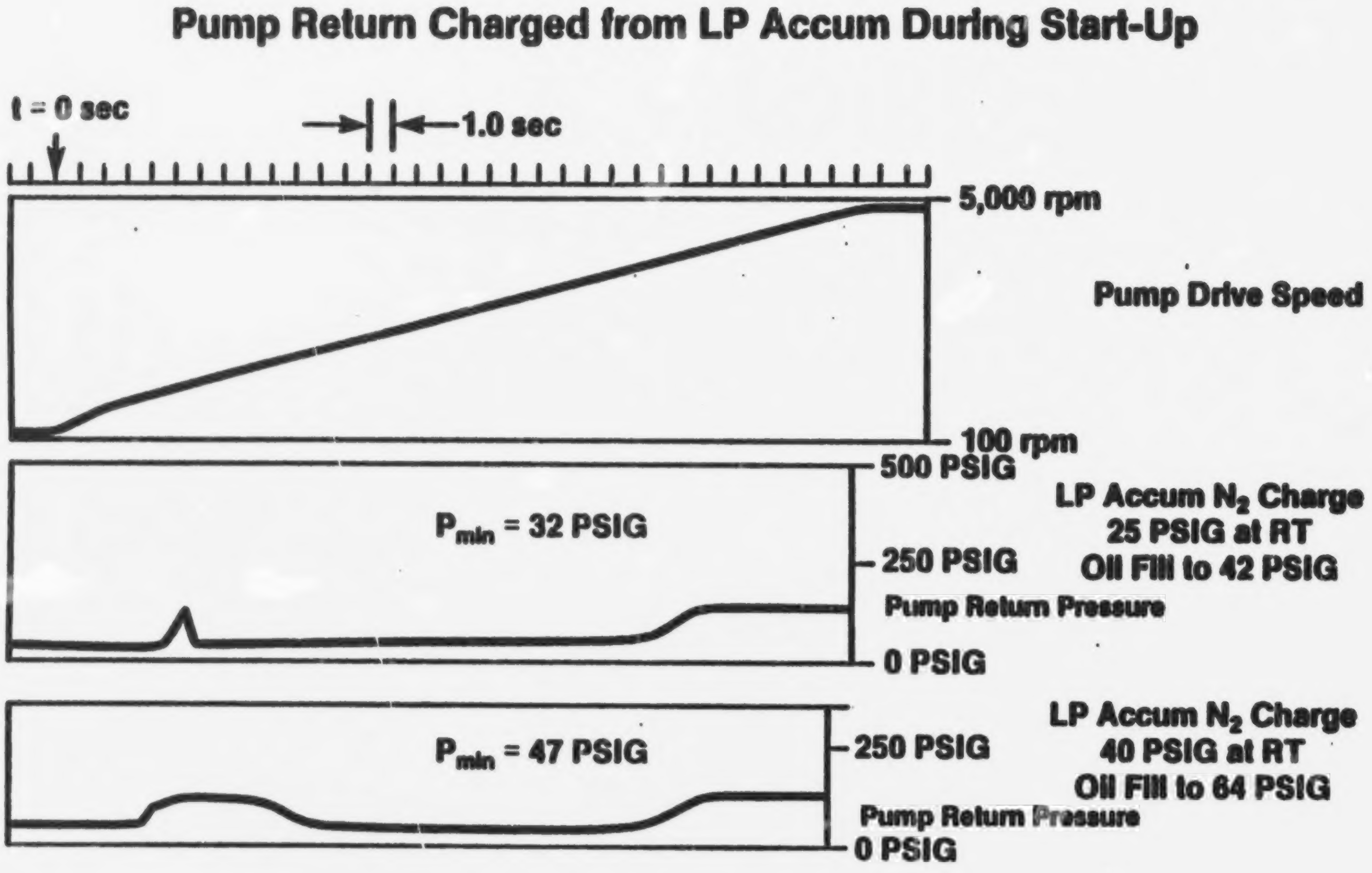

Figure 36. Fan Pitch Actuation System.

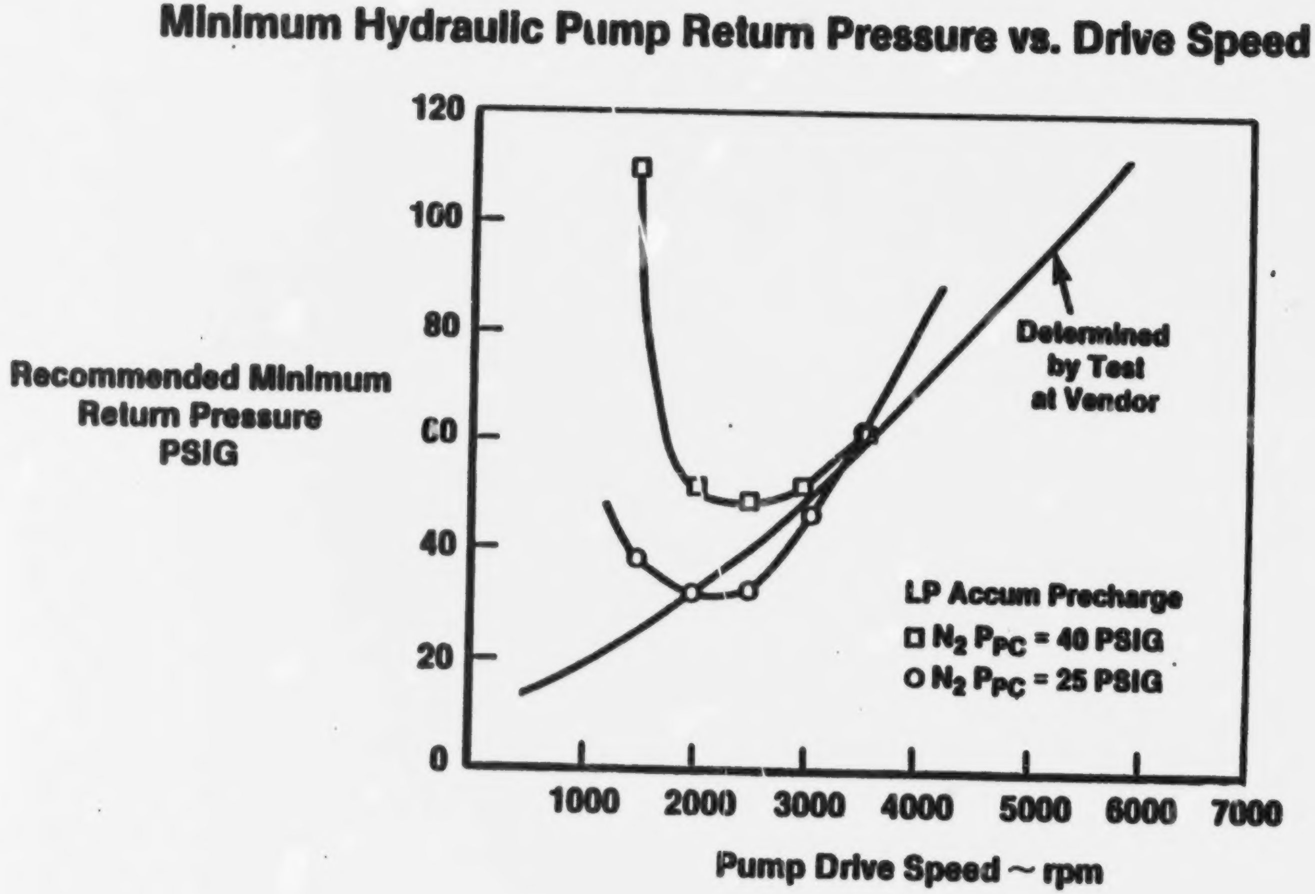

Figure 37. Fan Pitch Actuation System.

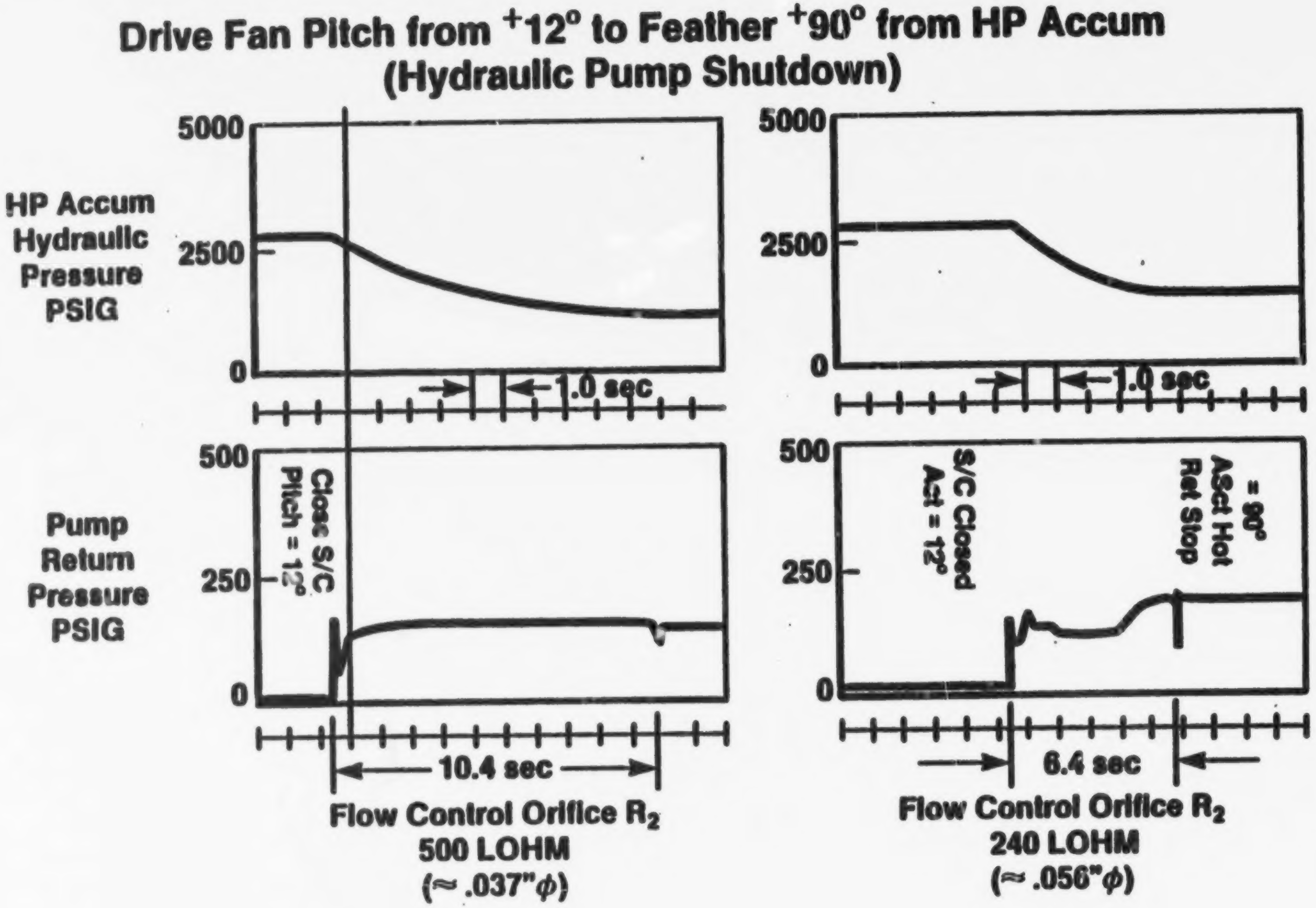

Figure 38. Fan Pitch Actuation System.

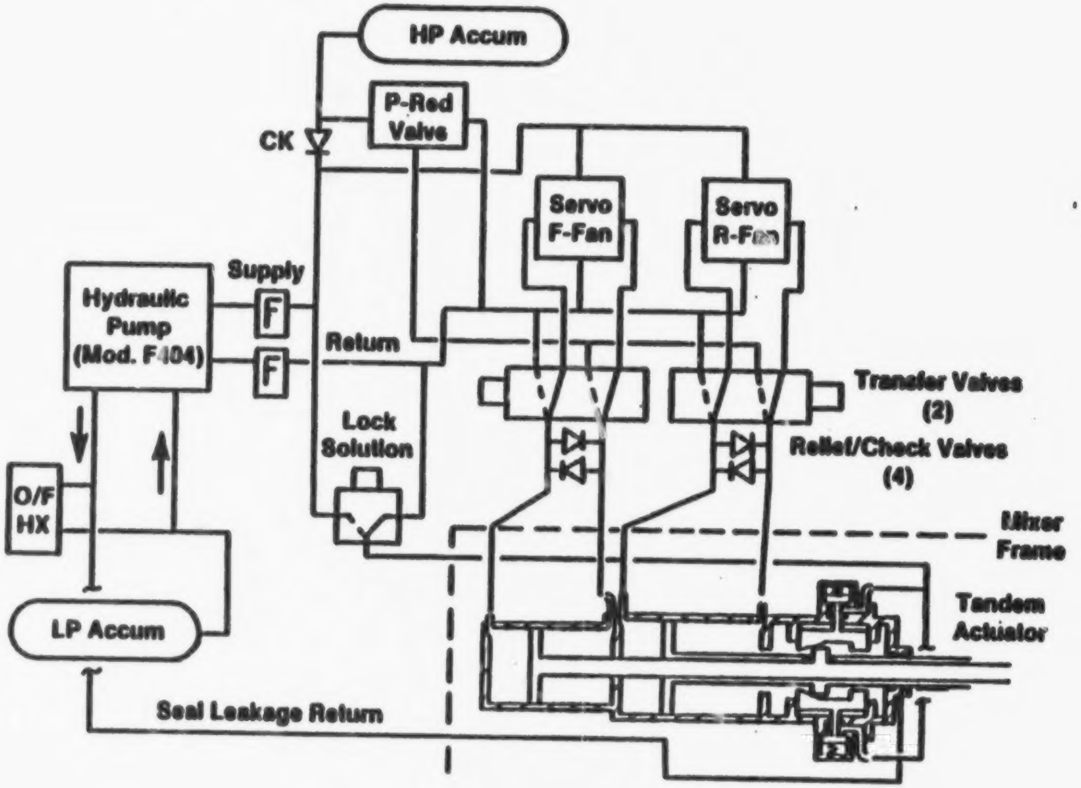
HP Accum
P-Red Valve
CK
Servo F-Fan
Servo R-Fan
Supply
Hydraulic Pump (Mod. F404)
F
F
Return
Transfer Valves (2)
Lock Solution
Relief/Check Valves (4)
O/F HX
Mixer Frame
Tandem Actuator
LP Accum
Seal Leakage Return

Figure 39. Schematic of Fan Pitch Actuation System - Before System Bench Test.

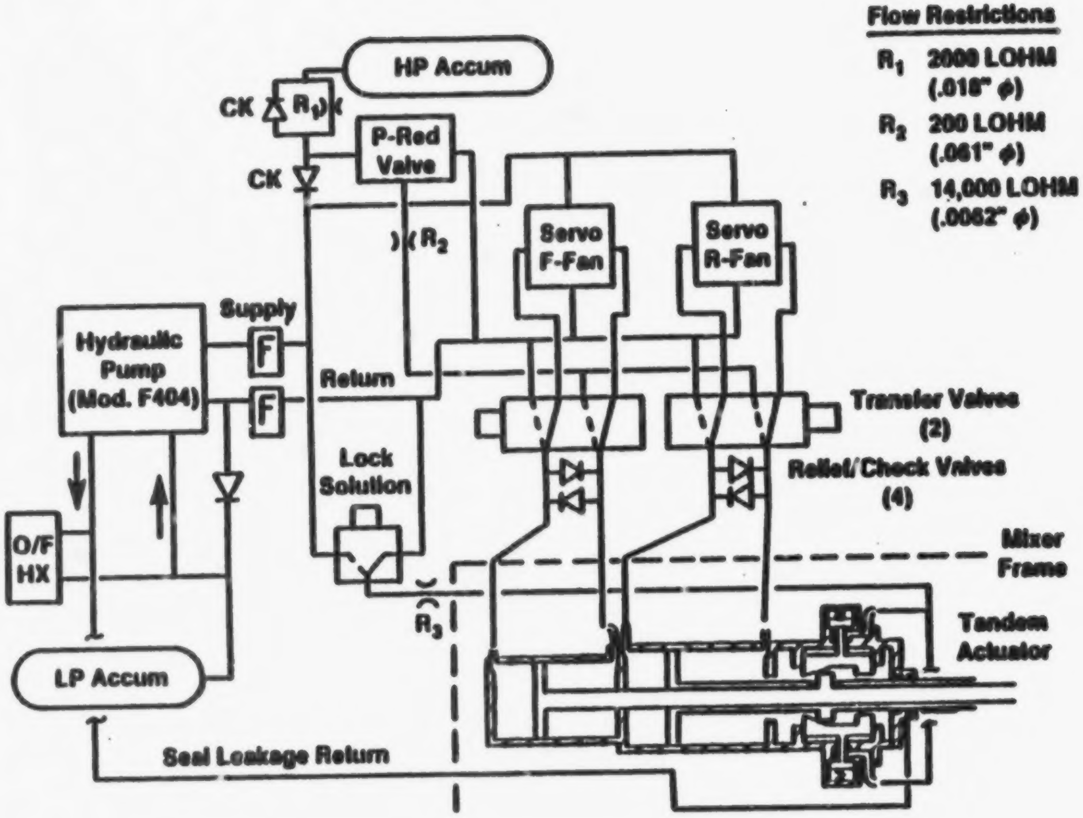
Flow Restrictions
R1 2000 LOHM (.018" ϕ)
R2 200 LOHM (.061" ϕ)
R3 14,000 LOHM (.0062" ϕ)
HP Accum
CK
R1
P-Red Valve
CK
R2
Servo F-Fan
Servo R-Fan
Supply
Hydraulic Pump (Mod. F404)
F
Return
F
Transfer Valves (2)
Relief/Check Valves (4)
Lock Solution
O/F HX
Mixer Frame
R3
Tandem Actuator
LP Accum
Seal Leakage Return

Figure 39. Schematic of Fan Pitch Actuation System - Engine Ground Test Configuration (Concluded).

This latter test configuration was used for engine test. This system successfully demonstrated the ability to control and actuate the fan pitch hydraulic actuation system over the full travel range from the full-exend to the full-retract position of the actuator. This includes the capability to engage (and disengage) the pitch lock to hold the actuator in the full-retract position.

5.2 FUEL SYSTEM TEST RESULTS

General

The HMU (Hydromechanical Control) is a fuel operated electro-hydromechanical component that interfaces with the control computer via the engine mounted Engine Control Unit (ECU) and performs the following primary functions:

> It controls HP rotor speed, schedules accel/decel fuel flows, provides for HP stator control, minimum fuel, limits HP compressor discharge pressure and other ancillary functions. In response to an electrical signal from the control computer, the HMU reduces engine fuel flow to maintain scheduled engine pressure ratio (P46Q2) and also limits inter-turbine temperature and IP shaft speed.

5.2.1 HMU (Hydromechanical Control)

The hydromechanical control is an unmodified F404 hydromechanical fuel control. A calibration check was made on the hydromechanical fuel control HP rotor speed governing schedule. Figure 40 is a plot of HP rotor speed versus power lever angle for compressor inlet temperature of 519° R (standard day).

The hydromechanical control is configured such that low power operation modulates fuel flow as a function of corrected HP rotor speed (XN25R) and at high power, the resultant fuel flow of the basic HP rotor speed control is downtrimmed through a torque motor input as a function of intermediate turbine speed (XN2), core engine exhaust temperature (T46), or engine pressure ratio (P46/P2), whichever provides maximum fuel downtrim. The features of the fuel flow cutback characteristics were tested. In each case, a reference value (RXN2, RT46, or RP46/P2) was set and the sensor value was increased until maximum fuel flow cutback (decel schedule) was achieved, then sensor value was decreased until fuel flow returned to the zero cutback condition (accel schedule).

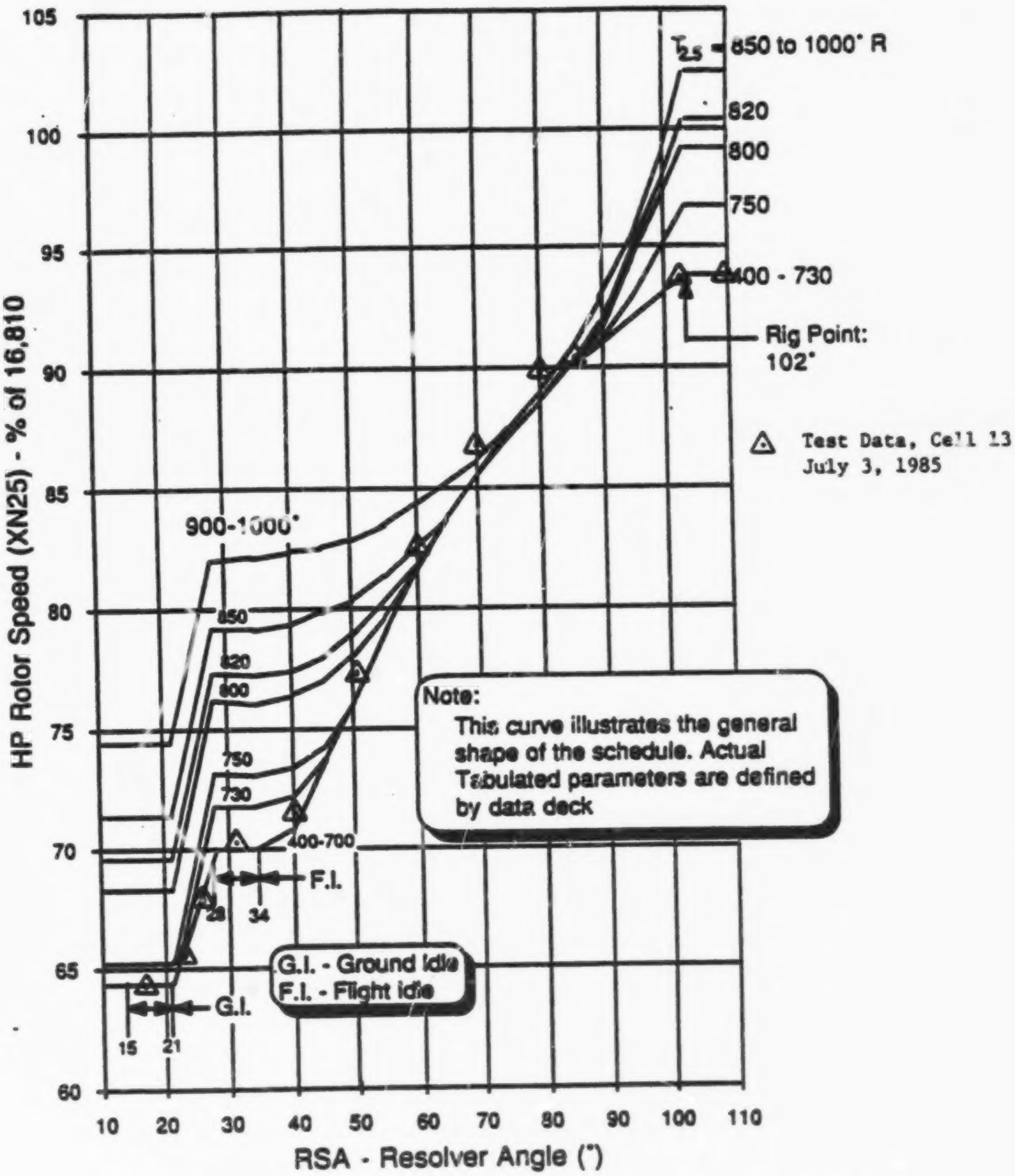

Note:
This curve illustrates the general shape of the schedule. Actual Tabulated parameters are defined by data deck

Figure 40. HP Rotor Speed Governing Schedule.

The cutback on intermediate turbine speed (XN2) results are as follows:

RXN2 = 12568 rpm

XN2 = 12570 rpm for maximum cutback

XN2 = 12550 rpm for minimum cutback

Hysteresis = 20 rpm.

The cutback on core engine exhaust temperature (T46) results are as follows:

RT46 = 1743° R

T46 = 1744° R for maximum cutback

T46 = 1743° R for minimum cutback

Hysteresis = 1° R.

The cutback on engine pressure ratio (P46/P2) results are as follows:

RP46/P2 = 3.276 units

P46/P2 = 3.2934 units for maximum cutback

P46/P2 = 3.2440 units for minimum cutback

Hysteresis = 0.0494 units.

These results indicate that the fuel cutback feature for power management (engine pressure ratio) and limit protection (core engine exhaust temperature and intermediate turbine speed) function properly and that the electrical circuitry is correct.

5.2.2 Duct Actuation Bleed System

A calibration test was conducted on the duct bleed LVDT and results are shown in Figure 41. Note that only the actuator was tested as the duct bleed valve was not available for this test. Full travel will be checked when installed on engine. Dynamic response of the duct bleed actuation system was checked by inputting, via the control computer, a step input command to the duct bleed valve torque motor and measuring the resultant actuator position and converting results of this test into an equivalent time constant. Results indicate an equivalent time constant of approximately 50 milliseconds, which meets design requirements. In addition, this test verified correct electrical circuitry.

Actuator Stroke (%)	Vo/Ve - Output Voltage Ratio
0	0.27
100	-0.30

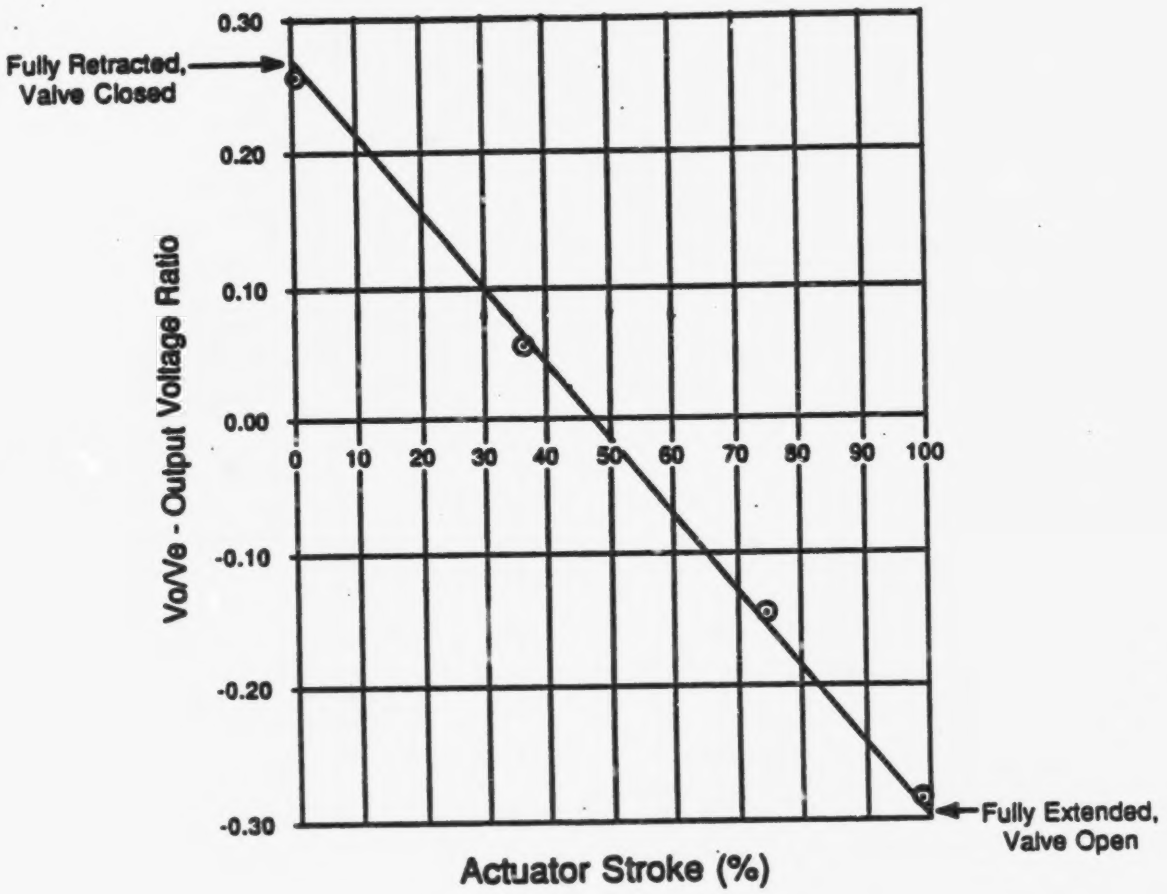

Note: 100% Stroke = 2.7 inches

⊙ = Test Data

Figure 41. Duct Bleed LVDT Characteristics.

5.2.3 Fuel Shutoff Valve Verification

The fuel shutoff valve and fan pitch transfer valves are energized in the run state and de-energized for shutdown, such as fuel off and fan pitch at feather. Normal shutdown is mechanized by a shutdown command (stopcock) to the overspeed unit. The stopcock signal was cycled to verify that this combined system functioned properly and that the electrical circuit is correct.

5.2.4 IP Stator Actuation

Dynamic response of the duct bleed actuation system was checked by inputting, via the control computer, a step input command to the duct bleed valve torque motor and measuring the resultant actuator position and converting results of this test into an equivalent time constant. Results indicate an equivalent time constant of approximately 50 milliseconds, which meets design requirements. In addition, this test verified correct electrical circuitry.

5.3 CONTROL COMPUTER TEST RESULTS

General

The control computer, interface circuitry, and overspeed protection system is mounted on standard cards and incorporated into rack mounted boxes. The control computer, interface circuitry, and overspeed protection system provides the following features:

- Excite, then condition signals from engine sensors and aircraft display signals and input these signals to the control computer
- Execute the control algorithms, provide output drivers for these control outputs, and process the aircraft data display outputs
- Communicate with a peripheral computer system
- Provide independent circuits for fan overspeed protection
- Use separate I/O equipment compatible with the control computer I/O bus for the engine sensors and control outputs

Control computer and peripheral computer software were modified as required; final validation was conducted on the software prior to delivery of the engine. This control bench test included inputting simulated sensor values, packed data words, and outputting driver signals and packed data words. Operation was verified by direct measurement, and comparison of the signals on the peripheral computer. Control computer and peripheral computer software were modified as required; final validation was conducted on the final software prior to initiation of systems testing.

Results

Operation of the control computer, interface circuitry, overspeed protection system and peripheral computer was successfully tested during functional checkout prior to the systems test.

5.3.1 Pitch Position Control

To determine proper operation of the pitch locks, the control computer commanded the pitch locks retracted, pitch lock pressure was monitored to verify locks were commanded retracted and pitch lock position feedback verified on the control computer readout. To determine proper pitch actuation the control computer commanded manual pitch positions of extend and retract, while running the hydraulic power unit. Operation was as commanded. Step inputs were applied to commanded position and compared to actual feedback position. Approximately a 50 millisecond response time was recorded for both the forward and rear actuator position.

5.4 TRANSIENT RESPONSE EVALUATION

Dynamic response of position control loops, such as duct bleed actuation, IP stator actuation, fuel override, etc. were conducted as reported in Section 5.2. No overall frequency response of fan speed control, or fuel downtrim features were tested during the systems bench test. Simulation of the controller operation using a digital transient engine model with an emulator for the control algorithms was used to verify correct dynamics.

5.5 FUNCTIONAL TEST OF ELECTRONIC CONTROL UNIT

General

The ECU is a modular solid-state component, supplied with power from the alternator. It provides signal excitation and signal conditioning for the following sensors:

5.5.1 HP shaft speed (XN25)
5.5.2 IP shaft speed (XN2)
5.5.3 Inter-turbine temperature (T46)
5.5.4 Inlet temperature (T2)
5.5.5 Fuel metering valve LVDT (XWF36)
5.5.6 IP compressor stator actuator LVDT (XLPVG)

Functional testing was conducted to ensure that the conditioned signals were scaled properly by the control computer. In each case, simulated sensor inputs were supplied to the ECU and compared to the control computer indicated value.

Results

Results of the testing indicated that operation of the ECU in conjunction with the control computer is satisfactory and that this configuration should be released for engine test.

5.5.1 HP Shaft Speed Scaling

A calibration test was conducted on the HP rotor speed signal as conditioned by the ECU. The results are shown in Table 5.

Table 5. HP Shaft Speed Scaling.

ECU Input,		Indicated HP Shaft Speed, rpm
rpm	Hz	
7570	1806	7558
9750	2326	9719
12000	2863	11920
15000	3579	14810
15810	3773	15692
16810	4011	17008

5.5.2 IP Shaft Speed Calibration

A calibration test was conducted on the IP shaft speed signal, as scaled by the ECU. The results are shown in Table 6.

Table 6. IP Shaft Speed Calibration.

ECU Input		Indicated IP Shaft Speed, rpm
rpm	Hz	
2603	1822	2481
3941	2759	3846
4968	3478	4891
6984	4889	6937
10010	7007	10000
13304	9313	13344
15924	11147	15930

5.5.3 Interturbine Temperature Scaling

A calibration test was conducted on the interturbine temperature signal as conditioned by the ECU. The results are shown in Table 7.

Table 7. Interturbine Temperature Scaling.

ECU Input		Indicated Interturbine Temperature ° F
° F	mvdc	
367	7.582	366
800	17.523	805
1200	26.975	1199
1464	33.094	1459
1651	37.330	1643
2000	44.856	1986

5.5.4 Inlet Temperature Scaling

A calibration test was conducted on the inlet temperature signal as conditioned by the ECU. The results are shown in Table 8.

Table 8. Inlet Temperature Scaling.

ECU Input		Indicated Interturbine Temperature
° F	ohms	° F
-80	7.4	-76.3
-20	8.8	-13.5
60	10.6	65.4
130	12.1	136.1
220	14.1	230.3
280	15.4	291.5

5.5.5 Fuel Valve Calibration

A calibration test was conducted on the fuel metering valve LVDT (Linear Variable Differential Transducer), with the output converted to fuel flow in the control algorithm's. The results are shown in Table 9.

Table 9. Fuel Valve Calibration.

Measured Fuel Flow, pph	Indicated Fuel Flow, pph
415	492
786	802
962	994
1981	2014
2648	2653
4013	4057
5072	5088
5505	5491
6972	6976
7259	7261

5.5.6 IP Compressor Stator Actuator LVDT

A calibration test was conducted on the IP compressor stator LVDT. The results are shown in Table 10.

Table 10. IP Compressor Stator Actuator LVDT.

Actuator Rod Extension, in	Indicated Rod Extension, in
0	0.0285
1.0	1.0050
2.125	1.9870
2.7	2.6997

5.6 FUNCTIONAL TEST OF THE EIU (ENGINE INTERFACE UNIT)

General

Three pressure transducers are housed in the engine mounted EIU. Excitation is provided by the control computer. Each transducer receives an air pressure input and, with excitation voltage applied, provides an output signal which is proportional to the input pressure.

A calibrated pressure source was used to conduct a calibration test on each of the three pressure transducers.

Results

Results of the testing indicated that operation of the EIU in conjunction with the control computer is satisfactory and that this configuration should be released for engine test.

5.6.1 Inlet Total Pressure (P2)

Table 11 provides the calibration data for the inlet total pressure transducer.

Table 11. Inlet Total Pressure.

Reference Pressure, psia	Indicated Pressure, psia
14.472	14.620
5.010	5.016
6.000	6.032
7.010	7.084
8.005	8.060
8.995	9.096
10.000	10.084
11.000	11.088
12.006	12.132
13.000	13.112
14.000	14.120
15.006	15.120
16.000	16.128
17.000	17.128
18.000	18.128
19.002	19.124

5.6.2 Duct Total Pressure (P15)

Table 12 provides the calibration data for the duct total pressure transducer.

Table 12. Duct Total Pressure.

Reference Pressure, psia	Indicated Pressure, psia
14.470	14.809
4.994	5.193
10.006	10.253
15.010	15.285
20.000	20.273
25.000	25.290
30.000	30.278
35.000	35.288
40.000	40.246
44.490	45.230
50.000	50.220

5.6.3 Interturbine Pressure (P46)

Table 13 provides the calibration data for the interturbine pressure transducer.

Table 13. Interturbine Pressure.

Reference Pressure, psia	Indicated Pressure, psia
14.47	14.81
5.01	5.20
10.00	10.29
15.00	15.27
20.00	20.30
25.00	25.29
30.00	30.27
35.00	35.27
40.00	40.25
44.97	45.20
49.87	50.08

5.7 CONCLUSIONS

1. The overall functioning of the GE36 demonstrator engine control system is satisfactory.
2. The pitch actuation system, as modified during systems testing, will provide pitch modulation for engine test operation.
3. The fuel system will provide the proper fuel scheduling, speed scheduling, HP stator scheduling and actuation, as well as actuation pressure required for other variable geometry.
4. Operation of the control computer in the wet bench environment is acceptable.
5. The ECU was functionally tested and provides satisfactory signal excitation and signal conditioning for input to the control computer.
6. The EIU was functionally tested and provides satisfactory signals for input to the control computer.

5.8 RECOMMENDATIONS

1. The control system as tested should be used for engine test.
2. Ensure that all connectors are properly installed and secured (lockwire or RTV) prior to engine running.
3. A source of uninterruptable power (120 vac, 60 Hz) be supplied to the control computer, overspeed unit, and peripheral computer. The system is designed such that loss of power to the control computer or overspeed unit will result in automatic shutdown of the engine. An uninterruptable power source would prevent such shutdowns.

6.0 ADDITIONAL COMPONENT TESTING

6.1 CARBON SEAL COMPONENT TESTING

Introduction

Flow tests of the propulsor sump air/oil seals were conducted to ensure proper assembly and provide predictions of vent flow quantity during engine testing. The sump air/oil seals are the two intershaft carbon seals, two circumferential carbon seals, 16 magnetic carbon seals, and several O-rings/gaskets. The results and description of these tests are presented below.

Overview

The propulsor sump air/oil seals were flow tested by pulling a vacuum on the sump cavity and measuring the leakage at various vacuum pressure levels. Since the intershaft seals are the major contributor to the total leakage, component tests of the two intershaft seals were conducted to establish acceptance guidelines for the assembly tests. During the assembly of the propulsor, three tests were performed to provide early verification of proper assembly. The tests were useful in identifying cracked carbon segments and providing estimates of vent flow levels for engine testing.

Test Set-Up and Procedure

For all of the tests, a vacuum pump was used to pull various vacuum levels in the sump cavity. A valve in the piping between the sump cavity and vacuum pump was used to set a desired vacuum pressure in the sump cavity. The exhaust of the vacuum pump was measured with a flowmeter and used as the total leakage of seals at the set vacuum pressure. The same vacuum pump was used for all tests with the assumption that any influence of the pump would be a constant and that the pump exhaust was simply the leakage flow.

Intershaft Seal Component Test Results and Conclusions

The intershaft seal (Figure 42) tests were conducted with tooling that simulate the OD land and inner mount of the shafts. A test of the intershaft seal assembly consisted of the carbon element, both races, the preload spring, and a mount element. Results for the forward intershaft seal test are shown

ORIGINAL PAGE IS
OF POOR QUALITY

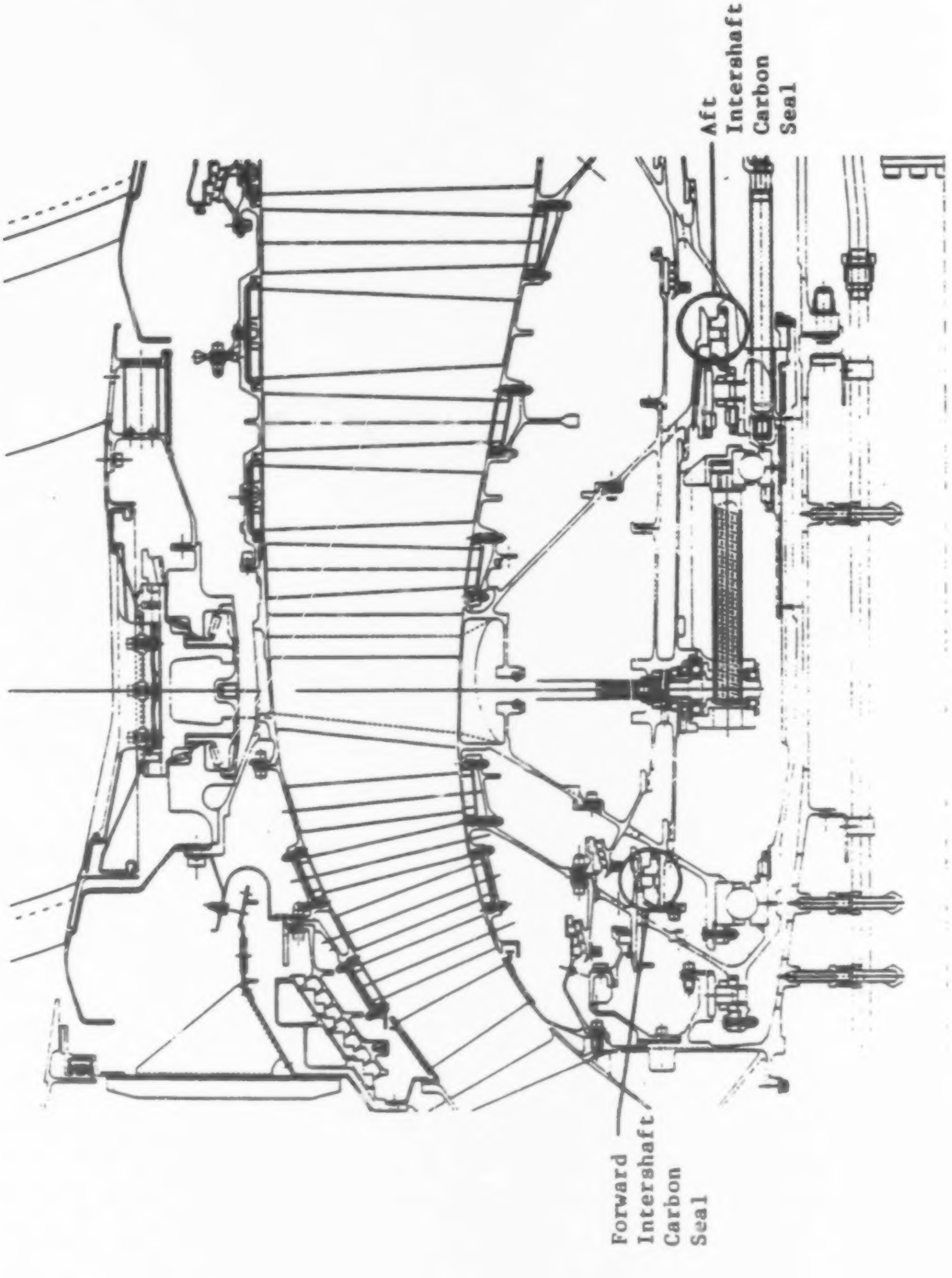
Aft Intershaft Carbon Seal
Forward Intershaft Carbon Seal

Figure 42. Forward and Aft Intershaft Carbon Seal.

in Figure 43 and are labeled component test. The seal tested in the component test was broken in transit to assembly and was never assembled and tested in the engine. However, the results do provide a guideline to the general leakage level for the forward intershaft seal. The aft intershaft seal assembly (Figure 42) was component tested but only limited data were obtained. For vacuum pressures of 3.2, 6.1, and 9.5 inches Hg, the corresponding leakage rates were 0.0103, 0.0152, and 0.201 lb/sec, respectively.

Assembly Test No. 1

The first assembly test was conducted after the forward actuation housing was installed. Figure 44 illustrates the test setup. Seals tested in this configuration are the forward intershaft carbon seal, four magnetic carbon seals that seal around the forward radial actuation rods, and several O-rings that seal the actuation housing and test fixture. Results of test No. 1 are shown in Figure 43. For Engine -001/1 (Engine 1, Build 1), the forward intershaft carbon seal used in the engine was a repaired seal. The OD dam of the carbon element had been damaged and was repaired with a graphite putty. The high flow characteristic shown in the curve is probably due to this repair and the resulting high spots on the OD surface. For Build 2, the carbon element was replaced with a good ring. Excellent correlation exists between the component test results and the assembly test No. 1 results. The results imply that the intershaft seal is the primary source of static leakage and the magnetic carbon seals and O-rings are properly assembled (negligible leakage).

Assembly Test No. 2

Test No. 2 was conducted after the 2B bearing housing was installed. At this time, all the significant rotating parts are assembled and balanced. Seals tested in this configuration are the seals of Test No. 1, the aft intershaft carbon seal, the aft circumferential carbon seal, four additional magnetic carbon seals for the aft actuation system, and additional O-rings. The fixture in Figure 44 that seals the forward end of the cavity is used along with a cap that seals across the aft end of the propulsor sump. The results

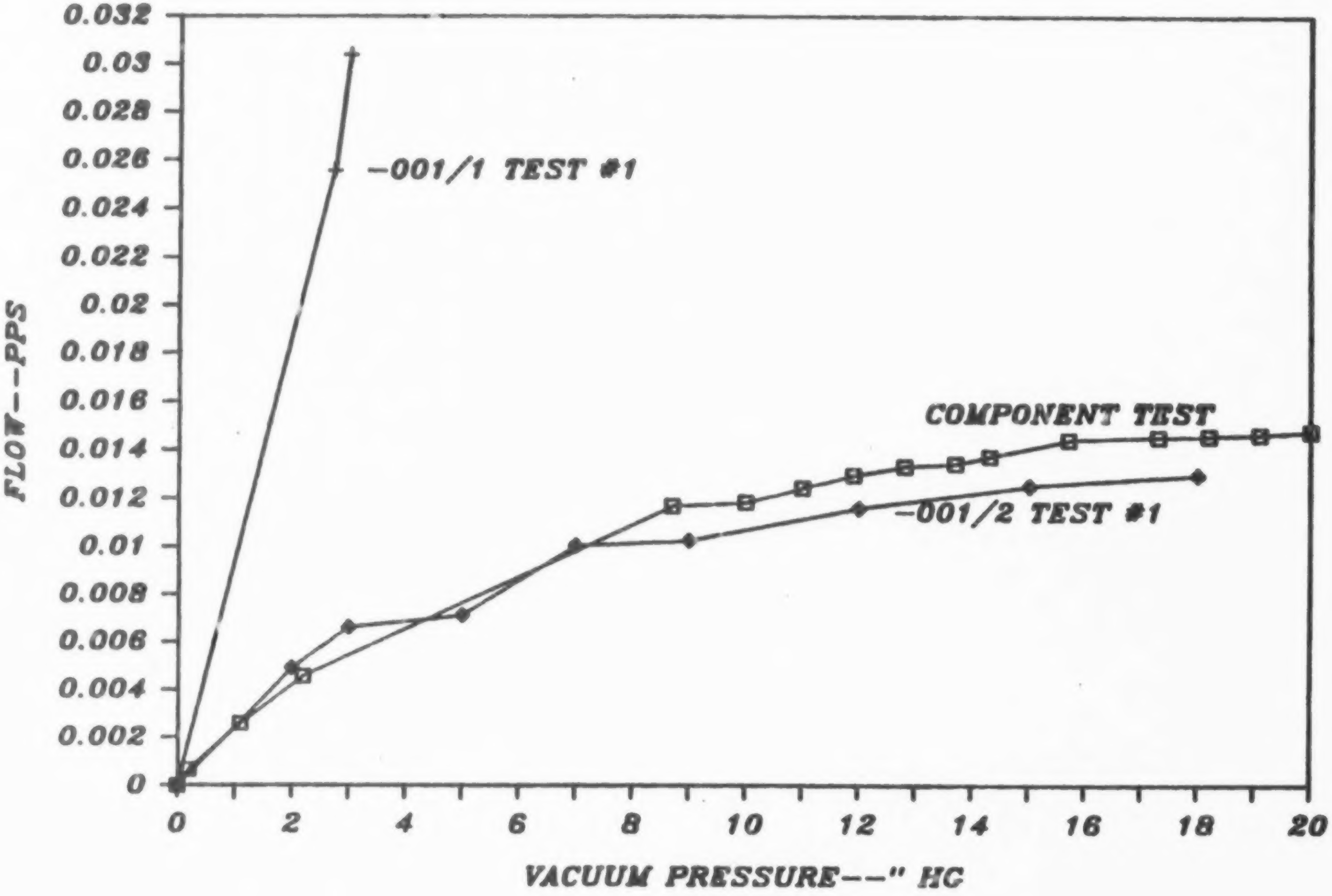

Figure 43. Forward Intershaft Seal Flow Test Results.

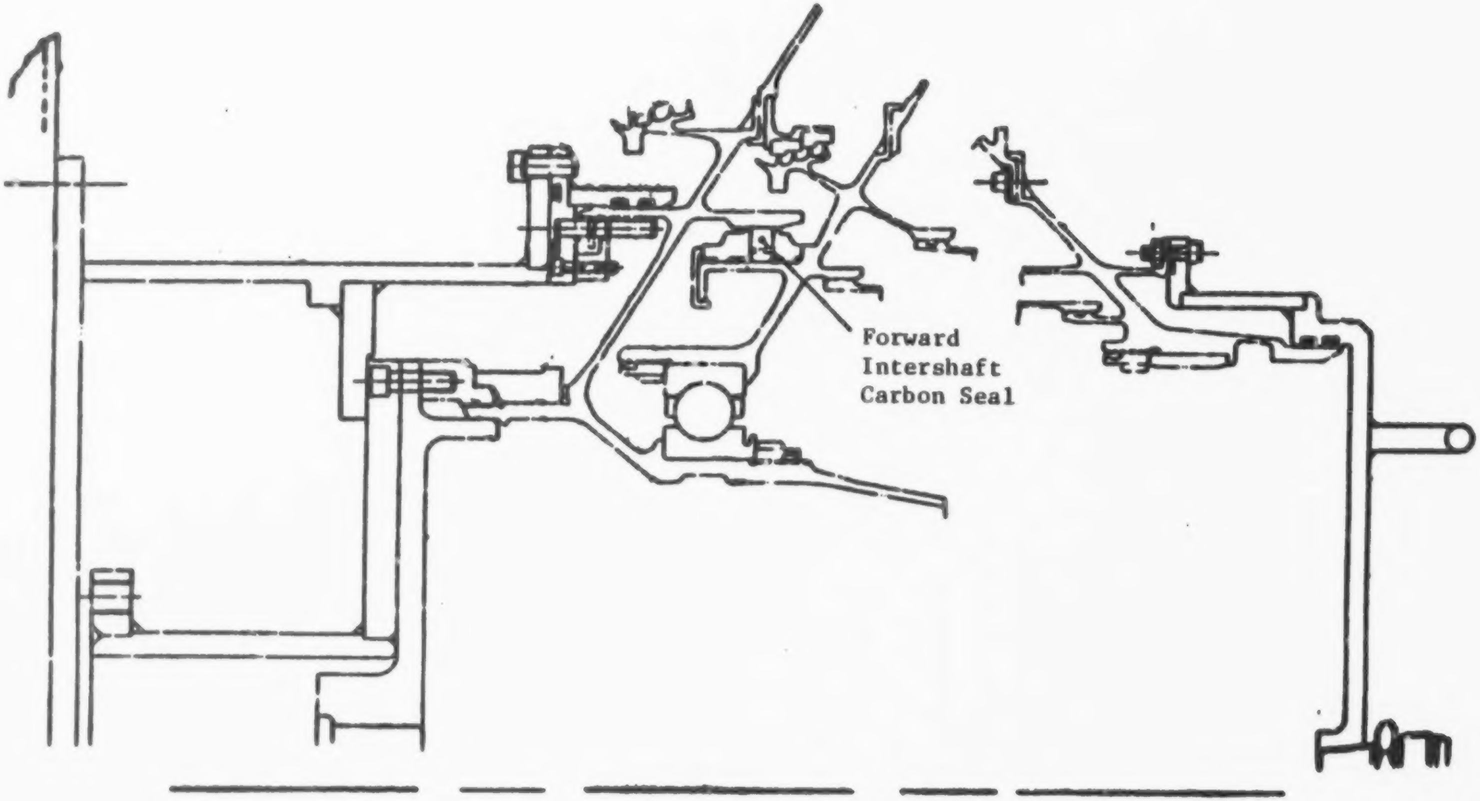
Forward
Intershaft
Carbon Seal

Figure 44. Test Setup for Assembly Test No. 1.

from these tests are shown in Figure 45. The sudden change in the Build 2 curve between 5 and 6 inches Hg corresponds to the calculated pressure differential that would cause the intershaft seals to blowdown. Blowdown is when the net radial force on the carbon element is inward resulting in the OD seal to open. In operation, the centrifugal force on the seal is significantly greater than the radial pressure force and blowdown will not occur. Note that the data show that Build 2 achieved a much higher vacuum level than did Build 1, indicating a much better seal for Build 2. It was discovered during the initial engine test of Build 1 that the forward circumferential carbon seal was damaged during engine assembly. This damage was not discovered during the component test for two reasons. Since this was the first of a new type of engine, limited knowledge and experience made it unclear as to what an adequate vacuum level was. It is obvious from the Build 2 data that a much higher vacuum level can be achieved with undamaged seals. The second reason has to do with the confusion caused by different pressure measurement locations. This will be discussed in further detail in the section on Broken Seal Determinations.

Assembly Test No. 3

Test No. 3 was conducted after the propulsor was assembled to the gas generator. The only fixtures required for this test are plugs for the various service lines to the sump cavity (oil supply, scavenge, and vents). This test was of the entire internal sump seal system. Results of these tests are shown in Figure 45. The final point of each characteristic curve is the maximum vacuum level that the test setup permitted. For Build 1 (repaired forward intershaft seal), the maximum vacuum was approximately 2 inches Hg and for Build 2 ("good" seal), the maximum levelwas approximately 6 inches Hg. The test data also imply that the test fixture used for tests No. 1 and 2 leaks.

Engine Vent Flow Predictions

Problems associated with transforming the assembly test results to engine operating conditions are low pressure ratio data limited by intershaft seal blowdown, lack of speed effects on seal leakage, and potential impact of vacuum pump exhaust on the test data. With these limitations, a rough estimate of the maximum propulsor vent flow is 0.09 lb/sec for Build 2.

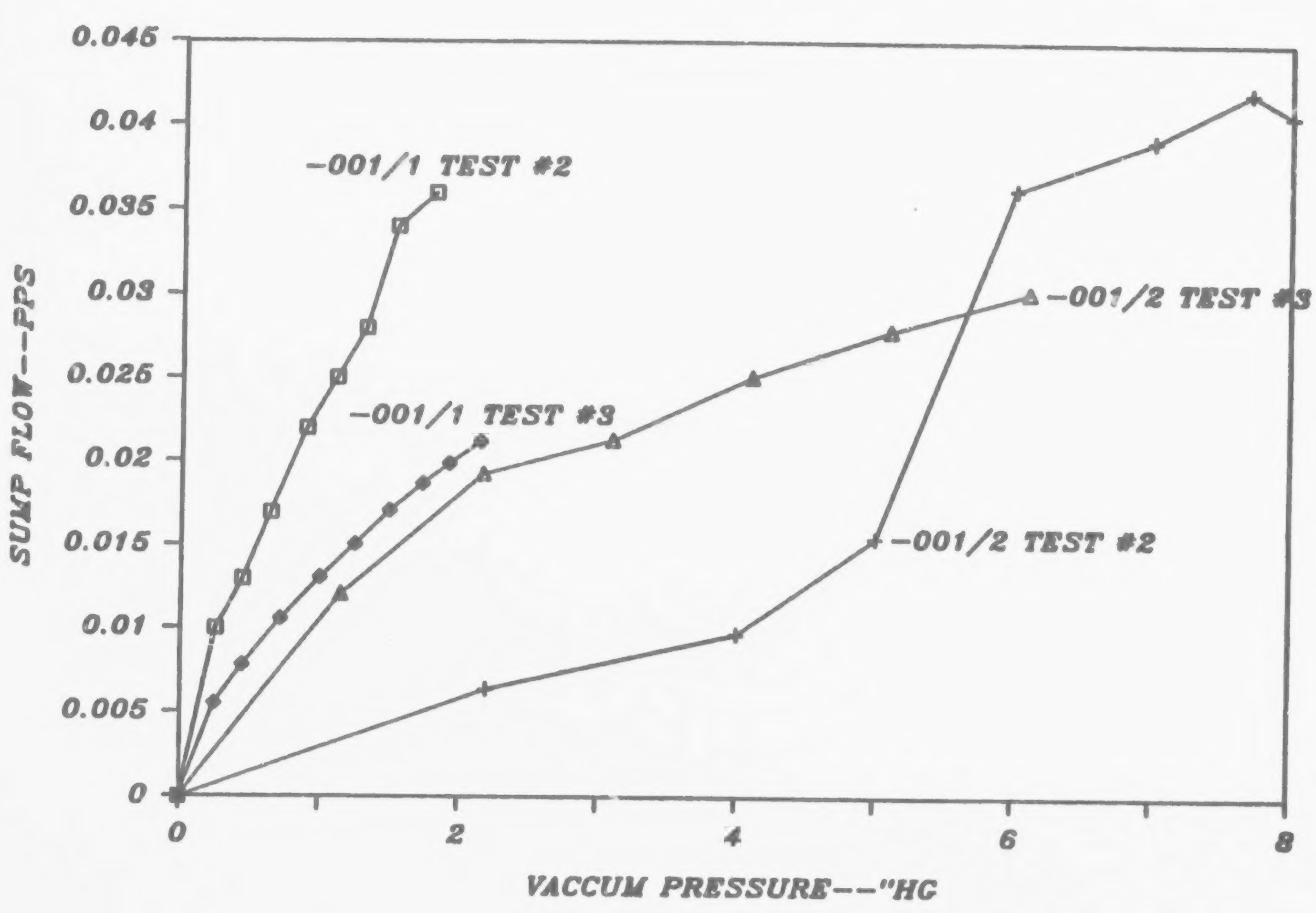

Figure 45. Engine -001 Sump Leakage, Tests 2 and 3 Results.

Broken Seal Determinations

During assembly of Builds 1 and 2, vacuum tests were conducted twice with seals that were broken during assembly.

One incident involved the aft circumferential carbon seal during Build 2. Test No. 2 setup was initially only able to pull a 0.05 inch Hg vacuum. The forward end test fixture was removed and checked but no signs of leakage were found. The seal was disassembled and one of the carbon segments was found broken. The seal was replaced and a maximum of 8 inches Hg vacuum was achieved.

The other incident involved the forward circumferential seal during Build 1. Figure 46 provides the test data. The curves labeled with an "A" were obtained when the broken seal was installed. Two curves for Test 3A are shown. The difference in the curves is the sump cavity pressure measurement location. For Curve 3A, the pressure was sensed at a point at the aft end of the sump cavity. The vacuum pump was attached to one of the service lines at the forward end. For Curve 3A?, the pressure measurement location was near the vacuum line attachment to the propulsor. Prior to the engine test, the 3A? curve was believed to be the correct characteristic since it was similar to expectations. Curve 3A was believed to be a bad data point. In hindsight, Curve 3A is the correct curve and Curve 3A? is influenced by the pressure measurement location. Curves 2B and 3B are the test results obtained after the broken seal was replaced.

6.2 IGV/OGV FREQUENCY TEST

Introduction

Bench frequency testing was conducted on the inlet guide vane (IGV) and outlet guide vane (OGV) assemblies to correlate analytical predictions.

Overview

Individual airfoils of the IGV and OGV fabricated assemblies were tested by driving them at resonance using an electromagnetic excitation. One airfoil was fully instrumented to identify modes and strain response factors for the engine gage location. All airfoils were tested to establish scatter. Results were corrected to engine temperature conditions and the potential operating

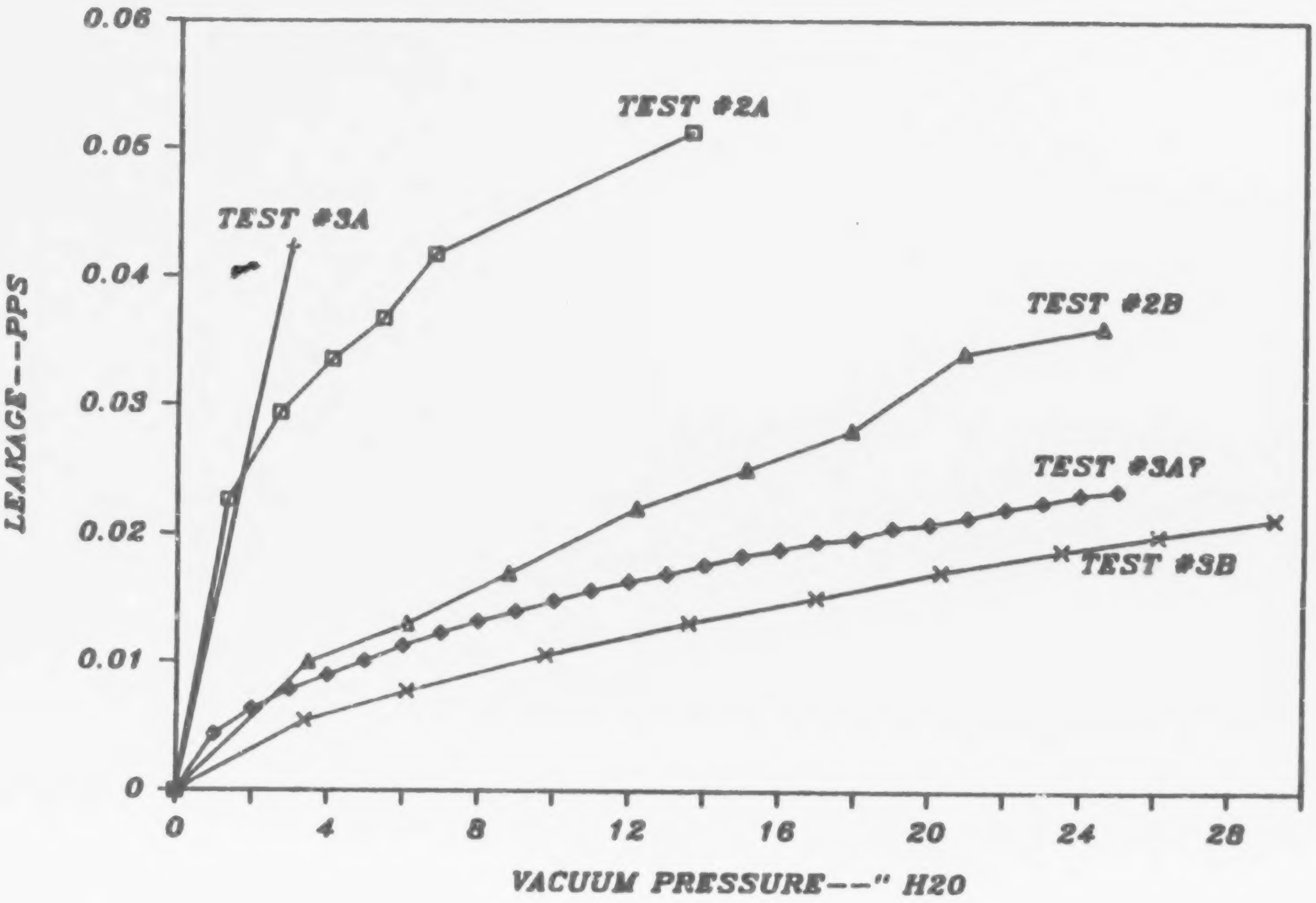

Figure 46. Engine -001 Sump Seal Leakage, Assembly Tests.

resonances were identified. Strain distribution results were used to select an engine gage location sensitive to the potential resonant modes and to establish scope limits for all modes.

Test Results and Conclusions

Figure 47 shows the IGV Campbell diagram based on test results. This indicated a potential second flex (2F) resonance in the operating range. The excitation source was downstream (Stage 1 blade passing frequency) and considered weak. The engine gage location was selected to be responsive to this mode.

Figure 48 shows the OGV Campbell diagram based on test results. This indicated a potential second torsion (2T) resonance with the Stage 12 frame airfoil passing frequency. Margin for a two stripe (2S) resonance was less than the design objective of 15%. However, the axial distance from the power frame to the OGV indicated that the excitation wake energy would be low for both modes. The engine gage location was selected to be responsive to both modes.

6.3 TURBINE BLADE DAMPER DEVELOPMENTAL VERIFICATION TESTS

Introduction

Build 1 engine testing at Peebles indicated all stages of turbine blades were highly responsive in the first flex (1F) mode. Build 1 testing was terminated following a high cycle fatigue (HCF) failure of Stage 1 which resulted in a gas generator stall.

Data review indicated less damping for the 1F mode than had been expected during detailed design. The design was to be modified to incorporate damping effective in the 1F mode for Build 2 engine testing. Component tests to verify and develop this damping mechanism were undertaken prior to finalizing the design modification.

Overview

Analysis indicated dampers near the tip of the airfoil would provide the most effective energy dissipation for 1F mode. Wire ties similar to those

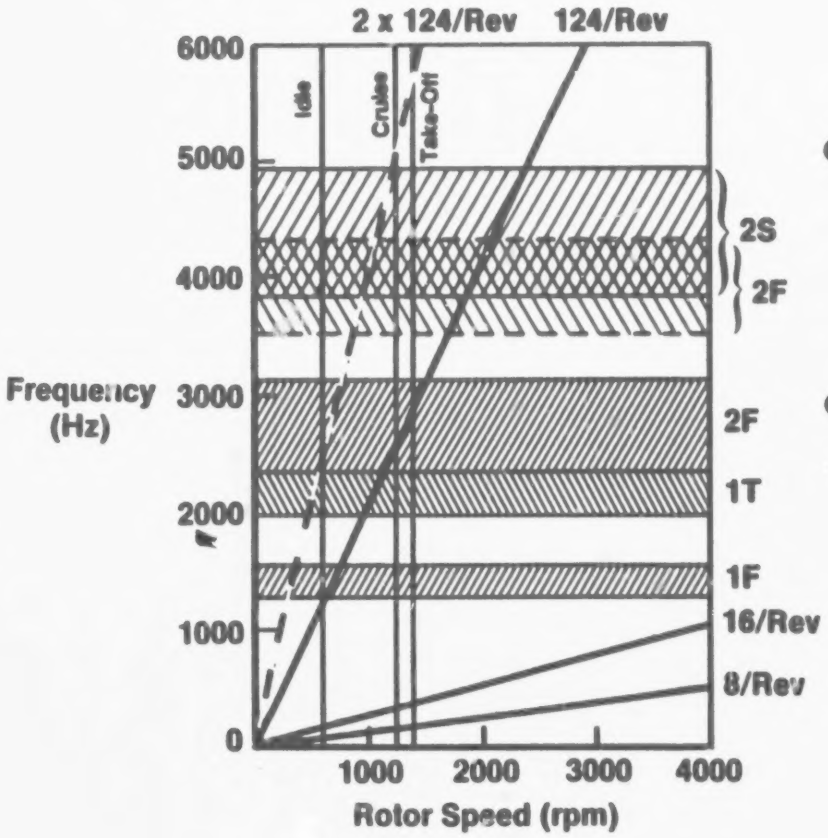

- Test Results Plotted:
  - +/-3 Sigma
  - Take-Off Temperature
- 2F Resonance
  - Weak (Downstream) Excitation
  - Engine Gage Responsive

Figure 47. IGV Frequency Test Results.

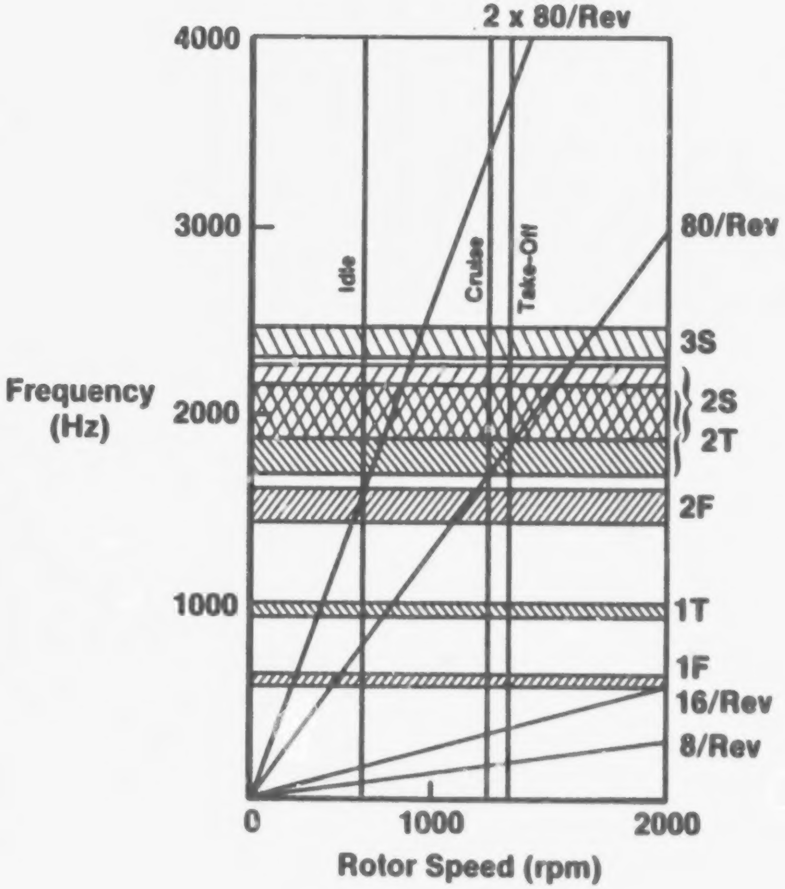

- Test Results Plotted:
  - +/-3 Sigma
  - Take-Off Temperature
- 2T Resonance
  - Difficult to Excite by Blade Passing
  - Low Wake Energy
- 2S Margin
  - Zero with +/-3 Sigma
  - 8% Minimun Tested
  - Low Wake Energy
- Engine Gages Responsive to 2T and 2S

Figure 48. OGV Frequency Test Results.

used in large steam turbine airfoils and pins which span between adjacent blades, as previously used in aircraft gas turbines, were two methods considered for accomplishing this. Airfoil inserts also were considered because they would not affect aerodynamic performance as wires or pins in the flowpath would.

Component bench testing of wire and insert dampers was conducted using Stage 1 and Stage 9 blades. While both methods provided effective damping, the insert results varied considerably while the wire results were predictable. Damping energy dissipation as a function of load (centrifugal load of the damper) was established from these tests. For most stages, the wire size required would result in relatively high stiffness and prevalent contact at "middle" blade locations; therefore, pin dampers between adjacent blades were selected.

Concurrent with the component tests, wear tests were conducted to select a damper material compatible with the turbine blade Hastelloy-X material. The two candidate materials were Inconel 718 and René 41. René 41 was selected based on the test results at different loads and temperatures.

To verify the pin damper design, a rotating spin rig (whirligig) test was conducted using Stage 1 blades; 12 blades were modified to incorporate the dampers and 12 were left unmodified as a control group. The blades were mounted in the engine spool and tested between 300 and 1400 rpm while shop air delivered through 24 nozzles was used to simulate the 1F excitation source; 74 nozzles were used to simulate the higher mode excitation source. All blades were instrumented to sense all six modes of interest. Two damper sizes, one heavier and one lighter than the projected optimum, were tested.

Test Results and Conclusions

Table 14 summarizes all damper testing and results. Figure 49 illustrates the whirligig test setup. The whirligig testing showed the undamped blades to be highly responsive in the 1F mode while higher order modes were difficult to drive.

The damped blade response was significantly less on an average basis and showed significantly less blade-to-blade scatter. There was no discernible difference between the two damper sizes, as seen in Figures 50 and 51. Based

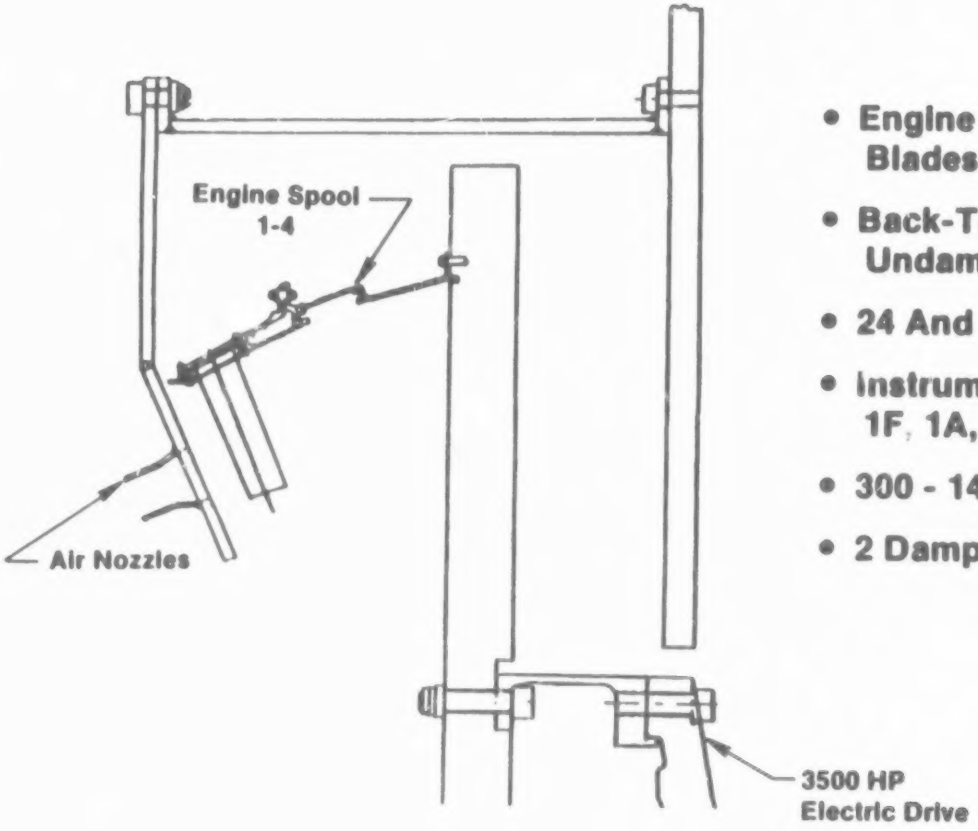
Engine Spool
1-4
Air Nozzles
3500 HP
Electric Drive

- Engine Hardware - Blades And Spools
- Back-To-Back Damped And Undamped (12 Each)
- 24 And 74 Nozzle Excitation
- Instrumentation Sensitive To 1F, 1A, 1T, 2F, 2T, And 2S
- 300 - 1400 rpm Test Range
- 2 Damper Sizes

Figure 49. Whirligig Damper Test.

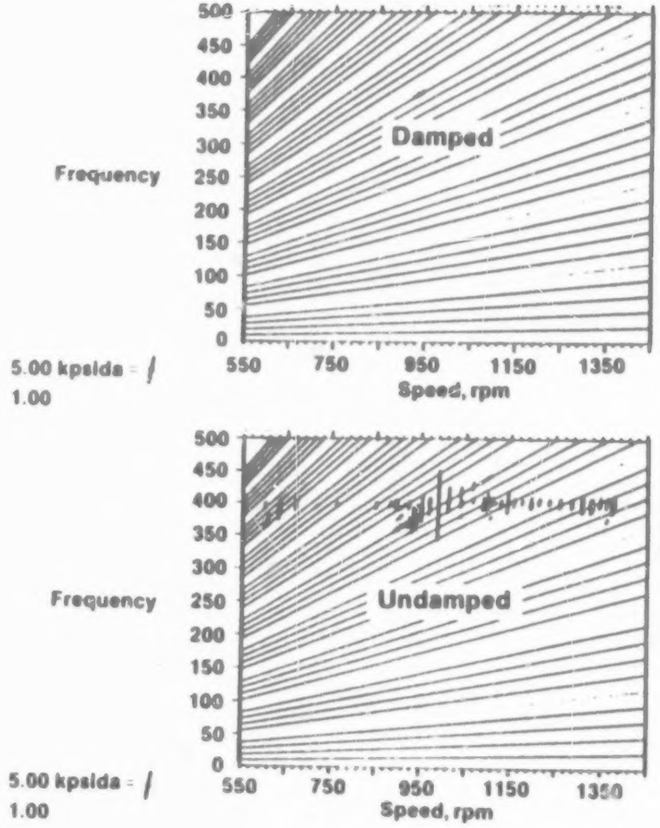

- Undamped Blades Highly Responsive
  - Unable To Control Excitation With 24 Nozzles
  - Testing Conducted With 12 And 6 Nozzles (2 x 12/Rev And 3 x 6/Rev)
- No Discernable Difference Between Two Damper Weights
- Significant Reduction In 1F Stress Level And Scatter With Dampers
- Unable To Drive Higher Order Modes
- Ability To Vary Excitation Energy Limited By Undamped Blades

Figure 50. Whirligig Test Results Summary.

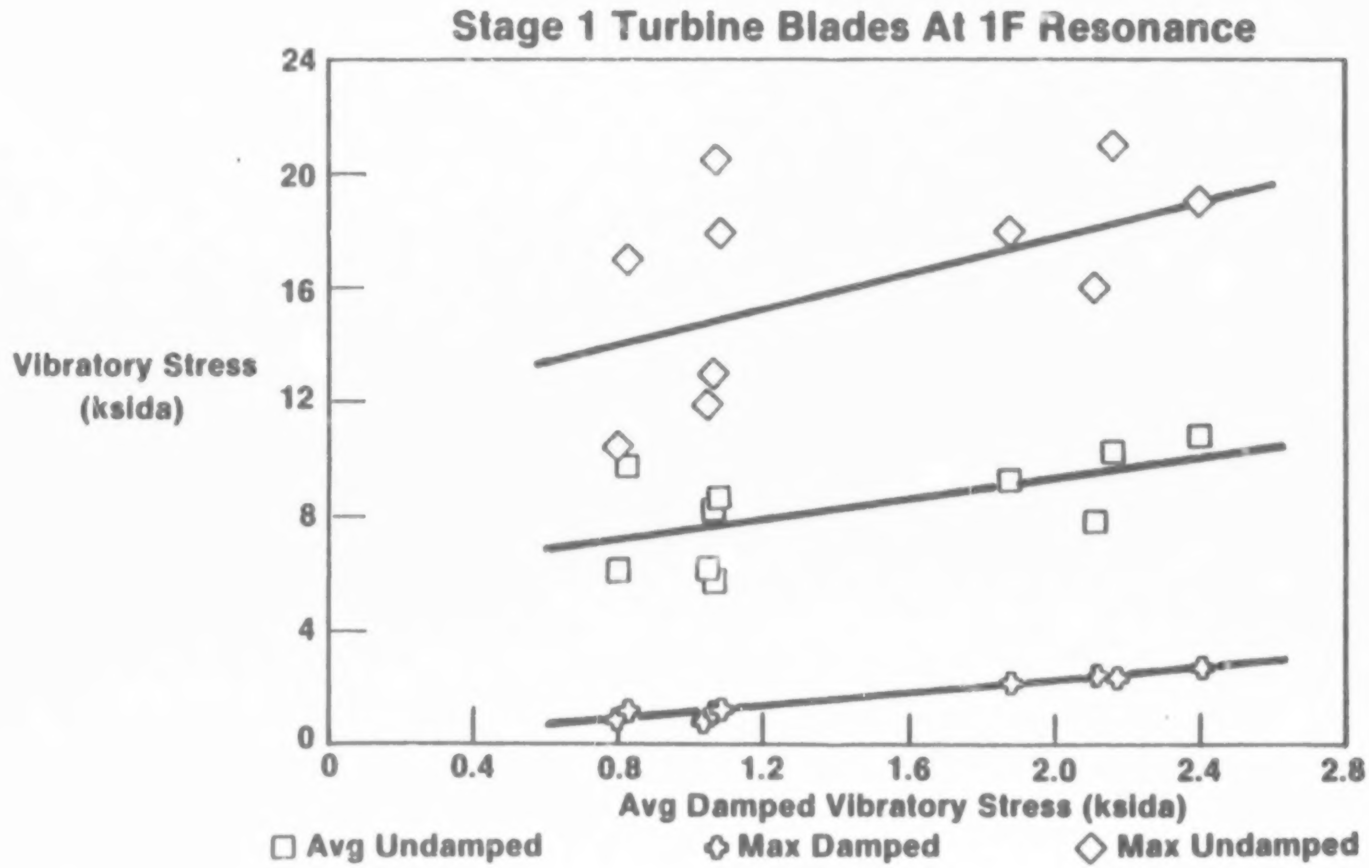

Figure 51. Whirligig Damper Test Results.

on the results of this test, damper pins were incorporated in the design of all 10 turbine blade stages and the Stage 12 power frame airfoils for Build 2. Figure 52 illustrates the final design.

Table 14. Turbine Blade Damper Development.

Test	Result	Conclusion
Component Bench - Wire Ties	Very Effective Damping	Must have Predictable Contact Load
Component Bench - Inserts	Variable Effectiveness, Unpredictable	Does Not Provide Desired Redundancy
Component Bench - Wear	0.003 Hast-X, 0.001 René 41: 104 Hours at 1300 rpm and 1 ksi 0.001 Hast-X, 0.000 René 41: 90 Hours at 700 rpm and 1 ksi 0.001 Hast-X, 0.003 IN718: 66 Hours at 1100 rpm and 1 ksi	
Whirligig - Damper Pins	Significant Reduction in Stress Level and Scatter	Damper Pins Provide Required Stress Reduction, Have Predictable Contact Load and Redundancy

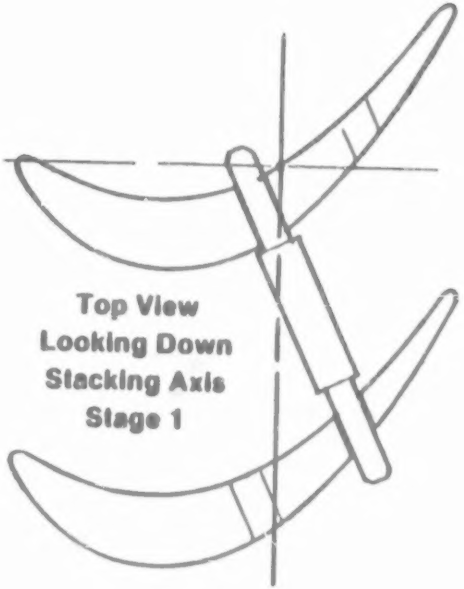
Top View
Looking Down
Stacking Axis
Stage 1

- Blade-To-Blade Damper Pins (René 41)
- Increased Tip Clearance (for Rub Avoidance)
  - + 0.050 Inch Stages 1, 3, 7, 9, 11
  - + 0.030 Inch Stages 2, 4, 6, 8, 10
- Reduced Tip Thickness
  (0.030 → 0.015)

Figure 52. Turbine Blade Fix.

7.0 SYMBOLS/ABREVIATIONS

Symbol	
A7	Final Aft Rotor Fan Blade Design
F404	Gas Generator Engine
F7	Final Forward Rotor Fan Blade Design
HCF	High Cycle Fatigue
Hg	Mercury
HPT	High Pressure Turbine
IGV	Inlet Guide Vane
Ksida	Ksi Double-Amplitude
LE	Leading Edge
LPT	Low Pressure Turbine
N	Nodal Diameter
OD	Outer Diameter
OGV	Outlet Guide Vane
PPS	Pounds per Second
P_T	Total Pressure
SFC	Specific Fuel Consumption (lb/lb hr)
UDF™	GE36 Unducted Fan Engine
W_2	Mass Airflow through Gas Generator (lb/sec)
1A	First Axial Vibratory Mode
1F	First Flexural Vibrational Mode
1R	First Radial Mode in Turbine Blades - Radial
2F	Second Flexural Mode
2S	Two-Stripe Vibratory Mode
2T	Second Torsional Mode

7.0 SYMBOLS/ABREVIATIONS

Symbol	
A/C	Aircraft
A7	Final Aft Rotor Fan Blade Design
CDP	Compressor Discharge Pressure (P33), psia
EGT	Exhaust Gas Temperature; HPT Exit Temperature
F404	Gas Generator Engine
F7	Final Forward Rotor Fan Blade Design
HCF	High Cycle Fatigue
Hg	Mercury
HMU	Hydromechanical Unit
HP	High Pressure System
HPT	High Pressure Turbine
HX	Heat Exchanger
IGV	Inlet Guide Vane
IP	Intermediate Pressure System (F404 Low Pressure System)
Ksida	Pounds-per-Square-Inch × 1000 (ksi) Double-Amplitude
LE	Leading Edge
LP	Low Pressure System (Propulsor Turbine and Fan)
LPT	Low Pressure Turbine
LVDT	Linear Variable Differential Transducer
N	Nodal Diameter
N_2	Nitrogen
OD	Outer Diameter
O/F	Oil/Fuel
OGV	Outlet Guide Vane
O/S	Overspeed
PLA	Power Level Angle
PPC	Precharge Pressure, psig
PPS	Pounds per Second
P_T	Total Pressure
P2	Inlet Pressure, psia
P15	Fan Bypass Duct Pressure, psia
P33	CDP (Compressor Discharge Pressure), psia

C-2

Symbol	
P46	HPT Exit Pressure, psia
P46/P2	Engine Pressure Ratio
RP46/P2	Reference P46/P2
RT46	Reference T46
RXN2	Reference XN2, rpm
SFC	Specific Fuel Consumption (lb/lb hr)
S/V	Servo Valve
T/M	Torque Motor
T2	Inlet Temperature
T25	HP Compressor Inlet Temperature, ° R
T46	EGT (Exhaust Gas Temperature); HPT Exit Temperature
UDF™	GE36 Unducted Fan Engine
W_2	Mass Airflow through Gas Generator (lb/sec)
XLPVG	IP Compressor Stator Actuator LVDT
XN2	IP Speed, rpm
XN25	HP Speed, rpm
XN25R	HP Speed Corrected to T25, rpm
XWP36	Fuel Metering Valve LVDT
1A	First Axial Vibratory Mode
1F	First Flexural Vibrational Mode
1R	First Radial Mode in Turbine Blades - Radial
2F	Second Flexural Mode
2S	Two-Stripe Vibratory Mode
2T	Second Torsional Mode

8.0 REFERENCES

1. GE, "Full Scale Technology Demonstration of a Modern Counterrotating Unducted Fan Engine Concept - Design," NASA Contract NAS3-24210, NASA CR-180867, December 1987, .
2. GE, "Full Scale Technology Demonstration of a Modern Counterrotating Unducted Fan Engine Concept - Engine Test," NASA Contract NAS3-24210, NASA CR-180869, December 1987 .
3. GE, "UDF^{TM} Airworthiness Executive Review," NASA Contract NAS3-24210, July 1986.
4. GE, "The Unducted Fan Engine - Quarterly Review," Number 8, NASA Contract NAS3-24210, May 13, 1986.
5. GE, "The Unducted Fan Engine - Quarterly Review," Number 7, NASA Contract NAS3-24210, November 18, 1986.
6. GE, "The Unducted Fan Engine - Quarterly Review," Number 6, NASA Contract NAS3-24210, August 16, 1985.

1. Report No.
CR-180868

2. Government Accession No.

3. Recipient's Catalog No.

4. Title and Subtitle
Full-Scale Technology Demonstration of a Modern Counterrotating Unducted Fan Engine Concept - Component Test

5. Report Date
December 1987

6. Performing Organization Code

7. Author(s)
GE36 Design and Systems Engineering

8. Performing Organization Report No.
535-03-01

9. Performing Organization Name and Address
GE Aircraft Engines
One Neumann Way
Cincinnati, Ohio 45215

10. Work Unit No.

11. Contract or Grant No.
NAS3-24210

12. Sponsoring Agency Name and Address
NASA Lewis Research Center
21000 Brookpark Road
Cleveland, Ohio 44135

13. Type of Report and Period Covered
Topical

14. Sponsoring Agency Code

15. Supplementary Notes

16. Abstract

The UDF™ engine is a new aircraft engine concept that is based on an ungeared, counterrotating, unducted, ultra-high-bypass turbofan configuration. This engine is being developed by GE to provide a high thrust-to-weight ratio powerplant with exceptional fuel efficiency for subsonic aircraft application. This report covers the component testing of pertinent components of this engine such as the fan blades, control and actuation system, turbine blades and spools, seals, and mixer frame.

17. Key Words (Suggested by Author(s))
Unducted Fan (UDF™); Counterrotation; Ultra-High-Bypass Fan; Propfan; Component Test

18. Distribution Statement
[redacted]

19. Security Classif. (of this report)

20. Security Classif. (of this page)

21. No. of Pages

22. Price